C 51.17/12:992/1

Tech Notes

January 1992

PB92-925901

PENNSYLVANIA STATE
UNIVERSITY

FEB 28 1992

DOCUMENTS COLLECTION
U.S Depository Copy

Technology fact sheets from Federal laboratories

NTIS

U.S. DEPARTMENT OF COMMERCE
National Technical Information Service
Center for the Utilization of Federal Technology

NOW! Work Directly with Government Labs

A New Directory to Expertise, Facilities, and Services

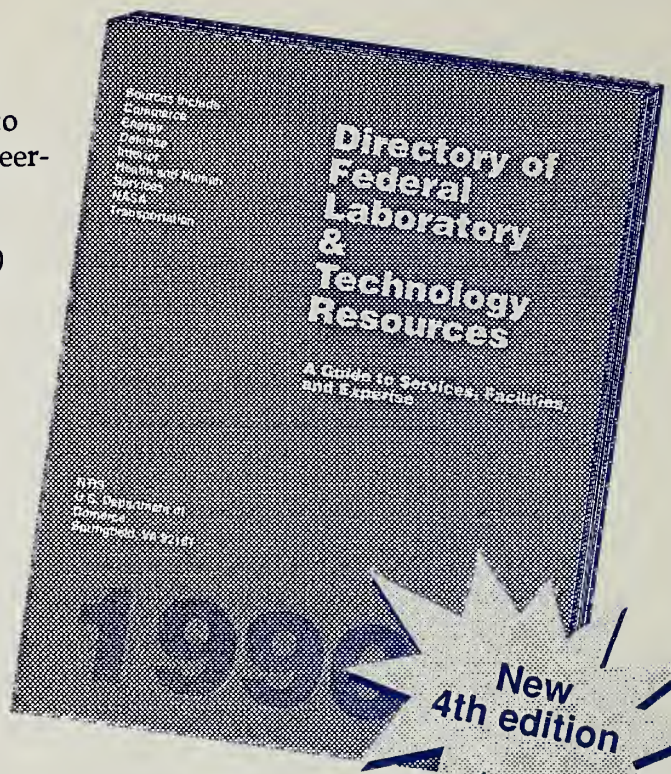

The 4th edition of this valuable directory guides you to hundreds of Federal agencies, laboratories, and engineering centers willing to share their expertise and equipment—and sometimes even their facilities—to aid in your research. Detailed summaries of more than 1,100 unique resources are arranged in 32 subject areas for easy reference

Aeronautics	Manufacturing
Agriculture and food	Materials
Biological sciences	Medicine
Building technology	Nuclear
Computers	Ocean sciences
Electrotechnology	Physical sciences
Energy	Transportation
Engineering	Plus others

The name, address, and phone number of a personal contact is listed for each entry, along with the descriptive summary.

Descriptions of 90 Technical Information Centers are included

These centers offer information services and expertise in areas such as fuels, cold regions, concrete, fisheries, toxicology, pesticides, plastics, and much more.

Four handy indexes make it easy for you to locate the resource you need:

- A Subject Index lets you look up your need by specific topic.
- The State Index arranges all the resources within a state.
- The Resource Name Index provides a quick reference if you already have a name of a specific Federal laboratory or service.
- An Agency Index provides a listing of all the resources by Government agency.

"The Directory will be popular in research or business libraries."

Reference Book Bulletin
American Libraries Association

"This directory is unusually well-indexed....It should be on the shelf of every Chamber of Commerce end economic development organization in the nation."

Mr. Brian McLaughlin
Information Services and Research
Syracuse, NY

Order your directory today.

Call the NTIS sales desk at (703) 487-4650. Refer to the NTIS order number, PB90-104480AAW, price $59.95 plus $3.00 for handling.

1990-91 *Directory of Federal Laboratory & Technology Resources—A Guide to Services, Facilities, and Expertise*

Tech Notes

Highlighting Selected U.S. Government Technology & Resources

January 1992

Contents

Agriculture & Food 1
Computers 4
Electrotechnology 7
Energy 17
Engineering 19
Environmental Science & Technology 36
Manufacturing, Machinery & Tools 38
Materials 44
Medicine & Biology 51
Natural Resources Technology & Engineering 54
Physical Sciences 55
Transportation & Components 59

Published monthly by the National Technical Information Service (NTIS), Tech Notes bring together individual one- to two-page fact sheets prepared by Federal agencies, their laboratories, or contractors. These fact sheets highlight current Federal technology determined to have commercial or practical application. Topics cover new processes, materials, techniques, software, instrumentation, and resources.

Some of the current sources are the Department of the Navy, Department of the Army, NASA, Department of Energy, Environmental Protection Agency, Department of the Interior, and the Department of Agriculture.

Special assistance is provided by the Federal Laboratory Consortium.

Change of address or questions concerning subscriptions should be sent to:
Subscriptions Department
National Technical Information Service
Springfield, VA 22161
(703) 487-4630

Suggestions, comments, or questions concerning Tech Notes should be directed to:
Tech Notes Editor
Room 300B F
National Technical Information Service
Springfield, VA 22161
(703) 487-4805

How to Use Tech Notes

Every Tech Notes fact sheet lists a source for additional information. The source of this information may be a special support package from the originating agency, a personal contact, a licensing opportunity, or a backup report available from NTIS.

Each fact sheet also is perforated to allow for easy removal for those subscribers who may wish to keep a special fact sheet file or route to others in their organization

Sources of Further Backup Information

Below are two representative examples of how each Tech Note fact sheet provides you with a source of further information. In most cases, this information is provided directly by the agency or its laboratory.

However, there are cases where NTIS is the source for backup documentation. In these cases, use the order form at the end.

Examples:

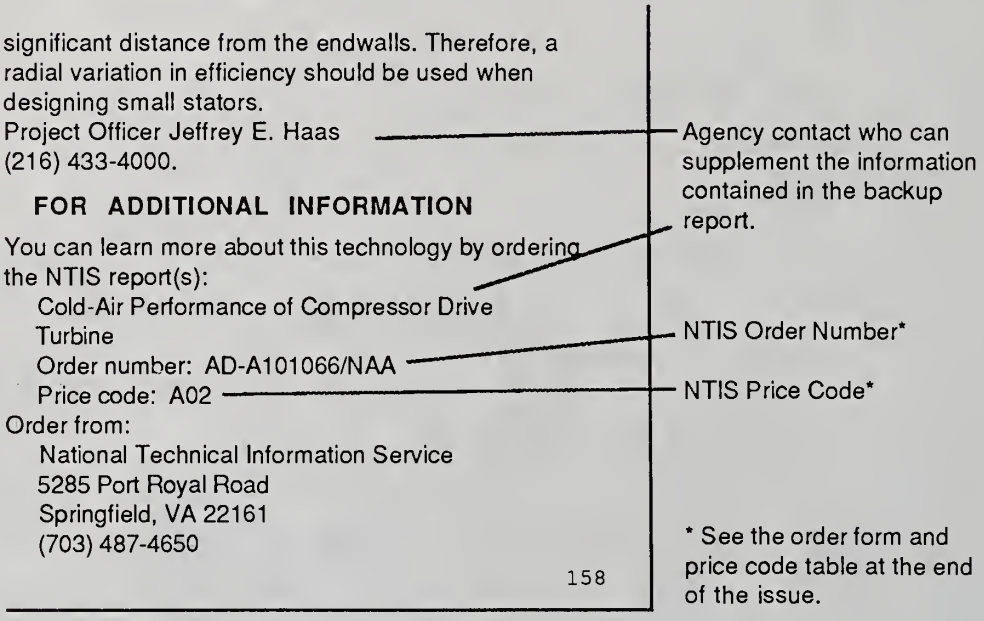
significant distance from the endwalls. Therefore, a radial variation in efficiency should be used when designing small stators.
Project Officer Jeffrey E. Haas
(216) 433-4000.
FOR ADDITIONAL INFORMATION
You can learn more about this technology by ordering the NTIS report(s):
Cold-Air Performance of Compressor Drive Turbine
Order number: AD-A101066/NAA
Price code: A02
Order from:
National Technical Information Service
5285 Port Royal Road
Springfield, VA 22161
(703) 487-4650
158
Agency contact who can supplement the information contained in the backup report.
NTIS Order Number*
NTIS Price Code*
* See the order form and price code table at the end of the issue.

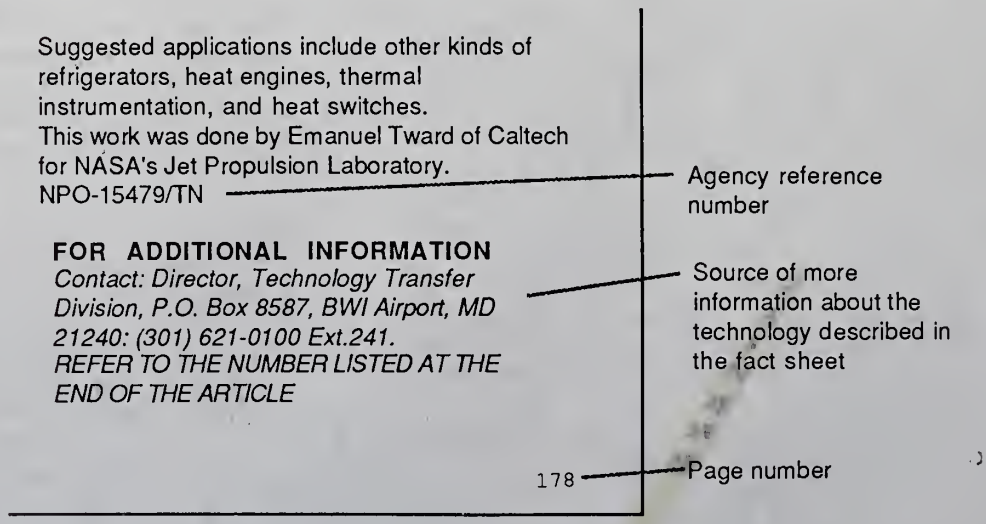
Suggested applications include other kinds of refrigerators, heat engines, thermal instrumentation, and heat switches.
This work was done by Emanuel Tward of Caltech for NASA's Jet Propulsion Laboratory.
NPO-15479/TN
FOR ADDITIONAL INFORMATION
Contact: Director, Technology Transfer Division, P.O. Box 8587, BWI Airport, MD 21240: (301) 621-0100 Ext.241.
REFER TO THE NUMBER LISTED AT THE END OF THE ARTICLE
178
Agency reference number
Source of more information about the technology described in the fact sheet
Page number

Tech Notes Title List for January 1992

Agriculture & Food

0001 Blocking Insect Immune Response

0002 Milk Doesn't Block Cereal's Iron

0003 No More Soggy Sandwiches

Other Items of Interest

0020 MRE Heaters Invented (Licensing Opportunity)

0024 Controlling Laboratory Processes From a Personal Computer—An operator can control processes via natural-language commands.

Computers

0004 Upgrades Bolster SANDAC V's Performance, Flexibility

Software

0005 Computer Language for Optimization of Design—Nonlinear methods are incorporated at the language level.

0006 Versatile, Fast Computer Core—The core speeds up the development of flight computers.

Electrotechnology

0007 Bi-Orthogonal PCM Communications System Employing Multiplexed Noise Codes (Licensing Opportunity)

0008 Behavior the Costas Loop in Reception of Telemetry—Effects of signal parameters and Doppler shift are computed.

0009 Circuit Detects Faint Flashes Against Bright Background—The rapidly varying component of a luminous-flus signal is extracted from the total signal.

0010 Designing Accelerated Tests of Electromigration—Error analysis helps in the selection of currents, temperatures, and durations.

0011 Digital Accumulators in Phase- and Frequency-Tracking Loops —Digital accumulators can degrade performances at low carrier-to-noise ratios.

0012 Effects of Frame Rates in Video Displays—High rates are needed in rapidly changing images.

0013 Improved Gas-Gap Heat Switch—Residual conductance in the 'off' state is reduced.

0014 Making High-Pass Filters for Submillimeter Waves—A process makes a thick metal mesh.

0015 Pulse-Width-Modulating Driver for Brushless dc Motor—The power supply for the motor is electrically isolated from other power supplies.

Testing & Instrumentation

0016 Silicon Moisture Sensor Detects Humidity in Electronics

Other Items of Interest

0018 Vaporization Would Cool Primary Battery—Less material would be needed in cooling by vaporization than in cooling by melting.

Energy

0017 Fuel Cells: Cutting Gasoline Consumption in Half

0018 Vaporization Would Cool Primary Battery—Less material would be needed in cooling by vaporization than in cooling by melting.

Engineering

0019 SUSV-Towed Snow Plow

0020 MRE Heaters Invented (Licensing Opportunity)

0021 Valve Regulates Sea Water Pressure

0022 Adaptive Control of Large Vibrating, Rotating Structures—The inherent passivity of structures is exploited to obtain convergence.

0023 Algorithm Computes Hypersonic Flow of Air—Nonequilibrium thermochemical effects are taken into account.

Software

0024 Controlling Laboratory Processes From a Personal Computer—An operator can control processes via natural-language commands.

0025 Damping Seals Would Help Support Turbopump Rotor—Tentative designs are presented.

0026 Growth of Instabilities in Two Types of Mixing Layers—Effects of feedback are examined.

0027 Incompressible, Viscous Flow About an Ogive/Cylinder—Calculated flow patterns agree closely with experimental ones. (Licensing Opportunity)

0028 Robot Grasps Rotating Object—Advanced techniques for sensing and control are combined.

Software

0029 Software for Multivariable Frequency-Domain Analysis—Outputs include frequency-response singular-value plots of multivariable transfer matrices.

Testing & Instrumentation

0030 Technique to Measure Liquid Level and Volume Device

0031 Adjustable Pitot Probe—The probe is readily positionable in the core of uniform flow in a hypersonic wind tunnel. (Licensing Opportunity)

0032 Collectors of Airborne and Spaceborne Particles—Simple units go directly into optical, electron, or x-ray analysis equipment.

Engineering (Cont.)

0033 Digital Pitch-and-Roll Monitor—A compact inclinometer is precise and prints out readings on demand.

0034 Integral Plug-Type Heat-Flux Gauge—The integral construction reduces the components of error caused by discontinuities. (Licensing Opportunity)

0035 Mixed-Mode-Bending Delamination Apparatus—Double-cantilever-beam and end-notch-flexure loads are applied simultaneously. (Licensing Opportunity)

Environmental Science & Technology

0036 Indoor Air Quality Simulator for Personal Computers

Testing & Instrumentation

0037 An Assessment of Soil-Gas Measurement Technologies

Other Items of Interest

0056 Air/Sea Temperature Probe Developed

Manufacturing, Machinery & Tools

0038 AGARD Handbook on Advanced Casting

0039 Composite Recycling

0040 Paint Spray Guide Developed

0041 Bearing-Cartridge Damping Seal—Ball bearings would carry reduced loads and be cooled more effectively. (Licensing Opportunity)

0042 Computer-Aided Design of Sheet-Material Parts—The old manual graphical 'development' technique is computerized. (Licensing Opportunity)

Testing & Instrumentation

0043 Computerized Profilometer for Inspection of Welds—Subjective inputs in inspection are reduced with consequent enhancement of precision. (Licensing Opportunity)

Materials

0044 Carbon Foam Features Exceptional Properties

0045 High-Temperature Polymers Reported

0046 Controlled Temperature Gradient Improves Freezing Alloy—Better microstructure increases fatigue life. (Licensing Opportunity)

0047 Correlating DSC and X-Ray Measurements of Crystallinity—The degree of crystallinity is roughly proportional to the heat of fusion.

0048 LaRC-RP41: a Tough, High-Performance Composite Matrix—A new polymer exhibits increased toughness and resistance to microcracking. (Licensing Opportunity)

0049 New Polyimide has Many Uses—Low-toxicity and low-mutagenicity monomer is the key to a new high-performance polyimide. (Licensing Opportunity)

0050 Superfiber for Strong, Light Fabrics—Polyolefin fiber resists chemicals and abrasion.

Other Items of Interest

0038 AGARD Handbook on Advanced Casting

0039 Composite Recycling

Medicine & Biology

0051 Chronic Adult Periodontitis Studied

0052 Confirmation for the Good Cholesterol

Testing & Instrumentation

0053 Biological Sensors

Other Items of Interest

0002 Milk Doesn't Block Cereal's Iron

Natural Resources Technology & Engineering

0054 Azimuthal Anisotrophy in Radar Backscatter From the Ocean—Minima are offset from the nominal crosswind directions.

Other Items of Interest

0037 An Assessment of Soil-Gas Measurement Technologies

Physical Sciences

0055 Molecular Engineering Theory Guides New Polymer Blends

Testing & Instrumentation

0056 Air/Sea Temperature Probe Developed

0057 Telescope Would Image X and (r) Rays—The advantages of focusing optics would be made available at high photon energies. (Licensing Opportunity)

0058 Ultra-High-Spectral-Resolution X-Ray/EUV Monochromator—Multilayer Bragg-reflection coats would be combined with diffraction gratings. (Licensing Opportunity)

Transportation & Components

0059 Research in Helicopter Noise—Progress in aeroacoustical theory and experiments is reviewed.

Agriculture & Food

0001 Blocking Insect Immune Response

0002 Milk Doesn't Block Cereal's Iron

0003 No More Soggy Sandwiches

Other Items of Interest

0020 MRE Heaters Invented (Licensing Opportunity)

0024 Controlling Laboratory Processes From a Personal Computer—An operator can control processes via natural-language commands.

Research Technology
Agricultural Research Service
U.S. Department of Agriculture

Blocking Insect Immune Response

Like humans, insects can fend off disease-causing organisms that might otherwise kill them. But exactly how these enduring organisms wage an immune defense has been uncertain.

Now, researchers have revealed the specific biochemical messages that trigger an immune response in the tobacco hornworm *(Manduca sexta).* Blocking these messages, they've discovered, weakens the insect's response.

"That leaves the hornworms vulnerable to deadly bacterial infections," says Ralph W. Howard, an ARS chemist who worked on the study.

Researchers might someday be able to use this information to snuff out pests—by using bacteria that's harmless to humans but fatal to bugs with weakened immune responses, he says. Howard is at ARS' Biological Research Laboratory in Manhattan, Kansas.

They injected hornworms with eicosanoid inhibitors, substances that block the production of certain hormones. In higher animals, eicosanoids control many physiological reactions, including immune defenses. Little is known about their role in insects and other invertebrates.

Next, scientists infected the insects with a red-pigmented strain of the bacterium *Serratia marcescens.* These naturally occurring bacteria are typically found on insects and in soil.

By clipping the tip off a hornworm's foreleg, the scientists could collect a few drops of its "blood"—a clear, greenish fluid called hemolymph. The samples were then grown on plates to count the bacteria present.

Hornworms that received inhibitors contained much more bacteria than the control group (insects whose immune systems were not blocked). The higher the dose of the inhibitors, the more bacteria were present. And that led to a higher death rate in the treated hornworms.

When eicosanoid production was blocked, the message telling the insect to wage a cellular-based defense was, in effect, silenced. The cellular immune response includes cells that engulf and destroy bacteria cells, a process known as phagocytosis.

"We knew about the infection and defense processes, but we didn't know what happened in between," says Stanley-Samuelson. "Now we've identified the biochemical pathways that mediate insect immune defense, and they're similar to those in humans. The next step is to find specific inhibitors that affect insects only."

Using this information to control pests is many years away, says Howard. But he speculates the inhibitors could be added to a bait that insects eat, which would damage their immune systems.

"Then we could hit them with a bacterial pathogen," he says. The compromised bugs couldn't withstand infections and would eventually die.

"It's an indirect approach, but these days we're looking for more sophisticated methods than just pouring on a chemical."

Ralph W. Howard is at the USDA-ARS Biological Research Unit, U.S. Grain Marketing Research Laboratory, Room 115, 1515 College Ave., Manhattan, KS 66502. Phone (913) 776-2706. ◆

Research Technology
Agricultural Research Service
U.S. Department of Agriculture

Milk Doesn't Block Cereal's Iron

Go ahead and drown your breakfast cereal with milk. It won't interfere with your body's ability to absorb iron from the cereal or other whole-grain foods such as brown rice, says ARS nutrition researcher Judith R. Turnlund.

Results of her study with eight healthy young women at the ARS Western Human Nutrition Research Center in San Francisco indicate that milk neither boosts nor blocks iron absorption. The findings should allay a concern, raised by earlier studies conducted elsewhere, that milk might inhibit the absorption of iron from foods eaten at the same meal.

"In our test," says Turnlund, "milk made no significant difference in the amount of iron our volunteers absorbed from their food."

Cereal products they ate included english muffins and whole-wheat hot cereal at breakfast, a brown rice casserole with stir-fried vegetables at lunch, and chapate, a spicy, tortilla-like bread, at dinner.

Turnlund's findings should be especially good news for women who are trying to boost their intake of milk or other calcium-rich dairy products to prevent osteoporosis. "They can go for the calcium, needed for strong bones," she says, "without worrying that they'll short themselves of the iron they need for good health."

Because they rely heavily on cereal grains for iron, vegetarians might also be heartened by the results. The study's outcome should also encourage people who are eating less red meat than before. "Any nutritional glitch that interferes with iron absorption will affect these people more than others," she explains. "We have shown that milk is not a glitch."

Why is iron absorption a special concern to these two groups of people? "If you eat little or no red meat, you have to be extremely careful to get enough usable iron in your food to avoid iron-deficiency anemia," explains Turnlund. "The form of iron from grains and vegetables, non-heme, is much more difficult to absorb than the heme iron in red meats. Because of this problem, we wanted to monitor milk's effect on cereal's iron."

To track volunteers' absorption of iron, Turnlund spiked the cereal component of each meal with a natural but rare form of iron that's easily traced. That iron, if not absorbed by the body, showed up in stool samples analyzed by a high-tech procedure called thermal ionization mass spectrometry.

The National Dairy Council sponsored the experiment.

Judith R. Turnlund is with the USDA-ARS Western Human Nutrition Research Center, Micronutrients Research Unit, P.O. Box 29997, San Francisco, CA 94129. Phone (415) 556-5662. ◆

Research Technology
Agricultural Research Service
U.S. Department of Agriculture

No More Soggy Sandwiches

Fed up with making jelly sandwiches that are soggy by lunchtime?

ARS scientists have a solution—an edible wrap that goes inside your sandwich to form a moisture barrier between the jelly and the bread.

Preliminary experiments show that the wrap, produced at ARS' Western Regional Research Center in Albany, California, can protect bread for 2 days.

Still, ARS research chemist Dominic W.S. Wong cautions that before the product can be used as an edible wrap in home or commercial kitchens, its all-natural ingredients must be approved for food use.

Those ingredients are lauric acid, from coconut oil, and chitosan, a derivative of chitin, a material in the shells of crab, shrimp, crawfish, and lobster. The film's bland taste won't interfere with the flavor of food products.

When heated, mixed, then spread out in sheets to dry, the lauric acid and chitosan make a flexible, silvery sheet. Wong and former ARS chemist Allen G. Pittman, along with colleague Francois A. Gastineau of France, developed the wrap.

Wong suggests the film might work equally well to protect the freshness of highly perishable produce such as cauliflower or cucumber.

Unlike today's most widely used plastic wraps, made from petrochemicals, the chitosan-based wrap is 100 percent biodegradable. And, although the idea of using lauric acid and chitosan for an edible film isn't new, the Albany team, according to chemist Pittman, is apparently the first to extensively test it for this use.

Dominic W.S. Wong is with the USDA-ARS Process Chemistry and Engineering Research Unit, Western Regional Research Center, 800 Buchanan St., Albany, CA 94710. Phone (415) 559-5860. ◆

Computers

0004 Upgrades Bolster SANDAC V's Performance, Flexibility

Software

0005 Computer Language for Optimization of Design—Nonlinear methods are incorporated at the language level.

0006 Versatile, Fast Computer Core—The core speeds up the development of flight computers.

Sandia National Laboratory

Upgrades Bolster SANDAC V's Performance, Flexibility

New capabilities have been developed for the Sandia Airborne Computer (SANDAC) that provide at least five times greater computational throughput, improved programming flexibility, resistance to electromagnetic interference, and other improvements.

SANDAC is a state-of-the-art, high-performance, ruggedized, miniaturized, parallel-processing computer developed at Sandia National Laboratories. It is small (about the size of a kitchen toaster) and tough enough to fly on missiles and run on batteries while offering supercomputer-like computing power for such things as high-speed navigation, guidance, and control.

SANDAC's ultra-high-performance capabilities are used by Sandia and defense agencies in the testing of various proof-of-principle exploratory systems including experimental missiles, reentry vehicles, complex space experiments, advanced aircraft prototypes, and other missions. Sandia also uses it in a variety of other projects including robotics, data gathering, and image recognition.

Despite its ultra-high-speed computational abilities, SANDAC, in a typical seven-module unit, weighs only seven pounds, uses just 35 watts of power, can operate in temperatures from $-20°C$ to $+70°C$ ($-4°F$ to $+160°F$), and can resist vibrations of 18 g's and shocks of 1,200 g's.

Expandable with modules

SANDAC is modular in both its hardware and logic design so that its computational capabilities can be easily expanded. It can be made up of anywhere from 1 to 15 parallel processor modules as needed for a particular use, plus a utility module and several memory and other optional modules. Each module measures 6.7×7 inches and is a little over half an inch thick. The ends of modules form the outside hardened case of the computer.

SANDAC is also unusual in that despite its leading-edge computational capability and high-level software tools, it uses commercially available parts.

SANDACs have evolved over a period of years at Sandia. They have been steadily improved through experience gained in building and applying earlier models in difficult, real-time experiments. The evolution has also taken advantage of the explosive growth of microprocessor technology and ever-increasing capabilities of recent software developments.

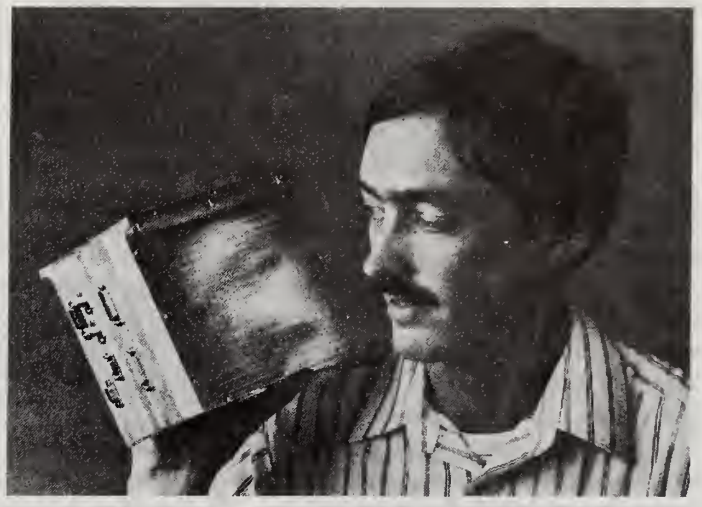

Sandia electrical engineer Glenn Russell displays the latest version of the SANDAC V computer. SANDAC is a state-of-the-art, ruggedized, miniaturized parallel-processing computer that runs on batteries and offers supercomputer-like performance for special airborne projects. It is also expandable; this is a six-module configuration.

The third-generation version, SANDAC V, first flew in 1988, but it has been improved with still more attributes since then.

Until recently SANDAC V has used the Motorola MC68020 microprocessor, with each processor module capable of carrying out 2.5 million instructions per second (MIPS)—a total of 37.5 MIPS for a full 15-module configuration. The most recent designs use the million-transistor MC68040 microprocessor, with a throughput of 15 million instructions per second, more than 5 times faster.

But the real strength of the MC68040, says Sandia electrical engineer Edward J. Nava, is in floating point operations, a key numerical manipulation. "We can see up to 30-times improvement in some floating point operations," he says, pointing out that one particular operation done in 4.5 microseconds (millionths of a second) with the 68020 is completed in 150 nanoseconds (billionths of a second) with the 68040—30 times faster. Another key floating point operation is carried out 18 times faster.

The new processor allows either greater computing power for the same space or smaller space requirements for a given computing power.

Both processor modules provide 1/2 megabyte (MB) of memory.

"SANDAC is a true multiprocessor," says Nava. "Each module can run independently. Yet each can access all resources available to any processor." He points out that this simultaneous access to all memory in any module is "transparent to the software," meaning that the user can write software without having to worry about the hardware architecture. "This greatly simplifies the software," he says.

The latest versions of SANDAC V also incorporate Sandia-developed EEPROM (electrically erasable, programmable, read-only memory) memory boards that allow memory contents to be retained indefinitely and make SANDAC V easily reprogrammable.

Although the primary programming language used with SANDAC is the C language, the most recent versions are also now capable of supporting the ADA language, which has been mandated by the Department of Defense for many weapon applications.

Recently a specialized SANDAC module has been developed that has been optimized for digital signal processing and digital control systems. This module is based on an AT&T DSP 32C single-chip digital signal processor.

The SANDAC external package has also been modified to minimize the computer's own radiated and conducted electromagnetic (EM) emissions as well as its susceptibility to external EM noise. The sensitivity of missile electronics systems to EM noise is always a concern.

Another new capability provides an interconnect that allows operation with any standard avionics hardware that has a dual-redundant MIL-STD-1553 interconnection, widely used in defense applications.

Nava says Sandia has also greatly increased the software development and testing capabilities related to SANDAC, including real-time software execution monitoring. The SANDAC V software strategy is to provide tools that allow the software development to occur at whatever level is consistent with the needs.

"Software generation is very easy now," says Nava. "Users can generate their own code without having to worry about all the hardware details."

Recently a capability has been developed that allows all application software to be loaded automatically from a Sundstrand disk. This allows users to develop software and store it on PC-compatible disks, which are then loaded during SANDAC power-up.

Nava says Sandia will probably continue to evolve and improve the computer while still calling it SANDAC V. All new improvements are designed to be compatible with current hardware, and a special effort has been made to maintain software compatibility with previous versions.

All SANDAC hardware and software design is done at Sandia. SANDAC V is produced under contract to Sandia by Honeywell Space & Strategic Avionics division, Clearwater, Florida. Potential users are subject to certain export-control laws.

FOR ADDITIONAL INFORMATION: Technical Contact: Edward Nava (505)846-1443, Department of Energy, Sandia National Laboratories, Albuquerque, NM 87185-5800.

Computer Language for Optimization of Design

Nonlinear methods are incorporated at the language level.

SOL is a computer language geared to the solution of design problems. SOL includes the mathematical modeling and logical capabilities of a computer language like FORTRAN but also includes the additional power of nonlinear mathematical programming methods (i.e., numerical optimization) at the language level (as opposed to the subroutine level).

The language-level use of optimization has several advantages over the traditional, subroutine-calling method of using an optimizer: first, the optimization problem is described in a concise and clear manner that closely parallels the manner of the mathematical description of the optimization; second, a seamless interface is automatically established between the optimizer subroutines and the mathematical model of the system being optimized; third, the results of an optimization (objective, design variables, constraints, termination criteria, and some or all of the optimization history) are put out in a form directly related to the description of the optimization; and finally, automatic checking for errors and recovery from an ill-defined model of the system or description of the optimization are facilitated by the language-level specification of the optimization problem. Thus, SOL enables rapid generation of models and solutions for optimum design problems with greater confidence that the problem is posed correctly.

The SOL compiler takes SOL-language statements and generates the equivalent FORTRAN code and system calls. Because of this approach, the modeling capabilities of SOL are extended by the ability to incorporate existing FORTRAN code into a SOL program. In addition, SOL has a powerful MACRO capability. The MACRO capability of the SOL compiler effectively gives the user the ability to extend the SOL language and can be used to develop easy-to-use shorthand methods of generating complex models and solution strategies. The SOL compiler provides syntactic and semantic checking for recovery from errors and provides detailed reports containing cross-references to show where each variable was used. The lists summarize all optimizations and include the objective functions, design variables, and constraints. The compiler checks for errors specific to optimization problems, so that simple mistakes will not cost hours of debugging time.

The optimization engine used by and included with the SOL compiler is a version of Vanderplatt's ADS system (Version 1.1) modified specifically to work with the SOL compiler. SOL allows the use of the more than 100 ADS optimization choices; for example, sequential quadratic programming, modified feasible directions, interior- and exterior-penalty-function methods, and variable-metric methods. Default choices of the many control parameters of ADS are made for the user, but the user can override any of the ADS control parameters for each individual optimization.

The SOL language and compiler were developed with an advanced compiler-generation system to ensure correctness and simplify the maintenance of programs. Thus, the syntax of SOL was defined precisely by a LALR(1) grammar, and the parser of the SOL compiler was generated automatically from the LALR(1) grammar with a parser generator. Hence, unlike in ad-hoc, manually coded interfaces, the lexical analysis of the SOL compiler ensures that the SOL compiler recognizes all legal SOL programs, can recover from and correct for many errors, and can report the location of errors to the user.

This version of the SOL compiler has been implemented on VAX/VMS computer systems and requires 204 KB of virtual memory to execute. Inasmuch as the SOL compiler produces FORTRAN code, it requires the VAX FORTRAN compiler to produce an executable program. The SOL compiler consists of 13,000 lines of Pascal code. It was developed in 1986 and last updated in 1988. The ADS and other utility subroutines amount to 14,000 lines of FORTRAN code and were also updated in 1988.

This program was written by Stephen J. Scotti of **Langley Research Center** *and Stephen H. Lucas of Vigyan Research Associates, Inc.*
LAR-14280/TN

FOR ADDITIONAL INFORMATION

CONTACT

COSMIC®
112 Barrow Hall
University of Georgia
Athens, GA 30602

(404) 542-3265

NASA Tech Brief
National Aeronautics and
Space Administration
Goddard Space Flight Center, Greenbelt, Maryland

Versatile, Fast Computer Core

The core speeds up the development of flight computers.

A versatile computer core serves as a state-of-the-art component and a tool for the development of computing systems that are required to process data rapidly, particularly as part of control tasks that involve relatively large volumes of input and output data. This core exploits new technology to enhance the performance needed in flight computers, the development of which has heretofore been relatively slow because of the limitations of central processing units and memories. Computing and other equipment specific to a flight system can be added around this core to develop flight systems rapidly without incurring the time and monetary costs of designing a new core.

The core consists of a Harris RTX2010 central processing unit, system memory, decoding logic, a watchdog timer, wait-state and timing circuitry. It also includes an RS232 interface for the development of programs and for monitoring the system. The core software kernel, which is stored in read-only memory, is based on the American National Standards Institute's Forth computing language. Inasmuch as Forth is the native (assembly) language of the central processing unit, this kernel provides a compact, robust, fast, interactive software-development environment that is extensible by the user.

The core consumes very little power, the amount depending on the operating frequency, the size and speed of the memory, and input/output requirements. For example, with a memory size of 256 Kb and a frequency of 10 MHz, it uses less than 100 mA at 5 V. In situations in which it is essential to minimize the consumption of power, external signals can be used to turn the core and the rest of the computing system off and on in duty cycles. Battery backup for memory is also available.

The central processing unit executes all native instructions in one or two cycles. Because most native instructions correspond to high-level Forth words, developing in Forth is equivalent to assembly-language programming. However, many "phrases" of words can be optimized by making them executable in single instructions (opcodes). This kind of optimization is called "code compression." The compression ratio (the number of Forth words that can be executed in one opcode in one clock cycle) typically lies between 1.5 and 3, but it can be as much as 5 in highly optimized segments of code. This much compression enables the central processing unit to have an operation throughput (measured in the number of instructions per unit time) greater than its clock speed. Running at 10 MHz, it can have an average throughput of 15 to 30 million instructions per second (MIPS), with bursts up to 50 MIPS. Previous flight computers have not been able to provide this much throughput in a comparable small size, low power, and low cost package.

This work was done by Douglas Ross of **Goddard Space Flight Center.**
GSC-13364/TN

FOR ADDITIONAL INFORMATION: *Contact: Director, Technology Transfer Division, P.O. Box 8757, BWI Airport, MD 21240; (301) 621-0100 Ext. 241*
REFER TO THE NUMBER LISTED AT THE END OF THIS ARTICLE .

Electrotechnology

0007 Bi-Orthogonal PCM Communications System Employing Multiplexed Noise Codes (Licensing Opportunity)

0008 Behavior the Costas Loop in Reception of Telemetry—Effects of signal parameters and Doppler shift are computed.

0009 Circuit Detects Faint Flashes Against Bright Background—The rapidly varying component of a luminous-flus signal is extracted from the total signal.

0010 Designing Accelerated Tests of Electromigration—Error analysis helps in the selection of currents, temperatures, and durations.

0011 Digital Accumulators in Phase- and Frequency- Tracking Loops —Digital accumulators can degrade performances at low carrier-to-noise ratios.

0012 Effects of Frame Rates in Video Displays—High rates are needed in rapidly changing images.

0013 Improved Gas-Gap Heat Switch—Residual conductance in the 'off' state is reduced.

0014 Making High-Pass Filters for Submillimeter Waves—A process makes a thick metal mesh.

0015 Pulse-Width-Modulating Driver for Brushless dc Motor—The power supply for the motor is electrically isolated from other power supplies.

Testing & Instrumentation

0016 Silicon Moisture Sensor Detects Humidity in Electronics

Other Items of Interest

0018 Vaporization Would Cool Primary Battery—Less material would be needed in cooling by vaporization than in cooling by melting.

Bi-Orthogonal PCM Communications System Employing Multiplexed Noise Codes

A technique that provides a practical means for implementing a true bi-orthogonal (or orthogonal) PCM system that employs perfect noise codes whose crosscorrelation function is zero. There is no existing noise coded bi-orthogonal (or orthogonal) PCM system whose crosscorrelation value between the noise codes used in the system is equal to zero (i.e. operates with a completely orthogonal noise code set) and whose noise codes are available in abundance. These two major attributes exist for the patented concept and provide a system that yields optimum transmission efficiency for a digital communications system while simultaneously providing a substantial anti jam (A/J) and low probability of intercept (LPI) protection. In addition, it would achieve this at a lower cost since chip by chip encryption would not be required due to the inordinately large quantity of available codes (in the code class used) for moderate practical time bandwidth products.

STATE OF DEVELOPMENT

The technique has been laboratory proven and is being considered for possible use by the United States Army.

APPLICATIONS

The concept can be used for any communications link whose requirements are for a transmission link that maximizes the transmission efficiency while being exceptionally resistant to interference and interception. An example would be for a reliable information distribution system that yields optimum transmission efficiency for a digital communications system.

PATENT STATUS

U.S. Patent Number 4,293,953

FOR ADDITIONAL INFORMATION: Charles Grzenda, Chief, Office of Research and Technology Applications, Center for C3 Systems, ATTN: AMSEL-RD-C3-SD, Fort Monmouth, NJ 07703, Telephone (908)544-3119.
Application Assessment Number 024.

NASA Tech Brief
National Aeronautics and
Space Administration

Behavior of Costas Loop in Reception of Telemetry

Effects of signal parameters and Doppler shift are computed.

A report presents a theoretical study of the behavior of a Costas loop in the reception of a radio carrier signal that is modulated in phase by a sinusoidal or square-wave subcarrier that is, itself, further modulated in phase by a nonreturn-to-zero binary data signal. The phase and frequency of the received signal may also be affected by a Doppler shift, and the instantaneous amplitude of the received signal is corrupted by additive white Gaussian noise. Signals of this type are ordinarily used in spacecraft telemetry, the sine-wave subcarrier being preferred for shorter signal paths and the square-wave subcarrier for longer signal paths.

The carrier component of the received signal is not completely suppressed, and the Costas loop reconstructs its carrier reference from this component. The residual-carrier modulation, Doppler shift, and noise degrade the ability of the Costas loop to lock onto the carrier signal. The study focuses on this degradation. As such, it extends a previous study of the performance of a Costas loop with a residual carrier but without phase-shift-keyed subcarrier modulation. In the previous study, it was assumed that the phase error of the Costas loop approaches zero at high signal-to-noise ratios. In this study, the phase error is assumed to remain small enough to keep the response of the loop within its approximately linear range, but it is not required to approach zero at high signal-to-noise ratios. This study also considers the maximum allowable telemetry rate for a specified tracking phase jitter and for a given combination of signal-to-noise ratio and bandwidth constraint.

It is shown both algebraically and by numerical examples that the Costas loop can be used to track the signals in the presence of the Doppler shift. The tracking performance is degraded in the sense that the mean-square phase jitter increases when a residual carrier is present. The tracking performance of a Costas loop is degraded further when the modulation index rises toward a critical value. At any signal-to-noise ratio, the loop ceases to lock onto the carrier when the critical value is reached. (The critical values for the square-wave- and sine-wave-subcarrier versions are different.) The performance can be optimized (in the sense that the mean-square tracking phase jitter can be minimized) by choosing the appropriate combination of (1) frequency of the subcarrier, (2) square or sinusoidal waveform of the subcarrier, (3) bit rate, and (4) noise bandwidth of the low-pass filters in the arms of the Costas loop.

This work was done by Tien M. Nguyen of Caltech for **NASA's Jet Propulsion Laboratory.** *"The Behavior of a Costas Loop in the Presence of Space Telemetry Signals."* *NPO-18084/TN*

FOR ADDITIONAL INFORMATION: *Contact: Director, Technology Transfer Division, P.O. Box 8757, BWI Airport, MD 21240; (301) 621-0100 Ext. 241*
REFER TO THE NUMBER LISTED AT THE END OF THIS ARTICLE

NASA Tech Brief
National Aeronautics and Space Administration
Marshall Space Flight Center, Alabama

Circuit Detects Faint Flashes Against Bright Background

The rapidly varying component of a luminous-flux signal is extracted from the total signal.

An electronic circuit detects flashes of light against a bright background in a camera or telescope image. The circuit was designed to detect lightning from a spacecraft in orbit far above the clouds. Usually, the sunlight reflected from the clouds makes lightning invisible to an observer in orbit. The circuit could also be used on Earth to detect lightning from a distance during the day or night, or to detect other flashes of light in safety-related, scientific, industrial, and military applications.

The circuit (see figure) includes the photocell that measures the luminous flux in the scene under observation. The output of the photocell includes a rapidly varying component that represents the lightning or other flash, plus a slowly-varying component that represents the slowly changing reflection of sunlight from the moving clouds or other bright background. The output of the photocell is fed to a first amplifier, which produces an inverted signal. The output of the first amplifier is fed back to its input via a low-pass filter and a noninverting amplifier.

Together, the low-pass filter and noninverting amplifier act as a low-frequency-nulling amplifier in that the feedback signal suppresses the low-frequency background signal at the input terminal of the first amplifier. Thus, the net output of the first amplifier consists mostly of the rapidly-varying flash signal. This output is sent to a second amplifier, where its amplitude is raised to about 150 times that of the input rapid-

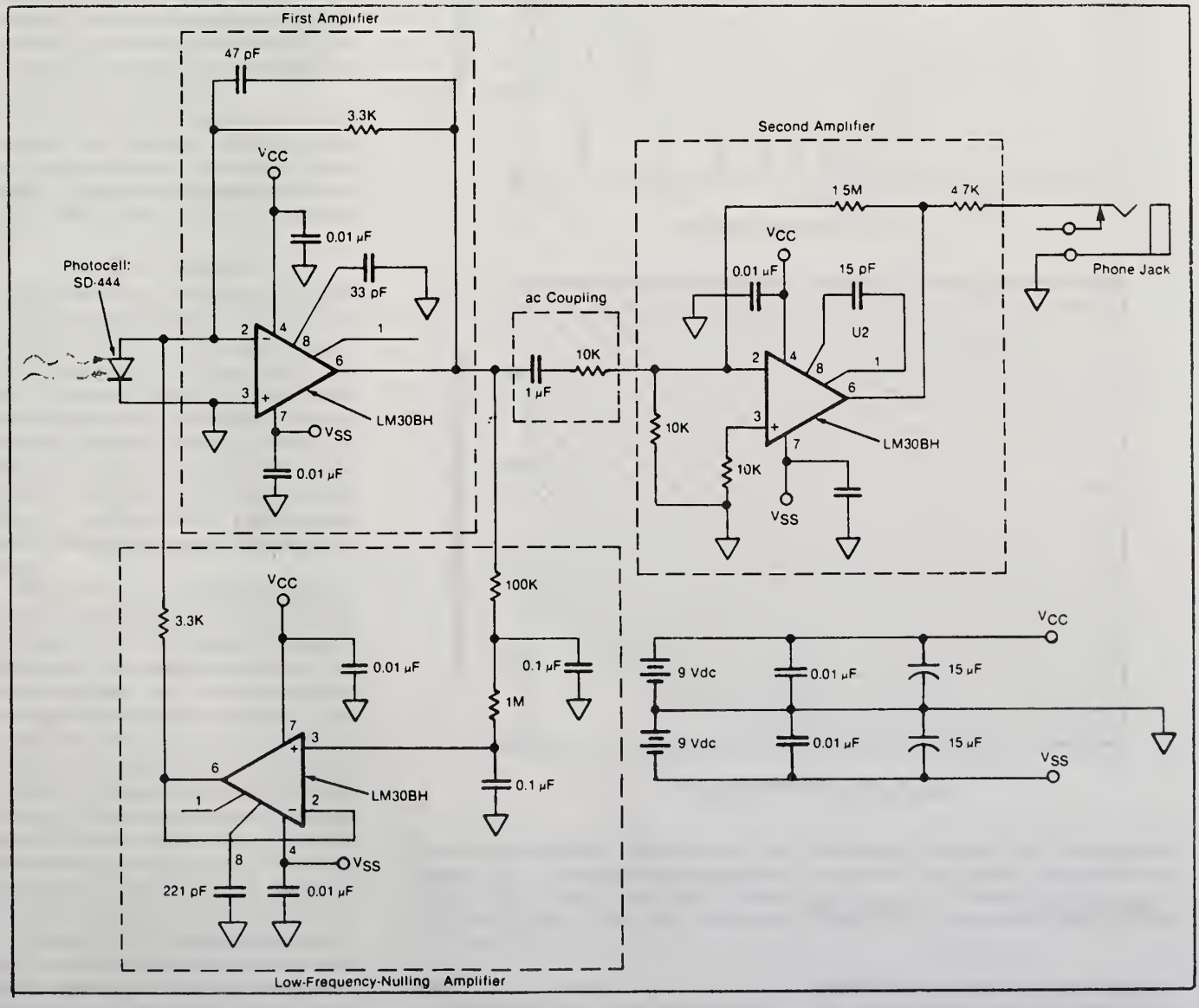

The Lightning Detector is a photocell-and-amplifier circuit that detects flashes of light against a steady or slowly varying bright background. The low-frequency-nulling amplifier is part of a feedback loop that suppresses the low-frequency background signal.

ly varying signals.

The output of the second amplifier is sent to a pair of earphones for aural monitoring and/or recorded on one track of a magnetic tape for future analysis. A timebase signal is recorded on the other track of the tape so that the time of each lightning pulse or other flash can be determined. A microphone can also be used to record verbal annotation on the tape.

A typical lightning pulse may appear as a single flash but usually consists of several strokes in rapid succession. The circuit can detect individual strokes, which have optical rise times of about 0.1 to 0.5 ms.

This work was done by O. Vaughan, M.L. Curtner, and D. Yeates of **Marshall Space Flight Center.**
MFS-28466/TN

FOR ADDITIONAL INFORMATION: *Contact: Director, Technology Transfer Division, P.O. Box 8757, BWI Airport, MD 21240; (301) 621-0100 Ext. 241*
REFER TO THE NUMBER LISTED AT THE END OF THIS ARTICLE

NASA Tech Brief
National Aeronautics and Space Administration
NASA's Jet Propulsion Laboratory, Pasadena, California

Designing Accelerated Tests of Electromigration

Error analysis helps in the selection of currents, temperatures, and durations.

A method for the design of accelerated tests of electromigration (as in microscopic conductors in integrated circuits) is based partly on a simplified mathematical model of electromigration and partly on error analysis. As in other accelerated-aging methods, the objective is to determine quickly what the operating life of tested components would be under normal operating conditions by extrapolation from lifetime measurements at operating stresses greater than normal. The design of an accelerated test involves a compromise between (1) reducing the testing time by increasing the stresses and (2) reducing the uncertainty in the extrapolated lifetime by decreasing the stresses.

In the case of electromigration, the stresses are the applied electrical current and the temperature. The median time to failure, t, is used as the measure of operating life and is assumed to be approximated by

$$t = AI^{-n} \exp(E_a/kT)$$

where A and n are constants, I is current, E_a is an activation energy, k is Boltzmann's constant, and T is the absolute temperature. This equation is first linearized by taking the natural logarithm of both sides, then applied to tests at different currents and temperatures. A minimum of three different combinations of current and temperature are necessary for the determination of n, E_a, and the value of t extrapolated to normal operating current and temperature.

The selection of currents and temperatures for these tests is guided by linear-regression and propagation-of-errors analyses of the linearized equation. The figure illustrates such a selection based on the results of such an analysis. In the upper part of the figure, each curve is a contour of constant normalized error $\delta \ln t$ (at normal operating current and temperature)/$\delta \ln t$ (at the test current and temperature). The upper right corner of this plot represents the point of maximum stress (maximum current I_{max} and maximum temperature T_{max}), which is determined by the capabilities of the testing equipment and the boundary of the electromigration-failure regime. The contours were generated by use of the stress points labeled 1 through 4, with all contours referred to point 3.

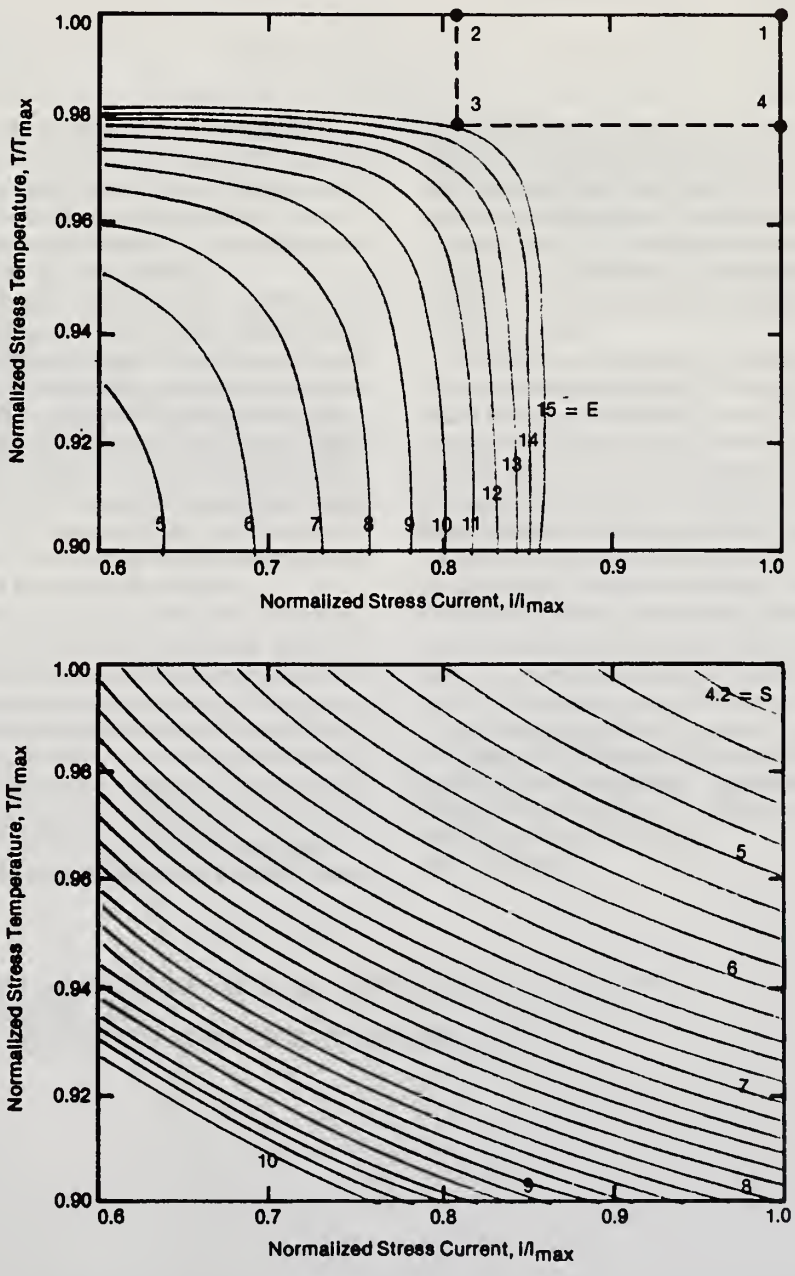

Error and Testing-Time Contours are used to select test currents and temperatures different from those represented by points 1 through 4. The contours of constant normalized error (E) were computed by using $I_{max}/I_{operating} = 10$ and $T_{max}/T_{operating} = 1.25$. The contours of constant normalized testing time (S) were calculated by using $n = 1.5$ and $E_a/kT_{max} = 10$.

In the lower part of the figure, each curve is a contour of constant normalized testing time, S, which is t (at the test current and voltage)/t (at I_{max} and T_{max}). These contours are computed for the

stress points shown in the upper part of the figure. Once a total test time is chosen, other stress points are determined from the intersections of the constant-time and constant-error contours. These intersections can be seen by superimposing the upper and lower parts of the figure.

This work was done by Martin G. Buehler of Caltech for **NASA's Jet Propulsion Laboratory.**
NPO-18012/TN

FOR ADDITIONAL INFORMATION: *Contact: Director, Technology Transfer Division, P.O. Box 8757, BWI Airport, MD 21240; (301) 621-0100 Ext. 241*
REFER TO THE NUMBER LISTED AT THE END OF THIS ARTICLE

NASA Tech Brief
National Aeronautics and
Space Administration

Digital Accumulators in Phase- and Frequency-Tracking Loops

Digital accumulators can degrade performances at low carrier-to-noise ratios.

A report describes an investigation of the deleterious effects of digital accumulators upon the performances of phase- and frequency-tracking electronic circuits. Digital accumulators are used extensively in these and other signal-processing circuits to compute averages and reduce processing rates. The report emphasizes problems encountered with respect to digital accumulators in the operation of receivers in the Global Positioning System (GPS). These receivers are required to track the phases and frequencies of the GPS carrier signals, which can be weak and are Doppler shifted by the high dynamics (high speeds, high accelerations, and sometimes high jerks) of the receiver with respect to the GPS spacecraft. Notwithstanding the emphasis on the GPS, the conclusions reached in this investigation are also applicable to more general receivers or other signal-processing systems that include digital accumulators.

The investigation focused on three different tracking loops: a digital phase-locked loop, a cross-product automatic frequency-control loop, and an extended Kalman filter. Algorithms that represent these loops were tested in a computer simulation. In addition, a hybrid analog/digital receiver was built to implement the algorithms, and the performances of the loops were measured to verify the simulations.

The report contains four sections. The first discusses the general problem and the questions that this investigation was intended to answer, reviews previous research on Doppler tracking in the presence of high dynamics, describes digital implementation of tracking loops, and introduces mathematical models that represent GPS signals under worst-case dynamics. The second chapter describes the hybrid analog digital receiver.

The third chapter describes the algorithms of the three loops. The results of the simulations and tests are presented in this chapter as various plots of frequency errors, amplitude losses, and probabilities of loss of lock vs. carrier-to-noise ratios, and as transient responses in terms of frequency errors and amplitude losses vs. time. The third chapter continues by comparing the performances of the three loops and ends by stating two conclusions: (1) simulations carried out without including the effects of digital accumulators can lead to erroneous predictions of performance, especially at low carrier-to-noise ratios, and (2) of the loops tested, the fourth-order version of the Extended Kalman filter performed the best.

The fourth chapter, which is very brief, summarizes the investigation, restating the first of the above-mentioned conclusions. It notes that at high carrier-to-noise ratios, the effects of digital accumulators are negligible, but that at low carrier-to-noise ratios, digital accumulators contribute substantial losses. It recommends that additional losses in threshold carrier-to-noise ratios should always be included in simulations to account for the digital accumulators. This could be done by including additional amplitude-suppression terms.

This work was done by Sami Hinedi and Joseph I. Statman of Caltech for **NASA's Jet Propulsion Laboratory.** *"Digital Accumulators in Phase and Frequency Tracking Loops."*
NPO-17909/TN

FOR ADDITIONAL INFORMATION: *Contact: Director, Technology Transfer Division, P.O. Box 8757, BWI Airport, MD 21240; (301) 621-0100 Ext. 241*
REFER TO THE NUMBER LISTED AT THE END OF THIS ARTICLE

NASA Tech Brief
National Aeronautics and
Space Administration

Effects of Frame Rates in Video Displays

High rates are needed in rapidly changing images.

A report describes an experiment on the subjective effects of the rates at which a display on a cathode-ray tube in a flight simulator is updated and refreshed. The experiment was conducted to learn more about the jumping, blurring, flickering, and multiple lines that an observer perceives when a line moves at high speed across the screen of a calligraphic CRT.

A horizontal line on an oscilloscope display was moved vertically at various speeds and viewed by several observers. The 1-mm-thick line approximates the lines used on 19- to 21-in. (48-to 53-cm) cathode-ray tubes in flight-simulation visual displays. The line was refreshed at a rate of either once or twice per update. A line that is refreshed once per update is drawn on the screen once. Its position is then recomputed (updated), and it is redrawn. A line that is refreshed twice per update is drawn on the screen twice in one position, its position is recomputed, and it is then redrawn twice in the next position. Lines are frequently refreshed more often than they are updated to avoid flickering.

The report presents data from the observations on plots of rates of refreshing and updating as functions of speed. The speed above which the picture appears to deteriorate can be found from such a plot. This speed can be related by calculations to simulated angular and linear velocities of the aircraft in the flight simulator.

For example, a visual display updated at 30 hertz and refreshed at 60 hertz appears to deteriorate at angular and linear velocities considerably less than those of modern high-performance aircraft. However, the speed at which deterioration appears to set in can be increased significantly by increasing the update rate. Refreshing at twice the update rate produces only minor improvement. To display rapidly changing flight scenery without apparent deterioration of the image, it may be necessary to use an updating rate of at least several hundred hertz.

This work was done by Gary V. Kellogg and Charles A. Wagner of **Ames Research Center**. *Further information may be found in NASA TM-100415 [N88-22033], "Effects of Update and Refresh Rates on Flight Simulation Visual Displays."*

Copies may be purchased [prepayment required] from the National Technical Information Service, Springfield, Virginia 22161, Telephone No. (703) 487-4650. Rush orders may be placed for an extra fee by calling (800) 336-4700.
ARC-12358/TN

FOR ADDITIONAL INFORMATION: *Contact: Director, Technology Transfer Division, P.O. Box 8757, BWI Airport, MD 21240; (301) 621-0100 Ext. 241*
REFER TO THE NUMBER LISTED AT THE END OF THIS ARTICLE

NASA Tech Brief
National Aeronautics and Space Administration
NASA's Jet Propulsion Laboratory, Pasadena, California

Improved Gas-Gap Heat Switch

Residual conductance in the "off" state is reduced.

Four modifications in the design of a gas-gap heat switch decrease its residual thermal conductance in the "off" state, thereby making it act more nearly like a true on/off switch. Gas-gap heat switches are used in cryogenic systems; for example, to connect and disconnect redundant coolers with a single load. Gas-gap heat switches have no moving parts and, therefore, offer reliability and long operating life.

In a gas-gap heat switch of the type described here (see figure), the gap is the space between interdigitating fins and slots machined into lengthwise-mating copper cylinders. The copper cylinders are sealed in a supporting stainless-steel tube, and the gap is made much less thermally conductive (the switch is turned "off") by evacuating it. The gap is made more thermally conductive (the switch is turned "on") by filling the evacuated gap with neon, nitrogen, hydrogen, helium, or other suitable gas from a gas-adsorption pump. The gas-adsorption pump could be, for example, a bed of charcoal that is heated to fill, and cooled to evacuate, the gap.

In many actual and potential applications, the "hot" side of the heat switch can be considerably hotter (e.g., at 300 K) than the cold side is (e.g., at 80 K). At such large differences in temperature, the residual conductance in the "off" state caused by parasitic radiation across the gap and conductance in the supporting cylinder can result in unacceptably high transfer of heat across the nominally "off" switch. In addition, differences among the thermal expansions of the hot and cold copper cylinders and the stainless-steel supporting cylinder can result in contact between the tips of fins and the bottoms of slots, with a consequent large increase in thermal conduction.

The four modifications reduce these undesired contributions to the "off"-state conduction. They are as follows:

1. Whereas previously the fins were made by electrical-discharge machining, in the improved version they were made by a carbide circular saw, then lapped by hand to the precise 0.002 in. (0.05 mm) gap dimension, then polished by hand, then electroplated with low-emissivity gold to reduce the radiative transfer of heat from the hot side to the cold side.
2. To reduce parasitic conductance along the supporting stainless-steel tube, the thickness of the wall of this tube was reduced from 0.004 in. (0.1 mm) to 0.002 in. (0.05 mm). Three circumferential stiffening ribs were added to prevent collapse under high differential pressures.

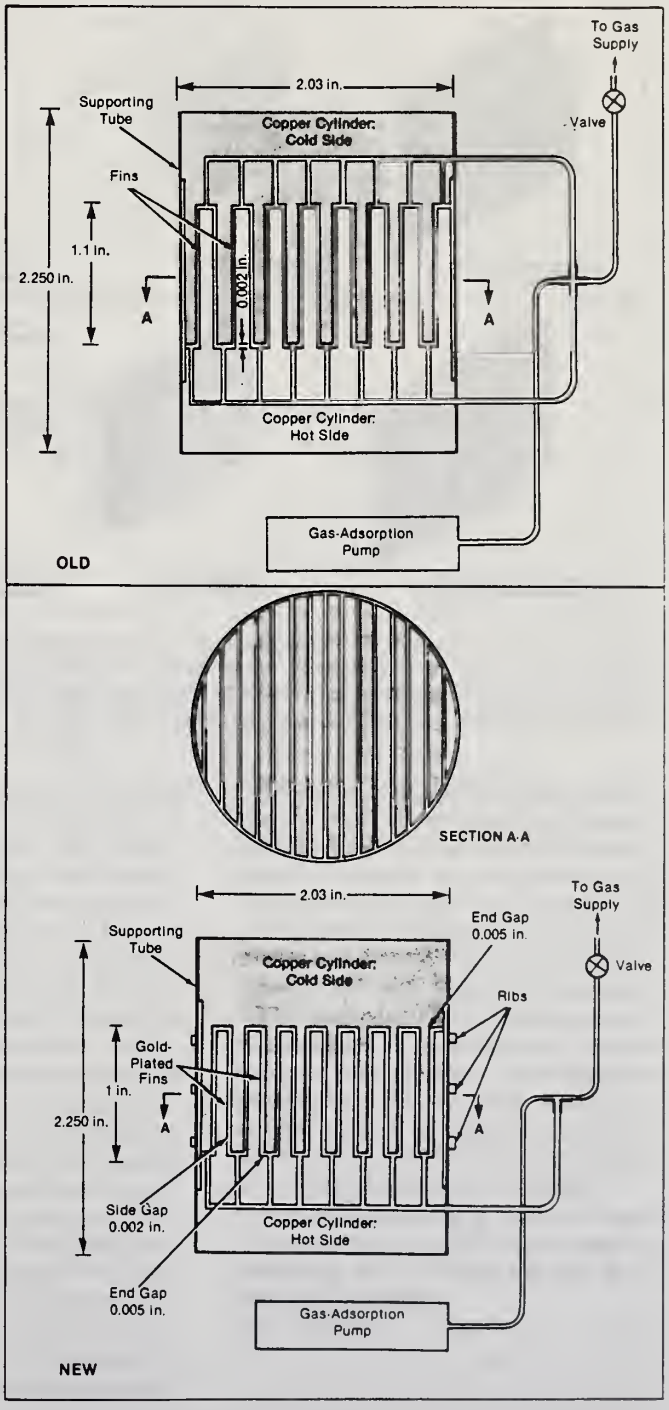

The **Old and New Versions** of the gas-gap heat switch differ in the surface finish of the fins, the thickness of the stainless steel supporting cylinder, the size of the gaps at the ends of the fins, and the plumbing for the gas.

3. To prevent contact caused by differential thermal expansion, the clearance between the tips of the fins and the bottoms of the slots was increased from the previous value of 0.002 in. (0.05 mm) to 0.005 in. (0.13 mm).
4. Whereas the gas flowed in and out through passages in both the hot and cold sides in the previous version, the modified version includes passages on the hot side only. This feature both minimizes the parasitic transfer of heat through the gas and simplifies construction.

This work was done by Chung K. Chan of Caltech for **NASA's Jet Propulsion Laboratory.** *NPO-18136/TN*

FOR ADDITIONAL INFORMATION: *Contact: Director, Technology Transfer Division, P.O. Box 8757, BWI Airport, MD 21240; (301) 621-0100 Ext. 241*

REFER TO THE NUMBER LISTED AT THE END OF THIS ARTICLE

NASA Tech Brief
National Aeronautics and Space Administration
NASA's Jet Propulsion Laboratory, Pasadena, California

Making High-Pass Filters for Submillimeter Waves

A process makes a thick metal mesh.

A micromachining-and-electroforming process makes rigid metal meshes with cells that range in size from 0.002 in. (0.05 mm) to 0.05 in. (1.27 mm) square. The meshes are electrically thick; that is, thicknesses are comparable to the sizes of the cells. These meshes are used as high-pass filters (dichroic plates) for submillimeter electromagnetic waves.

The figure illustrates some of the steps in the process. First, a standard undoped silicon wafer is cut to a shape (usually square) and to a size large enough to provide a 0.05-in. (1.27-mm) border around the mesh. To provide for an integral frame that will support the mesh during the process, the wafer is made at least 0.010 in. (0.25 mm) thicker than the final mesh is expected to be.

A high-speed dicing saw cuts parallel channels in the wafer. The wafer is rotated 90° on the saw table, and the saw cuts another set of channels parallel to each other and perpendicular to the first set of channels, forming a waffle pattern. The distance between adjacent channels defines the size of a cell, and the width of a channel defines the thickness of the wall between adjacent cells. The channels are cut to a depth slightly greater than the intended thickness of the grid. The saw blade is exchanged for a much thicker grinding wheel, and a swath 0.05 in. (1.27 mm) wide is ground off around the edge of the wafer to provide for the frame. At this stage, the wafer forms the inverse of the final mesh.

The wafer is cleaned and placed in a vacuum evaporation channel with the channel side facing a vapor-deposition source and with a collimating baffle between the wafer and the source boat. A layer of titanium 50 to 100 Å thick is deposited on the wafer and is followed by a layer of gold 2,500 to 5,000 Å thick. (The thin titanium layer helps the gold adhere to the silicon.) The baffle, with its 10:1 ratio of length to width, causes most of the metal to be deposited only on the edge swath, the bottoms of the channels, and the tops of the squares; little or no metal condenses on the sidewalls of the channels.

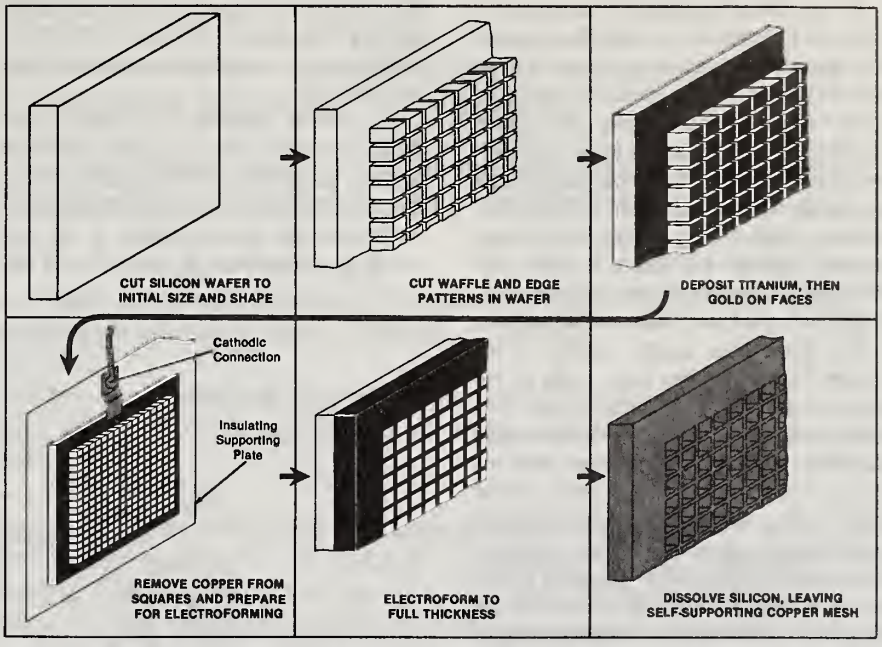
CUT SILICON WAFER TO INITIAL SIZE AND SHAPE
CUT WAFFLE AND EDGE PATTERNS IN WAFER
DEPOSIT TITANIUM, THEN GOLD ON FACES
Cathodic Connection
Insulating Supporting Plate
REMOVE COPPER FROM SQUARES AND PREPARE FOR ELECTROFORMING
ELECTROFORM TO FULL THICKNESS
DISSOLVE SILICON, LEAVING SELF-SUPPORTING COPPER MESH

A **Series of Steps** involving cutting, grinding, vapor deposition, and electroforming creates a self-supporting, electrically thick mesh. The width of the holes is typically 1.2 times the cutoff wavelength of the dominant waveguide mode in a hole. To obtain a sharp frequency-cutoff characteristic, the thickness of the mesh should be made greater than one-half of the guide wavelength of the mode in the hole.

The evaporated metal layers on the tops of the squares are cut or ground off, and the wafer is cleaned again. The wafer is attached to an electrically insulating supporting plate, and a cathodic contact is clipped to the copper layer on the perimeter of the wafer. The wafer is immersed in a copper electroforming bath at an initial current density of 30 mA/cm^2 followed by a longer exposure at 20 mA/cm^2 until the channels and the edges become filled with copper. Because little or no copper had been vapor-deposited on the sidewalls of the channels, the electroformed copper builds up from the bottom; there is little or no lateral growth of copper that could cause voids by blocking a channel before the bottom is completely filled. This makes it possible to use narrow channels and, consequently, to make thin walls; the thickness of a wall can be as little as one-fifth the thickness of the mesh (the height of the wall).

When the channels are filled with copper, the wafer is removed from the electroforming bath and rubbed on fine emery paper to remove any copper that has grown on the squares and to flatten out any asperities on the frame. The silicon is etched away in hot potassium hydroxide, leaving the copper mesh and its frame.

The new process is not limited to square silicon wafers. Round wafers can also be used, with slightly more complication in grinding the periphery. The grid can be in any pattern that can be produced in an electroforming mandrel. Any platable metal or alloy can be used for the mesh.

This work was done by Peter H. Siegel of Caltech and John A. Lichtenberger of Metalplate Co. for **NASA's Jet Propulsion Laboratory.**
NPO-17992/TN

FOR ADDITIONAL INFORMATION: *Contact: Director, Technology Transfer Division, P.O. Box 8757, BWI Airport, MD 21240; (301) 621-0100 Ext. 241*
REFER TO THE NUMBER LISTED AT THE END OF THIS ARTICLE .

NASA Tech Brief
National Aeronautics and Space Administration
NASA's Jet Propulsion Laboratory, Pasadena, California

Pulse-Width-Modulating Driver for Brushless dc Motor

The power supply for the motor is electrically isolated from other power supplies.

A high-current pulse-width-modulating driver for a brushless dc motor features optical coupling of the timing signals from its low-current control circuitry to its high-current motor-driving circuitry. This optical coupling makes it possible to provide high electrical isolation of the motor-power supply, thereby helping to prevent the fast, high-current motor-driving pulses from being coupled through the power supplies into the control circuitry, where they could interfere with the low-current control signals.

The driver (see figure) controls motor current by varying the duty cycle of the motor-drive voltage. Null or zero motor current results when the motor-drive-voltage waveform exhibits a 50 percent duty cycle. The direction and magnitude of net motor torque is determined by the duty-cycle variation about the 50 percent point. The motor is connected to its power supply via an H-bridge circuit of n-channel, enhancement-mode power, metal oxide/semiconductor field-effect transistors (MOSFET's) and p-channel power MOSFET's. By use of these two types of MOSFET's, each type connected in the polarity opposite that of the other type, it is possible to simplify the power-MOSFET-gate-driving part of the circuit in that it becomes unnecessary to supply a gate-driving voltage in excess of the supply voltage (as would be necessary if the H-bridge circuit contained all n-channel power MOSFET's).

The input control voltage is received differentially by amplifier U_2, which is capable of operating over the full ±10-V range of the input signal. The pulse-width-modulator circuit U_1 compares the input voltage (scaled through U_2) to a voltage proportional to the motor current (scaled through instrumentation amplifier U_5, as described more fully below). U_1 varies the duty cycle in such a way as to reduce the comparison (difference) voltage to zero.

The output of U_1 is optically isolated from the output transistor stages by optoisolator U_3, which couples signals through an optical link only. The output of U_3 is inverted by inverting buffer U_4, which generates the gate-driving voltages for the power MOSFET's of the H-bridge (Q_1 through Q_4, Q_6, and Q_7). Transistor Q_5 delays the turn-on of these MOSFET's until the gate-voltage waveforms have stabilized.

U_5, which operates in a balanced differential configuration, provides feedback voltage proportional to the motor-driving current. The use of two 8.25-MΩ resistors to couple the current signal to U_5 provides a net isolation of more than 4 MΩ for the motor-driving circuitry. In keeping with the concept of isolation of the high-current stages of the driver, separate voltage regulators are provided for the circuits associated with the output H-bridge.

This work was done by Phil M. Salomon of Caltech for **NASA's Jet Propulsion Laboratory.**
NPO-17142/TN

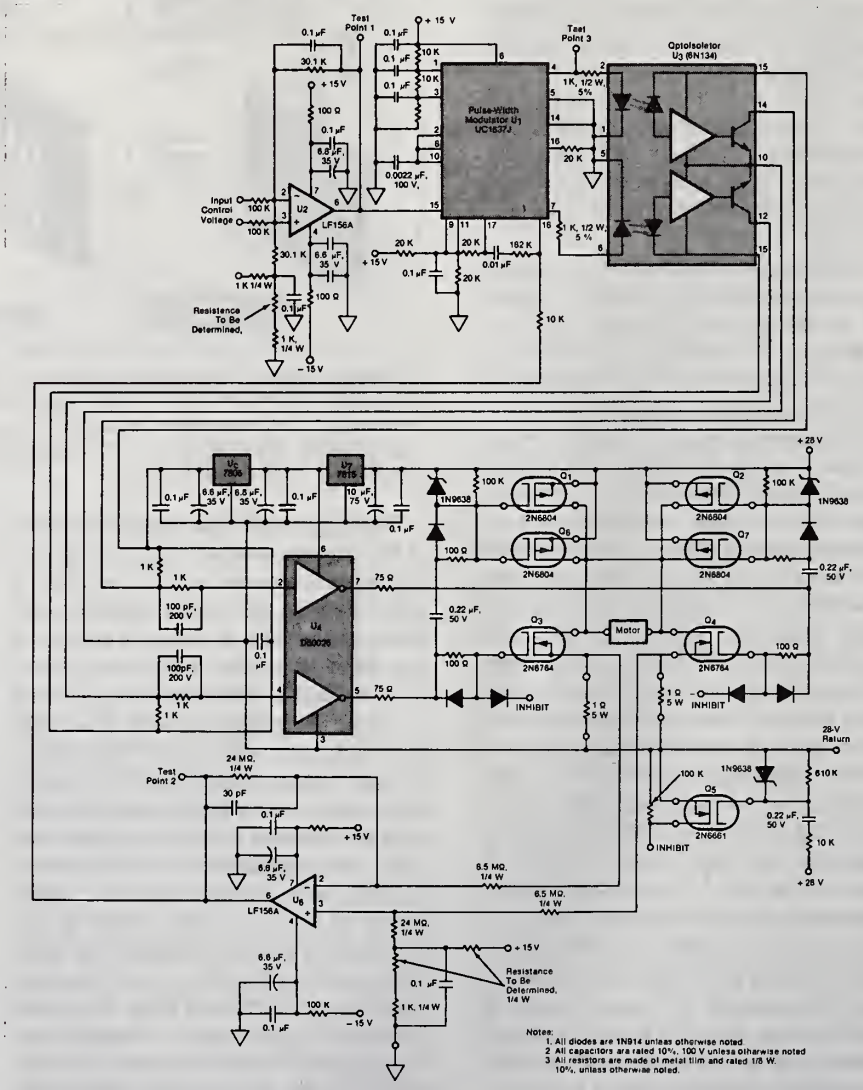
Test Point 1
+ 15 V
Test Point 3
Optoisolator U3 (6N134)
Pulse-Width Modulator U1 UC1637J
Input Control Voltage
LF156A
Resistance To Be Determined,
+28 V
Motor
INHIBIT
28-V Return
Test Point 2
Notes:
1. All diodes are 1N914 unless otherwise noted.
2. All capacitors are rated 10%, 100 V unless otherwise noted
3. All resistors are made of metal film and rated 1/8 W. 10%, unless otherwise noted.

The **Pulse-Width-Modulating Driver** features optical coupling of the timing signals (for electrical isolation of the motor and its power supply) and a complementary power-MOSFET H-bridge output circuit (to simplify the H-bridge-gate-driving circuitry).

FOR ADDITIONAL INFORMATION: *Contact: Director, Technology Transfer Division, P.O. Box 8757, BWI Airport, MD 21240; (301) 621-0100 Ext. 241*
REFER TO THE NUMBER LISTED AT THE END OF THIS ARTICLE

Technology Application

Sandia National Laboratory

Silicon Moisture Sensor Detects Humidity in Electronics

Extremely sensitive moisture sensors for making accurate humidity measurements inside packages of electronics have been fabricated at Sandia National Laboratories.

The sensors are made of silicon - the same basic material used in the manufacture of integrated circuits. They have many other advantages as well over other sensors now used for the evaluation of electronic packaging.

Accurate humidity measurements inside electronic packages containing integrated circuits (ICs) are critical in assessing the long-term performance and reliability of the IC.

"We have found that these sensors are very sensitive to small changes in humidity," report Sandia researchers Michael J. Kelly, Terry R. Guilinger, David W. Peterson, Melanie R. Tuck, and James N. Sweet.

"For example, the response of a typical sensor increased 800 percent when the relative humidity it was exposed to changed from 1 percent to 40 percent. In addition to this excellent sensitivity, the sensors quickly respond to rapid humidity changes, not only in cases where the change is from low relative humidity to high relative humidity but in the opposite direction as well."

The capacitor-type sensors use a material known as oxidized porous silicon (OPS) as the moisture-adsorbing dielectric between the two electrodes of the capacitor.

The Sandia researchers report that in addition to their high sensitivity, the sensors offer other advantages. One is consistent performance at temperatures above 100 degrees Celsius. Another is that they can be made by manufacturing methods that are completely compatible with standard techniques used to fabricate ICs.

Uses other than the application in microelectronic packaging are being considered. The Sandia group is evaluating the sensor's suitability for industrial drying applications. Industrial drying consumes about 5 percent of the total energy used in the industrial sector each year, and it is estimated that as much as 10 percent of this energy is wasted due to inadequate control of the humidity within the drying chambers of process equipment. They point out that improvements in humidity sensing would result in energy savings and increased productivity.

The Sandia researchers say the "complete compatibility" of equipment and procedures used to form the sensors with those used in standard IC wafer fabrication opens the door to the manufacture of so-called smart sensors, in which sensor and microelectronic logic elements are combined on the IC chip.

"With sensing and signal-processing aspects fully integrated, additional applications are envisioned," they say. "An example would be inclusion of a smart humidity sensor within the advanced heating, ventilation, and air conditioning (HVAC) systems being used for environmental control in building interiors."

The oxidized porous silicon (OPS) used as the moisture adsorbing dielectric is formed in a two-step process. First, the researchers make porous a very thin layer on the top of the silicon wafer by a simple electrolysis process. This process involves making the silicon wafer the anode in an electrochemical cell containing hydrofluoric acid.

Then this porous material is converted into OPS - simply porous silicon dioxide - by a high-temperature treatment in either oxygen or steam. Metal electrode layers are then deposited on the OPS and the back of the wafer to complete the capacitor structure.

When water vapor contacts the sensor, it permeates through the porous volume between the electrodes, resulting in a net change in the dielectric constant of the porous volume. This is in turn monitored by measuring the capacitance of the device. These measurements have proved to be very sensitive to small humidity changes. *Technical Contact: Michael J. Kelly (505)844-4031.*

FOR ADDITIONAL INFORMATION: Department of Energy, Sandia National Laboratories, Albuquerque, NM 87185-5800.

Energy

0017 Fuel Cells: Cutting Gasoline Consumption in Half

0018 Vaporization Would Cool Primary Battery—Less material would be needed in cooling by vaporization than in cooling by melting.

Department of Defense Fact Sheet

Strategic Defense Initiative Organization

Fuel Cells: Cutting Gasoline Consumption in Half

Researchers at Argonne National Laboratory have developed an electrical generator with no moving parts. This generator, known as a monolithic solid oxide fuel cell (MSOFC), can use gasoline, methane gas, and jet or diesel fuel with an efficiency of twice that of current automotive engines. Present automotive fuels consume 63% of all oil. MSOFCs could cut that amount in half. An MSOFC could also run on methanol, which is produced from coal.

Like a battery, the fuel cell converts chemical energy into electricity. The breakthrough in the Argonne fuel cell lies in their selection of the ceramic for the cell electrolyte and electrode plates, the novel manufacturing process to construct the cell, and the efficient layout of the fuel cell components.

The MSOFC also uses waste heat, created when oxygen and hydrogen react in the cell core, to preheat the oxidizer and vaporize the fuel. Further, the cell construction permits the hydrogen fuel to be regenerated within the cell, rather than in a separate fuel reformer.

The MSOFC could reach an energy conversion efficiency of 72%. The cell's extremely compact structure can yield estimated power densities of 4,000 kW/m^3 and 10kW/kg - an order of magnitude better than other fuel cells.

The MSOFC simplifies space-based power systems that must regenerate hydrogen fuel from the combustion product (water), because the MSOFC can use the same unit for producing power and for regenerating fuel. The MSOFC's high operating temperature permits waste heat to be rejected at a high temperature, which minimizes the size of the radiator. The MSOFC can operate in either an open or a closed cycle.

In earth-based applications, the MSOFC design could power cars, vans, and small trucks with twice the fuel efficiency of internal combustion engines at competitive engine costs. It could also power recreational vehicles, such as golfcarts and snowmobiles, as well as lawnmowers and motorcycles. It could even propel boats or aircraft. The MSOFC could produce stationary power, such as for power plants, back-up generators, and power at remote sites.

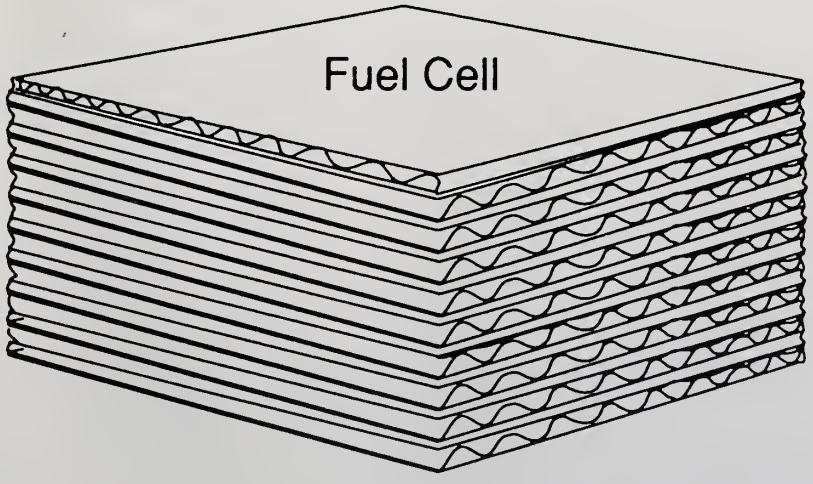

Ztek (Waltham, Mass.), is commercializing a zirconia solid oxide fuel cell. The zirconia cell is shaped flat, so it is much easier to make than tubular or monolithic fuel cells. Like the monolithic, the zirconia cell is light, compact, and efficient, suitable for supplying power in space.

The zirconia cell operates at 1000 degrees Celsius, allowing the radiator to be very compact. For low detectability, however, the system can employ a larger radiator, which rejects heat at a lower temperature. The fuel cell can supply power for utilities because of its high efficiency and low cost. It can serve as a heat source, converting waste gas into water and carbon dioxide.

The zirconia cell can also act as a regenerator, storing energy when not in use, and providing bursts of power when needed. The fuel cell is a very clean system with less pollution than burning coal, oil, or natural gas.

In the chemical industry, the basic zirconia process can be used for making sulfuric acid, or other chemicals. The process can supply residential power in remote areas, generating electricity, heat, and cooling.

FOR ADDITIONAL INFORMATION: Technology Applications Office, Strategic Defense Initiatives Organization, OSD/SDIO/TNI, The Pentagon, Washington, DC 20301-7100; (703)693-1563.

NASA Tech Brief
National Aeronautics and
Space Administration
NASA's Jet Propulsion Laboratory, Pasadena, California

Vaporization Would Cool Primary Battery

Less material would be needed in cooling by vaporization than in cooling by melting.

The temperature of a discharging high-power-density primary (i.e., nonrechargeable) battery would be maintained below a specified level by the evaporation of a suitable liquid from a jacket that surrounds the battery, according to a proposal. A pressure-relief valve would regulate the pressure and, thereby, the boiling temperature of the liquid. Because the latent heat of vaporization of a typical material is an order of magnitude larger than the latent heat of fusion of itself or another material, the mass and volume of liquid needed to produce a given amount of cooling would be much less than the mass and volume of material needed to produce the same amount of cooling by melting. This technique could be used to cool batteries in situations in which engineering constraints on volume, mass, and location prevent the attachment of cooling fins, heat pipes, or the like.

Water has been proposed as the evaporative-cooling liquid for an $Li/SOCl_2$ battery that is being developed. The maximum operating temperature for this battery should be maintained below 100 to 110 °C. Water boils at 100 °C at atmospheric pressure and has a heat of vaporization of 2.3×10^6 J/kg. The battery has a total mass of 25 to 30 kg and contains nine cells, each of which produces an average of about 20 to 30 W of heat during a complete discharge lasting 5 h.

A first-order thermal analysis predicts that if the battery has an initial temperature of 50 °C, a total mass of 0.5 kg of water would suffice to limit the maximum temperature of the battery to 110 °C; 1.5 kg of water would suffice to limit the temperature to 100 °C. About 10 times these masses of a solid-to-liquid or solid-to-solid phase-change material would be required to achieve the same cooling effects.

In the spacecraft application for which this technique was originally conceived, the steam produced in cooling the battery would be directed via tubing to a small reservoir located near tanks containing liquid hydrogen and liquid oxygen. This very cold reservoir would condense the steam. This would prevent the steam from escaping and contaminating the spacecraft. In a terrestrial or other application in which contamination by steam is not an issue, the steam could be vented to the environment.

This work was done by Pradeep Bhandari and Robert N. Miyake of Caltech for **NASA's Jet Propulsion Laboratory.**
NPO-17805/TN

FOR ADDITIONAL INFORMATION: *Contact: Director, Technology Transfer Division, P.O. Box 8757, BWI Airport, MD 21240; (301) 621-0100 Ext. 241*
REFER TO THE NUMBER LISTED AT THE END OF THIS ARTICLE

Engineering

0019 SUSV-Towed Snow Plow

0020 MRE Heaters Invented (Licensing Opportunity)

0021 Valve Regulates Sea Water Pressure

0022 Adaptive Control of Large Vibrating, Rotating Structures—The inherent passivity of structures is exploited to obtain convergence.

0023 Algorithm Computes Hypersonic Flow of Air—Nonequilibrium thermochemical effects are taken into account.

Software

0024 Controlling Laboratory Processes From a Personal Computer—An operator can control processes via natural-language commands.

0025 Damping Seals Would Help Support Turbopump Rotor—Tentative designs are presented.

0026 Growth of Instabilities in Two Types of Mixing Layers—Effects of feedback are examined.

0027 Incompressible, Viscous Flow About an Ogive/Cylinder—Calculated flow patterns agree closely with experimental ones. (Licensing Opportunity)

0028 Robot Grasps Rotating Object—Advanced techniques for sensing and control are combined.

Software

0029 Software for Multivariable Frequency-Domain Analysis—Outputs include frequency-response singular-value plots of multivariable transfer matrices.

Testing & Instrumentation

0030 Technique to Measure Liquid Level and Volume Device

0031 Adjustable Pitot Probe—The probe is readily positionable in the core of uniform flow in a hypersonic wind tunnel. (Licensing Opportunity)

0032 Collectors of Airborne and Spaceborne Particles—Simple units go directly into optical, electron, or x-ray analysis equipment.

0033 Digital Pitch-and-Roll Monitor—A compact inclinometer is precise and prints out readings on demand.

0034 Integral Plug-Type Heat-Flux Gauge—The integral construction reduces the components of error caused by discontinuities. (Licensing Opportunity)

0035 Mixed-Mode-Bending Delamination Apparatus—Double-cantilever-beam and end-notch-flexure loads are applied simultaneously. (Licensing Opportunity)

U.S. Army Corps of Engineers
Cold Regions Research & Engineering Laboratory
72 Lyme Road, Hanover, New Hampshire 03755-1290

SUSV-Towed Snow Plow

PROBLEM/HISTORY

The U.S. Army's light forces have limited snow removal capabilities. Therefore, many military support vehicles have limited usefulness in operations during which a snow cover is present. Since many roads and trails will not have been kept open prior to hostilities, truck-mounted snow plows (if available) would be ineffective. In most instances, heavy tracked vehicles are required to move deep snow.

Light forces have been equipped with a large number of tracked, over-snow vehicles known as SUSVs (Small Unit Support Vehicles). Over-snow vehicles can be equipped with front- or rear-mounted plow blades, but to do so, the SUSV would require extensive design changes.

SOLUTION

CRREL engineers determined that a snow plow towed by the SUSV could enhance winter operations with minimal changes to the SUSV itself. From a series of 1/12-scale tests it was determined that a special linkage could be attached to the SUSV's pintle hook mounting bracket and thereby could control the attack angle of the plow. A 1/2-scale plow and 4-bar parallel linkage towing assembly were designed. This 1/2-scale plow, towed by a SUSV, has been tested in snow depths up to 30 inches with good results. It is estimated that the SUSV will have enough tractive reserve to pull the full-scale plow.

STATUS

A video tape describing the design and performance of the 1/2-scale plow is available from CRREL. The full-scale plow is being designed, and testing is scheduled for February 1992 in Alaska.

An Operational Needs Statement for the towed snow plow is being prepared by the 6th Infantry Division (Light) for the U.S. Army Engineer School.

FOR ADDITIONAL INFORMATION: Contact: Mr. Paul Richmond, U.S. Army Cold Regions Research and Engineering Laboratory, 72 Lyme Road, Hanover, New Hampshire 03755-1290; (603)646-4461, FTS 561-4461.

MRE Heaters Invented

Figure 1. Inventors Stan Black (left) and Jim Jenkins (right) with flank Petty Officer, Bob Janas (center) are shown holding an MRE, MRE Heater, and the MRE box in which the other two are placed while heating.

Two senior engineers from the Naval Civil Engineering Laboratory (NCEL), Port Hueneme, California, invented a technology, which led to the development of a Meals Ready-to-Eat (MRE) Heater (Figure 1). This chemical reaction (flameless) heater provides a more efficient and safer means of preparing field rations (MREs) over the present method of igniting chemical tablets. Additionally, the heater is such a small and compact device that a serviceman or woman can carry an ample supply in a backpack without any appreciable increase in weight.

The invention allows the serviceman or woman to heat an MRE with only a slight delay in their duties. While marching, the serviceman or woman can open the plastic bag containing the MRE Heater; place the MRE in the bag next to the Heater; add water to the bag to start the chemical reaction; place the MRE package in his pocket or backpack while it heats; then, in approximately 15 minutes, the meal will be hot and ready-to-eat. Not only can this process take place while the serviceman or woman is marching, but more importantly, there is no flame to draw the attention of the enemy and subsequent enemy fire. This invention could save the lives of servicemen and women on the battlefield.

For Additional Information:

Backup material on this effort is available from:

Navy Domestic Technology Fact Sheet Reader Reply Service
Code E211
Naval Surface Weapons Center
Dahlgren, VA 22448-5000
(703) 663-8921

Refer to 160601/TN

Valve Regulates Sea Water Pressure

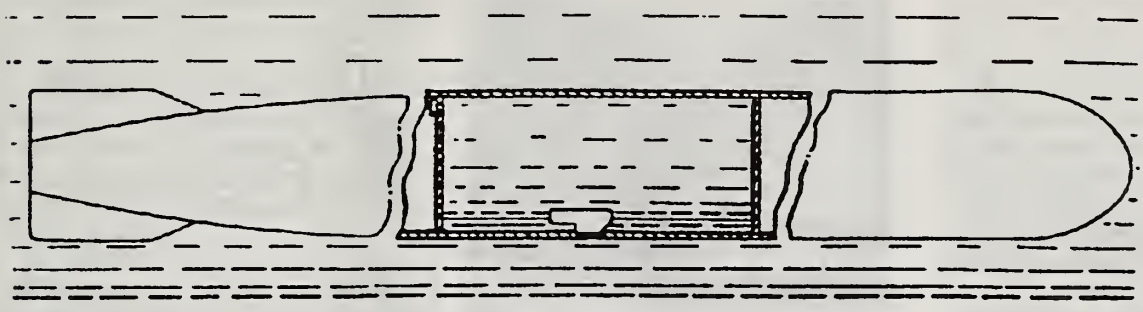

Figure 3. Valve to regulate sea water pressure

The Naval Ocean Systems Center (NOSC), San Diego, California, has developed a valve for pressurizing fluid within a tank submerged in sea water. The valve (Figure 3) regulates the pressure within the tank, independent of the pressure outside the tank—a downstream regulator valve. The valve takes advantage of sea water depth pressure by allowing sea water to displace fuel in the tank.

The valve will solve the problem of maintaining a constant tank pressure independent of upstream (feed) pressure variations by activating the piston to move against a determined spring force, closing the entrance area of the upstream (feed) flow.

For Additional Information:

Backup material on this effort is available from:

Navy Domestic Technology Fact Sheet Reader Reply Service
Code E211
Naval Surface Weapons Center
Dahlgren, VA 22448-5000
(703) 663-8921

Refer to 160903/TN

NASA Tech Brief
National Aeronautics and Space Administration
NASA's Jet Propulsion Laboratory, Pasadena, California

Adaptive Control of Large Vibrating, Rotating Structures

The inherent passivity of structures is exploited to obtain convergence.

A globally convergent theoretical method provides for the adaptive set-point control of the orientation of, along with suppression of the vibrations of, a large structure. Developed for controlling the attitudes of large, somewhat flexible spacecraft, the method may also be useful in such terrestrial applications as controlling movable bridges or suppressing earthquake vibrations in bridges, buildings, and other large structures.

The method utilizes the inherent passivity properties of the structure to attain a mathematical condition essential to adaptive convergence on the commanded set point. Under this condition, the system is said to be "robustly stabilized against spillover dynamics," meaning that it maintains stability and convergence in the presence of errors in the mathematical model of the dynamics of the structure and actuators.

The new method offers the advantage of avoiding the command-generator-tracker (CGT) condition typically associated with model-following solutions to the same control problem. The tracking condition that replaces the CGT condition is satisfied by the same conditions that assure the strictly positive real (SPR) property of the structure. More specifically, the control architecture in the new method is based on proportional-integral feedback from position and velocity sensors (see figure), and the CGT condition is replaced by the most stringent sufficient condition for global asymptotic stability, which requires the existence of an output feedback matrix, K, such that the closed-loop system is SPR.

An important feature of the new method is that stability conditions are satisfied if the ratio of position feedback to velocity feedback is chosen sufficiently small relative to a quantity that depends on the intrinsic structural damping, modal frequencies, number of actuators, and the controllability of the rigid-body modes relative to the flexible-body modes at the actuator/sensor locations. Such conditions are relatively mild and can always be satisfied by design, making use of coarse ground test data.

The characterization of the closed-loop stability properties is based on a new Lyapunov function. This function, in itself, extends application of many prior techniques based on positivity theory (both adaptive and nonadaptive) to the more-realistic case in which rigid-body modes are present in the dynamics, and, as a consequence, the problem of controlling the attitude is solved simultaneously with, and as an integral part of, the problem of suppressing the vibrations.

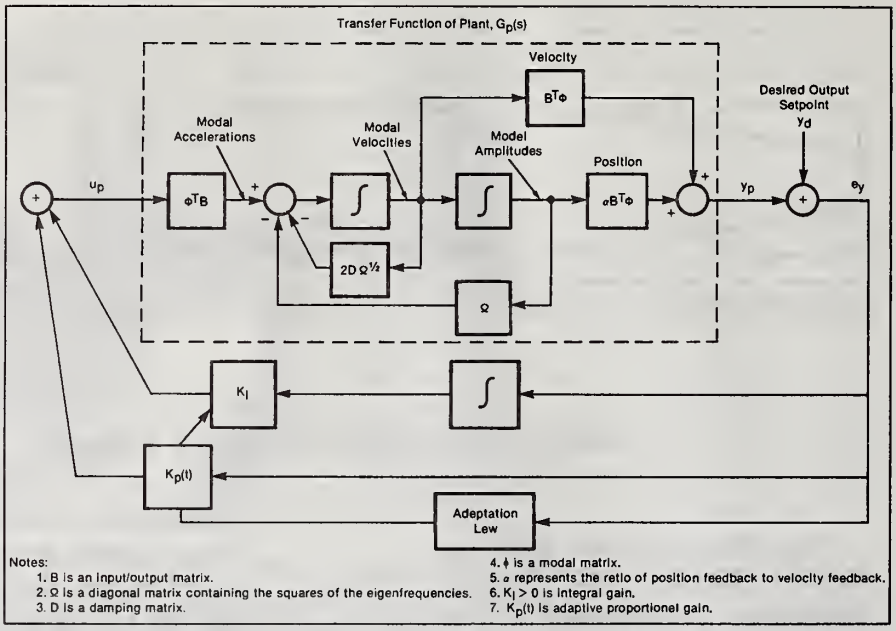

The Adaptive Set-Point Control Architecture is Applied to a Flexible Structure that is weightless or otherwise free and that is equipped with collocated torque actuators and position and velocity sensors.

This work was done by David S. Bayard of Caltech for **NASA's Jet Propulsion Laboratory.** *NPO-17471/TN*

FOR ADDITIONAL INFORMATION: *Contact: Director, Technology Transfer Division, P.O. Box 8757, BWI Airport, MD 21240; (301) 621-0100 Ext. 241*
REFER TO THE NUMBER LISTED AT THE END OF THIS ARTICLE

NASA Tech Brief
National Aeronautics and Space Administration
Ames Research Center, Moffett Field, California

Algorithm Computes Hypersonic Flow of Air

Nonequilibrium thermochemical effects are taken into account.

An algorithm simulates the three-dimensional hypersonic flow of air or another mixture of gases around a blunt body. It accounts for nonequilibrium thermochemical effects via a two-temperature mathematical model of molecular excitations and equations for finite-rate chemical reactions. These equations are fully coupled to the fluid dynamical equations.

The mathematical derivation of the algorithm begins, as is customary, with the Navier–Stokes equations for the flow of a viscous, incompressible fluid. These equations are put in conservation-law form, then transformed into generalized coordinates that conform to the body at its surface. The resulting intermediate set of equations represent the conservation of the masses of the various chemical species, the conservation of total mass, the conservation of momentum, the total thermochemical energy density, and the molecular-vibrational component of the thermochemical energy density. The latter two equations represent the two-temperature model, in which the following are assumed: (1) the translational and rotational components of molecular kinetic energy equilibrate immediately, so that they are represented by a single translational temperature, T; and (2) a single vibrational temperature, T_v, characterizes the vibrational state of all polyatomic species present and equals the temperature of all electrons.

The vibrational component of heat conduction is incorporated via a mathematical model for the rate of exchange of energy between the vibrational and translational modes. The diffusion of chemical species is approximated by a combination of binary-diffusion models. Customary models for viscosity and the translational/rotational component of heat conduction are also included. The finite-rate equations represent the following chemical reactions:

$$N_2 + M \rightleftharpoons 2N + M$$
$$O_2 + M \rightleftharpoons 2O + M$$
$$NO + M \rightleftharpoons O + N + M$$
$$NO + O \rightleftharpoons N + O_2$$
$$O + N_2 \rightleftharpoons N + NO$$
$$N + O \rightleftharpoons NO^+ + e^-$$

where M can be any of the other species shown. The algorithm incorporates assumptions about the dependencies of the forward and reverse reactions upon T and T_v. The finite-rate equations for these reactions are solved simultaneously with the global conservation-law equations. Without some kind of simplifying approximation, the resulting set of equations would be too large to be solvable on any but the most advanced supercomputers. Here, the size of the problem is reduced by use of an underrelaxation computational process that limits the rate at which the gas can be computed to dissociate and ionize and prevents wild swings in mass fractions and temperatures. The gas is computed to relax gradually and stably to its steady-state compositions and temperatures. The simulation is not time-accurate, but it achieves the proper steady state.

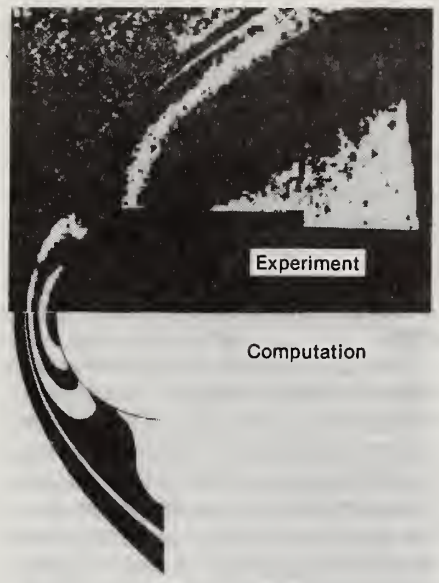

These interferograms show the density fringes in a flow of dissociating nitrogen across a circular cylinder at a speed of 5.59 km/s. The upper fringe pattern was observed in an experiment. The lower fringe pattern is computed from a flow simulated by the algorithm.

The algorithm has been tested by comparison of its predictions with those of other algorithms and with measurements. It has been found to compute hypersonic flows accurately (see figure). The benefits of the explicit formulation are particularly evident where the complexity of the body requires the use of patched coordinate grids.

This work was done by Grant Palmer of **Ames Research Center**. *Further information may be found in AIAA paper 89A-43217, "The Development of an Explicit Thermochemical Nonequilibrium Algorithm and Its Application to Compute Three Dimensional AFE Flowfields."*

Copies may be purchased [prepayment required] from AIAA Technical Information Service Library, 555 West 57th Street, New York, New York 10019, Telephone No. (212) 247-6500.

ARC-12623/TN

FOR ADDITIONAL INFORMATION: *Contact: Director, Technology Transfer Division, P.O. Box 8757, BWI Airport, MD 21240; (301) 621-0100 Ext. 241*
REFER TO THE NUMBER LISTED AT THE END OF THIS ARTICLE

Controlling Laboratory Processes From a Personal Computer

An operator can control processes via natural-language commands.

A computer program provides natural-language process control from an IBM PC or compatible computer. This program sets up a process-control system that can either run without an operator or be run by workers who have limited programming skills.

The complex environment of the typical research laboratory requires flexible process control. Sometimes process-control schedules require frequent changes, even several times per day. These changes may include the addition, deletion, or rearrangement of steps in a process. The program facilitates such changes.

The program includes three smaller programs. Two of them, written in FORTRAN77, record data and control research processes. The third program, written in Pascal, generates the FORTRAN subroutines used by the other two programs to identify the user commands with device-driving routines (device drivers) written by the user. The program also includes a set of input data that allows the user to define the user commands to be executed by the computer.

To set up the system, the operator writes the device-driving routines for all of the controlled devices. Once set up, this system requires only an input file that contains natural-language command lines that tell the system what to do and when to do it. The operator can make up custom commands for the operation of, and the taking of data from, external research equipment, at any time of the day or night, even when the operator is not in attendance.

This process-control software system requires a personal computer operating under MS-DOS with suitable hardware interfaces to all controlled devices. The program requires a FORTRAN77 compiler and device drivers written by the user. This program was developed in 1989 and requires 62K bytes of memory.

This program was written by H. Will and M.A. Mackin of **Lewis Research Center.**
LEW-14907/TN

FOR ADDITIONAL INFORMATION

CONTACT

COSMIC®
112 Barrow Hall
University of Georgia
Athens, GA 30602

(404) 542-3265

NASA Tech Brief
National Aeronautics and
Space Administration

Damping Seals Would Help Support Turbopump Rotor

Tentative designs are presented.

A report describes an engineering study of the proposed use of damping seals as major load-carrying members of the high-pressure-oxygen turbopump of the Space Shuttle main engine. The damping seals would be incorporated into the bearing packages at the preburner-pump and turbine-end locations on the pump rotor. This exploration of the damping-seal concept was motivated by the need to increase the operating lives of the ball bearings that support the rotor by relieving them of damaging transient lateral loads.

A damping seal of the type in question is a leaky thin-layer liquid bearing somewhat reminiscent of a labyrinth seal. It is formed by directing some of the pumped fluid (in this case, liquid oxygen) into the volume defined by the roughened or pocketed inner surface of a stator member and the smooth outer surface of a rotor member that fits in the stator member with a small radial clearance. The damping seals are required to act in parallel with, and remove most or all of the radial load from, the ball bearings during operation. The damping seals and ball bearings must act in concert to suppress the bending-mode vibrations of the rotor. The overall result should be longer bearing lives and a rotor-supporting system that is almost fully redundant.

The modified bearing packages are required to be robust and simple and to allow the proper transfer of loads to the damping seals. This means, among other things, the smooth transfer of loads from the ball bearings to the seals as the pump approaches the operating speed. The installation of the seals must not impose any additional bearing loads (for example, because of slight misalignments caused by accumulations of manufacturing tolerances) and must not compromise the integrity of the pump in any other way. The seals are required to function with the pressure gradients available in the unmodified pump design. The damping seals are also required to prevent rotation of the outer races of the ball bearings.

During the design study, specifications for the required performance, design envelope, and boundary conditions were developed. Various seal and bearing-package design concepts were evaluated, and final designs were selected and analyzed. Alternatives to standard damping seals were also evaluated. After selection of the best bearing-package design concepts, preliminary mechanical designs were prepared and analyzed.

Three damping-seal designs — two at the preburner-pump location and one at the turbine-end location — were developed and analyzed. An alternative that was developed for the turbine-end location consisted of a pocketed hydrostatic bearing with an unique geometry of stationary pockets and a rotating feed. The dynamic performance of the rotor/bearing system was evaluated. It was found that two critical speeds that excite bending-mode vibrations of the rotor will have to be traversed below the running speed. However, the dynamic behavior was computed to be very well controlled, and the response of the rotor was computed to be very heavily damped.

This work was done by O. Pinkus, J. Walowit, C. Lee, and F. Gillham of Mechanical Technology, Inc., and P. Buckman of Aerojet Tech Systems for **Marshall Space Flight Center.** *"Damping Seal Rotor Support in Turbomachinery."* *MFS-27227/TN*

FOR ADDITIONAL INFORMATION: *Contact: Director, Technology Transfer Division, P.O. Box 8757, BWI Airport, MD 21240; (301) 621-0100 Ext. 241*
REFER TO THE NUMBER LISTED AT THE END OF THIS ARTICLE

NASA Tech Brief
National Aeronautics and
Space Administration

Growth of Instabilities in Two Types of Mixing Layers

Effects of feedback are examined.

A report discusses issues involved in the computation of the growth of instabilities and vorticity in the mixing (shear) layer between two parallel flows that have different speeds and are separated initially by a flat surface. The study focusses upon the degree to which these growing flow structures hasten or retard their own further growth, and upon the related question of the differences between flows computed according to mathematical models of S-layer and T-layer mixing.

An S (for "space") layer is a shear layer that develops downstream of a point where the two streams are brought into tangential contact. This kind of shear layer is better suited to experimental study in a laboratory where, for example, it can be formed at the downstream edge of a thin splitter plate. A T (for "time") layer is a shear layer in which infinitesimal wrinkles grow and roll up into vortexes, developing in time from an initial tangential velocity discontinuity at the plane separating the half spaces that contain the initial uniform flows. A T-layer is better suited to theoretical study because the differential equations that describe its development are parabolic in time (as opposed to elliptic for the S-layer) and, therefore, an initial perturbation can be specified according to the linear theory and its growth treated by linear/weakly nonlinear and computational techniques.

The author notes that despite the similarities between S- and T-layers, the common practice of interpreting observations of S in terms of calculations with T may be misleading. One of the physical questions associated with the difference between T- and S-layers is whether distant vortexes, which have already paired once or several times downstream in the S-layer, can induce perturbations upstream that seed the subharmonic instability. If so, the downstream development of the S-layer would not depend on perturbations imposed upstream but the S-layer would create its own perturbations and continue to develop downstream. To examine this question, the author offers a model of the S-layer that introduces the elliptic nature of real flow indirectly to some level of approximation in the solution for the T-layer.

The method of comparison between the S- and T-models is to assume that the vorticity of the S-layer is given parabolically by a Galilean mapping of that of the T-layer, to satisfy the appropriate boundary conditions in the S-layer and compute the velocity induced at any point in the S-layer by its vorticity field, and to compare this velocity to that which can be derived from the velocity of the T-layer at corresponding points by a Galilean transformation of the velocity itself. The purpose of these calculations is to assess approximately how far the flow in the S-layer is from parabolic and, in particular, to what extent the perturbations induced upstream by large downstream concentrations of vorticity exert the retarding or hastening effect described above. The results of the calculations suggest that this elliptic influence, or the feedback, in a mixing layer is relatively small, at least for flows in which the normalized difference between the two initial velocities is relatively small. Thus, the transformation method used in this study offers a suitable tool for the study of such flows.

This work was done by Upender K. Kaul of Sterling Federal Systems for **Ames Research Center.** *"Do large structures control their own growth in a mixing layer? An assessment."* *ARC-12567/TN*

FOR ADDITIONAL INFORMATION: *Contact: Director, Technology Transfer Division, P.O. Box 8757, BWI Airport, MD 21240; (301) 621-0100 Ext. 241*
REFER TO THE NUMBER LISTED AT THE END OF THIS ARTICLE

NASA Tech Brief
National Aeronautics and Space Administration

Licensing Opportunity

Incompressible, Viscous Flow About an Ogive/Cylinder

Calculated flow patterns agree closely with experimental ones.

Theoretical predictions and observations of incompressible viscous flow about a body of revolution at an angle of attack are compared in a report. This study was a test of modern numerical methods for the solution of the equations of fluid dynamics, and was conducted as a step toward future work on more difficult problems.

The body consisted of a solid circular cylinder at the downstream end and tapered in an ogive of revolution to a point on the axis at the upstream end. The cylinder had a length-to-diameter ratio of 1, and the ratio of the length of the ogive to the diameter of the cylinder was 3.5, yielding an overall length-to-diameter ratio of 4.5.

The ogive/cylinder was placed in a towing tank and a camera was mounted to move along with it. The tank was filled with salt water seeded with small particles. When illuminated by a fan of laser light and photographed, the particles produced streak images, the lengths and directions of which indicated the local velocity of the flow about the body. Observations were made at angles of attack of 30° and 45°. Previous studies had shown that the flow is steady at angles of attack up to 60°.

For the simulation, the flow was represented by the Navier-Stokes equations in mass-averaged variables, with terms for pseudocompressibility. The pseudocompressibility allows the use of an implicit finite-difference scheme and relaxes the requirement of incompressibility during the convergence process. Upon reaching the steady state, the effect of the pseudocompressibility on a solution becomes negligible, and the solution is essentially that of the Navier-Stokes equations of incompressible flow.

The computational mesh conforming to the ogive/cylinder was generated by a two-dimensional Poisson-grid generator in the plane of the body axis. The plane was then rotated about the axis to generate a three-dimensional wrapped mesh. The outer boundary was spherical and located six body lengths from the tip of the ogive.

The equations were solved numerically by use of the INS3D computer code. Implicit second-order and explicit fourth-order numerical dissipation was added to damp out high-frequency oscillations. The solution was advanced in time until the steady state was reached.

The computed and photographed crossflows at various positions along the ogive and at both angles of attack were in qualitative agreement. In general, the crossflow, which develops along the body, produces a pair of leaside vortices. An analysis of the development of the symmetric vortical flow field reaffirms the utility of the impulsive-flow analogy in understanding the qualitative nature of the flow.

This work was done by Gregory G. Zilliac of **Ames Research Center**. *Further information may be found in NASA TM-88329 [N90-11254], "A Computational/Experimental Study of the Flow Around A Body of Revolution at Angle of Attack."*

Copies may be purchased [prepayment required] from the National Technical Information Service, Springfield, Virginia 22161, Telephone No. (703) 487-4650. Rush orders may be placed for an extra fee by calling (800) 336-4700.

Inquiries concerning rights for the commercial use of this invention should be addressed to the Patent Counsel, Ames Research Center. Refer to ARC-11793/TN.

Ames Research Ctr.
Technology Utilization Officer: Laurance Milov
Mail Code 223-3
Moffett Field, CA 94035
(415) 694-4044
Patent Counsel:
Darrell G. Brekke
Mail Code 200-11
Moffett Field, CA 94035
(415) 694-5104

FOR ADDITIONAL INFORMATION: *Contact: Director, Technology Transfer Division, P.O. Box 8757, BWI Airport, MD 21240; (301) 621-0100 Ext. 241*
REFER TO THE NUMBER LISTED AT THE END OF THIS ARTICLE

NASA Tech Brief
National Aeronautics and
Space Administration
NASA's Jet Propulsion Laboratory, Pasadena, California

Robot Grasps Rotating Object

Advanced techniques for sensing and control are combined.

An experimental robotic system semiautomatically grasps a rotating object, stops the rotation, and pulls the object to rest in a fixture. The system, based on a combination of advanced techniques for sensing and control, was constructed to test concepts for the robotic recapture of spinning artificial satellites. Potential terrestrial applications for the technology to be developed with the help of this system could include tracking and grasping of industrial parts on conveyor belts, tracking of vehicles and animals, and soft grasping of moving objects in general.

The system (see figure) consists of a sensing-and-perception (S&P) subsystem and a manipulator-control-and-mechanization (MCM) subsystem. The S&P subsystem acquires and tracks the position, orientation, linear velocity, and angular velocity of the spinning object [in this case, a 350-lb (159-kg) mockup of a satellite] and sends tracking data to the MCM subsystem. The S&P subsystem includes charge-coupled-device video cameras, video digitizers, frame buffers, a custom-made "pipeline" video-data processor that finds high-contrast edges in the video images, and buffers that store the output of this processor. The S&P subsystem also includes a microcomputer programmed to control the other S&P equipment and to perform the various computing tasks involved in acquisition, tracking, and the analysis of images.

The MCM subsystem grapples the spinning object and brings it to rest without exerting excessive forces on the object or on itself. This subsystem includes two robot arms with hands that include special grappling tools mounted on pneumatically driven parallel fingers. A microcomputer that communicates with the S&P microcomputer and with the robot-controlling microprocessors performs the control computations for each arm. Data from force and torque sensors on the robot arms are passed back to the computers via the robot-controlling microprocessors.

Ultimately, of course, it would be desirable to develop a robotic system that could acquire a view of the rotating object, track it, grasp it, and bring it to a stop, all automatically. A fully autonomous acquisition algorithm is being developed, but at present, acquisition requires so much computation that it cannot be performed rapidly enough on currently available computers to keep up with a moving object in real time. Therefore, the experimental system is designed to execute a semiautomatic acquisition procedure: A human operator guides the system into an approximate overlap of each video image of the rotating object with a superimposed wire-frame video image that represents the state of the rotating object in the mathematical model of the object in the computer. Once the desired overlaps are achieved, the operator commands the system to begin the automated operations of tracking, grasping, despinning, and pulling into the fixture.

In experiments, the system has successfully grappled the satellite mockup at rotational speeds up to 2 rpm. At higher speeds, delays in communication and inaccuracies in the control subsystems cause the robot hands to miss the grasping pads on the mockup. The use of faster computers and improved robot-control software should improve the grappling capability and help reduce the transient grappling forces.

This work was done by Brian H. Wilcox, Kam S. Tso, Todd E. Litwin, Samad A. Hayati, and Bruce B. Bon of Caltech for **NASA's Jet Propulsion Laboratory.**
NPO-18016/TN

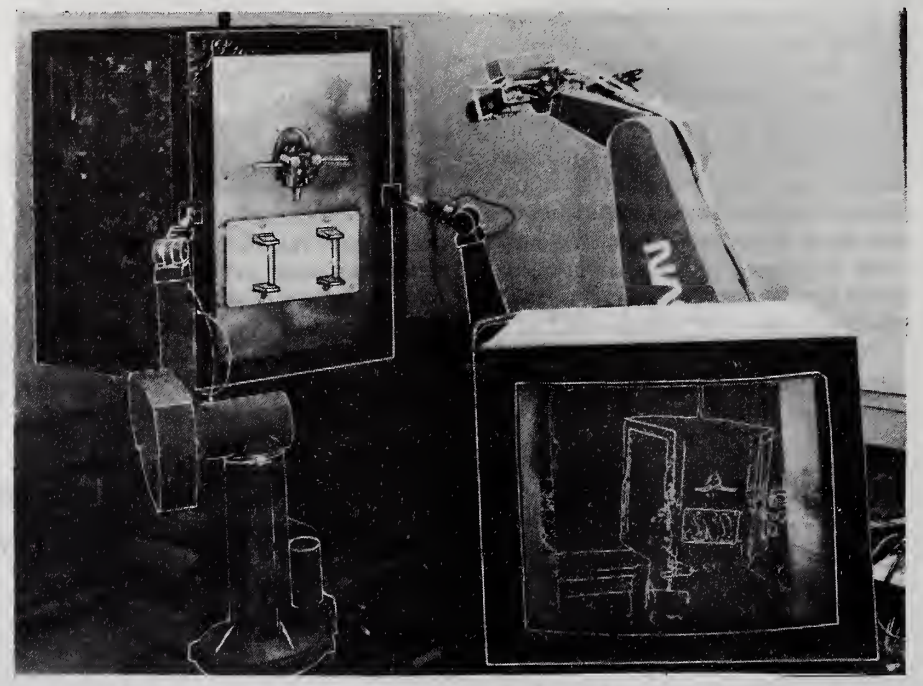

The Test Bed of the NASA Telerobot Project is being used to investigate the robotic capture of a spinning mockup of a satellite. The technology is also potentially applicable to industrial robots and robotic vision systems that are required to acquire, track, and possibly grasp moving objects.

FOR ADDITIONAL INFORMATION: *Contact: Director, Technology Transfer Division, P.O. Box 8757, BWI Airport, MD 21240; (301) 621-0100 Ext. 241*
REFER TO THE NUMBER LISTED AT THE END OF THIS ARTICLE

Software for Multivariable Frequency-Domain Analysis

Outputs include frequency-response singular-value plots of multivariable transfer matrices.

FREQ (Multivariable Frequency Domain Singular Value Analysis Package) is a software package of subroutines that perform frequency-domain analysis of (1) continuous- or discrete-multivariable linear systems, (2) any continuous system for which one can calculate the transfer matrix at points on the imaginary axis, or (3) any discrete system for which one can calculate the transfer matrix at points on the unit circle. Many approaches in the field of the analysis of, and the synthesis of controllers for, linear, multivariable, time-invariant systems involve loop-shaping procedures. Within these procedures, design parameters are chosen to shape frequency-response singular-value plots of selected transfer matrices. FREQ computes, within one unified framework, many of the most-used multivariable transfer matrices. The matrices are evaluated at frequency-response values selected by the user, and singular values and vectors are computed. FREQ also tabulates maximum and minimum singular values against frequency.

A document that describes FREQ includes an example with data taken from a study in which a fine-pointing attitude-control system was designed for a large, flexible hoop/column space antenna. The control system was designed to exhibit stability robustness with respect to high-frequency, unmodeled components of the dynamics of the antenna, and a prototype version of FREQ was employed to obtain the robustness-barrier-design plots. As other applications of FREQ indicated new users' needs and preferences, FREQ evolved through a sequence of applications in the analysis and design of controls. The current version of FREQ provides a body of tested software that incorporates most of the desired properties and options needed by the practicing engineer.

Four different versions of FREQ are available from COSMIC. The user may choose between single- and double-precision versions and between brief and complete versions. To use the brief versions, the user must have access to the numerical linear-algebra packages LINPACK (real and complex versions) and EISPACK in the same precision as that of the version of FREQ being used. The single-precision brief version is LAR-14119, the single-precision complete version is LAR-14120, the double-precision brief version is LAR-14121, and the double-precision complete version is LAR-14122.

The double-precision version is recommended for such 32-bit computing equipment as a DEC VAX or Sun Microsystems workstation. The brief version offers the economy of less code to compile and store. In addition, if the brief version is installed on a super-computer or minicomputer, the computer may already have a version of LINPACK with the Basic Linear Algebra Subprograms (BLAS) subpackage optimized to its architecture. The use of this version of LINPACK will result in a more efficient package. All four versions of FREQ may be purchased together as a package (COS-10024).

The user gains access to FREQ by writing a program in FORTRAN 77 that makes calls to subroutines in the FREQ package. FREQ is written in ANSI standard FORTRAN 77 (with minimal extensions in the double-precision versions to support the use of the COMPLEX*16 data type) and is intended to be independent of the specific computing equipment (except that some FORTRAN compilers do not support COMPLEX*16). Representative memory requirements (in bytes) on a VAX computer running VMS 5.2 and using VAX FORTRAN 5.1-10 are 59K for single-precision brief, 75K for single-precision complete, 73K for double-precision brief, and 91K for double-precision complete. The amounts stated here for the brief versions do not reflect the size of the required proprietary routines. This program contains copyrighted material and was developed in 1989.

This program was written by Ernest S. Armstrong of **Langley Research Center** *and Daniel P. Giesy of Planning Research Corp. LAR-14119/TN, LAR-14120/TN, LAR-14121/TN, and LAR-14122/TN.*

FOR ADDITIONAL INFORMATION

CONTACT

COSMIC®
112 Barrow Hall
University of Georgia
Athens, GA 30602

(404) 542-3265

Technique to Measure Liquid Level and Volume Device

Scientists at the Naval Surface Warfare Center, Silver Spring, Maryland, have developed a device that uses an optical attenuation technique to measure liquid levels and volumes without contaminating the liquid under observation. The device provides an accurate, extended measurement range (from empty to full) without contacting either the fluid or its container via a single light-source, detector, and associated electronics. The device is applicable to transparent and translucent fluids in containers of similar optical transmission characteristics. Figure 4 is a schematic diagram of the device.

The function of the optical source is to emit a constant output within a specific wavelength band; for example, white source with appropriate filters or monochrometer, or a laser diode. The source wavelength is chosen to match the spectral properties of the fluid to be measured. Sources are commercially available to match absorption characteristics of most fluids, including the 1300 nanometers required for water-based fluid measurements. The source may be used directly, through a lens, or remotely located from the measurement area by coupling into an optical fiber. The detector can be similarly configured. Analysis circuitry used to convert detector output to liquid level or volume measurements is comprised of standard off-the-shelf components. It processes the detector output to determine the attenuation of the optical beam for subsequent correlation to the parametric measurements.

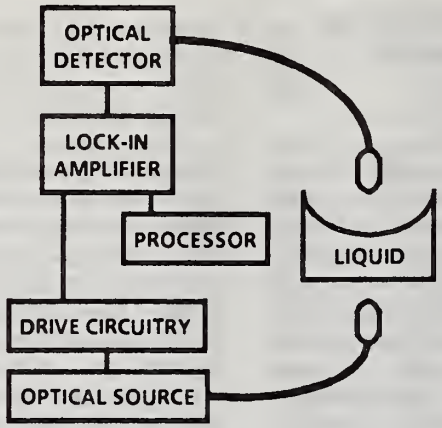

Figure 4. Schematic liquid level and volume sensor

Potential users of this device include medical and chemical laboratories and manufacturing facilities having production lines for filling liquid containers.

For Additional Information:

Backup material on this effort is available from:

Navy Domestic Technology Fact Sheet Reader Reply Service
Code E211
Naval Surface Weapons Center
Dahlgren, VA 22448-5000
(703) 663-8921

Refer to 160503/TN

NASA Tech Brief
National Aeronautics and Space Administration
Langley Research Center, Hampton, Virginia

Licensing Opportunity

Adjustable Pitot Probe

The probe is readily positionable in the core of uniform flow in a hypersonic wind tunnel.

Pitot probes are generally used to measure the pressures of high-velocity fluid streams in wind tunnels. In a hypersonic wind tunnel, the air is heated up to about 3,000 °F (about 1,600 °C) to prevent liquefaction of the nitrogen and oxygen in the flow. The transducers used to measure the pitot pressures must be protected from the hostile temperatures to prevent thermally induced measurement errors and possible damage to the transducers. Therefore, the pressure transducers are usually mounted outside of the test section, connected to the tips of the probes through relatively long tubes. The large volume of such a connecting tube causes an undesirable increase in the "settling time" of the pressure probe, the shortness of which can be essential to accurate measurements. Also, a free-stream pitot pressure probe is typically mounted on the wall of a tunnel or on an injection mechanism, and its position can be adjusted within only a limited range. Accordingly, in the design of a new cooled, readily positionable pressure probe, the transducer is mounted relatively close to the tip of the probe.

The probe is formed of a pair of mating cylindrical housings: the transducer housing and the pitot-tube housing. A small hole is bored through the transducer housing along its centerline. A hole slightly larger than the body of the sensor portion of the transducer is bored from one end along the same line to a depth large enough to provide a pressure-sensing chamber beyond the tip of the transducer. The transducer mounting post, in the vicinity of the pressure-sensing chamber, is surrounded by a cooling-water annulus, which has full-depth webbing 180° apart to divide it in half. It also has cross-connecting water passages at full depth to force the water to flow completely around the volume area to be cooled. A thermocouple sheathed in stainless steel is inserted from the other end into the pressure-sensing chamber to monitor the temperature. The transducer housing also contains a pressure annulus and a larger annulus that accommodates a boss on the pitot-tube housing.

The pitot-tube housing has a pressure annulus that matches the boss. The pitot pressure is delivered from the pitot tube, which points into the free stream, to the pressure-sensing chamber via a metal bellows that connects the pitot tube to its housing. The pitot tube is supported by an adjustable wedge fairing attached to the top of the pitot-tube housing with a semicircular foot. This foot extends over the transducer housing with a radial clearance and allows the pitot tube to rotate to any orientation within 360°.

Because of the design of the wedge fairing, the probe can be adjusted both radially and circumferentially. In addition, the pressure-sensing transducer in the adjustable probe is cooled internally by water or other cooling fluid passing through the annulus of the cooling system.

This work was done by George C. Ashby, Jr., W. Eugene Robbins, and Lewis A. Horsley of **Langley Research Center**.

This invention is owned by NASA, and a patent application has been filed. Inquiries concerning nonexclusive or exclusive license for its commercial development should be addressed to the Patent Counsel, Langley Research Center. Refer to LAR-14232/TN.

Langley Research Ctr.
Technology Utilization
Officer John Samos
Mail Stop 139A
Hampton, VA 23665
Patent Counsel
George F. Helfrich
Mail Code 279
Hampton, VA 23665
(804) 864-3523

FOR ADDITIONAL INFORMATION: *Contact: Director, Technology Transfer Division, P.O. Box 8757, BWI Airport, MD, 21240; (301) 621-0100 Ext. 241*
REFER TO THE NUMBER LISTED AT THE END OF THIS ARTICLE

NASA Tech Brief
National Aeronautics and Space Administration
NASA's Jet Propulsion Laboratory, Pasadena, California

Collectors of Airborne and Spaceborne Particles

Simple units go directly into optical, electron, or x-ray analysis equipment.

Brushlike collectors capture samples of dust and other particles in space vacuum or air for optical, scanning-electron-microscope, and/or x-ray analysis. The collectors gently decelerate the particles without damaging them, minimizing the tendency of some particles to rebound. Depending on the design of a specific collector of this type, it can capture particles ranging upward in size from fractions of a micrometer to a few micrometers.

A collector of this type resembles a stubby, round brush. It consists of an array of fibers embedded in a matrix. In a typical application, the collector would be oriented with the fibers parallel to the direction of the impinging particles (see figure). The free ends of the fibers can be tapered to facilitate the entry of the particles into the interstices of the array. As particles arrive, they are accepted and retained. The fibers can be clustered loosely or tightly to suit the expected sizes and rebound properties of the particles.

A collector of this type can be fabricated by embedding parallel fibers in the matrix material, then etching the matrix away to the desired depth with an oxygen plasma to expose the ends of the fibers, leaving enough of the matrix material to form a supporting base. The oxygen plasma can also be used to thin and taper the ends of the fibers as necessary.

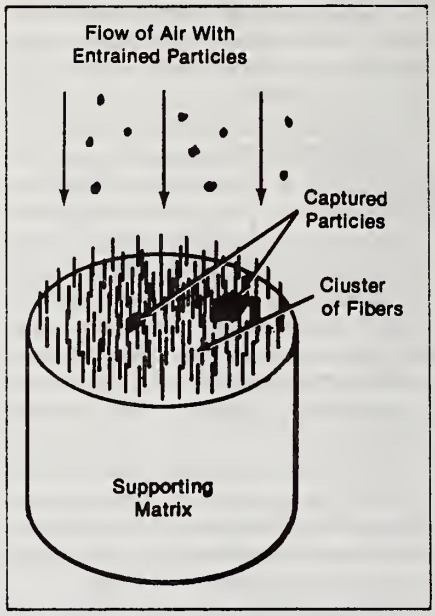

Particles Flow Into a Brushlike Array of fibers with the airstream. The fibers trap particles for subsequent analysis.

After samples have been captured, the collector serves as a holder for analyzing them. Viewed on end, the fibers appear black and thus provide a contrasting background for microscopic inspection. The known sizes and spacing of the fibers provide a reference scale for determining the sizes of the captured particles. A reference grid can also be etched into the array.

The fibers can be made of carbon, a low-atomic-number material. This improves contrast in scanning electron microscopy (by minimizing backscatter and secondary electrons) and in x-ray analysis (by minimizing x-ray background). The fibers are electrically conductive, and it should not be necessary to apply conductive coats to the captured particles. The fibers are also good thermal conductors and should readily dissipate heat generated by impacts of particles.

Unlike collectors of other types, the carbon-fiber units are not ordinarily coated with sticky materials, which may not endure well under some collection conditions. Furthermore, particles in fiber collector are fixed and do not sink below the surface as they do in a viscous adhesive.

This work was done by Robert E. Frazer of Caltech for **NASA's Jet Propulsion Laboratory.** *NPO-18183/TN*

FOR ADDITIONAL INFORMATION: *Contact: Director, Technology Transfer Division, P.O. Box 8757, BWI Airport, MD 21240; (301) 621-0100 Ext. 241*
REFER TO THE NUMBER LISTED AT THE END OF THIS ARTICLE

NASA Tech Brief
National Aeronautics and
Space Administration
Langley Research Center, Hampton, Virginia

Digital Pitch-and-Roll Monitor

A compact inclinometer is precise and prints out readings on demand.

The measurement of angle with respect to the local vertical is important in wind-tunnel testing and other applications. This problem is compounded if it is necessary to make this measurement in two axes simultaneously. In some wind tunnels, models can be set to roll angles over a 360° range and to pitch angles over a reasonably wide range. Sensors are generally employed to determine the attitudes of such models, but it is always necessary to verify the calibration of the sensor(s) in each model before and after a wind-tunnel test. Conventional inclinometers, which are generally used for this task, have distinct disadvantages in weight, size, readability, and the like. Other types of angle sensors are available but have either limited range or limited accuracy.

Consequently a small, highly accurate inclinometer has been developed. This inclinometer monitors both pitch and roll simultaneously and can provide printed output on demand. The inclinometer includes three mutually perpendicular accelerometers and signal-conditioning circuitry that converts the outputs of the sensors to digital values of pitch and roll. The accelerometers are mounted on an inclinometer base. Three digital multimeters have been modified to supply power to the accelerometers and digitize their outputs. A small programmable calculator computes the angles, and a printer provides hard-copy output.

The displays of the multimeters provide visual readout of pitch and roll directly in degrees. The system can be operated from 115 Vac or from internal batteries. The system has a resolution of 0.001° and an accuracy of approximately ±0.005°. The computer program provides for using an alternate reference instead of reading absolute angles. This simplifies mounting the inclinometer on a model at some location other than the zero-reference surface.

This inclinometer is based on work done in support of the National Transonic Facility, which has used this inclinometer or its prototype since 1984. In addition to its wind-tunnel applications, this system could be useful in any application involving steady-state, precise sensing of angles, such as the calibration of robotic devices and positioners.

This work was done by Tom D. Finley of **Langley Research Center.** *Jeff Brown of Virginia Governor's School, and Ryland Campbell of Wyle Laboratories.*
LAR-14247

FOR ADDITIONAL INFORMATION: *Contact: Director, Technology Transfer Division, P.O. Box 8757, BWI Airport, MD 21240; (301) 621-0100 Ext. 241*
REFER TO THE NUMBER LISTED AT THE END OF THIS ARTICLE

NASA Tech Brief
National Aeronautics and Space Administration
Lewis Research Center, Cleveland, Ohio

Licensing Opportunity

Integral Plug-Type Heat-Flux Gauge

The integral construction reduces the components of error caused by discontinuities.

A new heat-flux gauge eliminates measurement errors caused by temperature discontinuities associated with conventional gauges. The new gauge yields more accurate surface heat-flux data for verifying aerodynamic and heat-transfer models.

The figure shows a schematic of the new heat-flux gauge mounted into a metal or alloy specimen. The gauge comprises the following items: (1) an annulus fabricated part way through the specimen thickness, (2) a wall extending from the bottom of the annulus to the active surface of the gauge, (3) a cylindrical thermoplug that is surrounded by the annulus, (4) thermocouple thermoelements attached to the side and back of the thermoplug, (5) a thermocouple with a hot junction mounted near the active surface of the gauge, and (6) a cover enclosing the thermoplug and thermocouples.

Conventional gauges are generally mounted by screwing or welding them into position. Sharp temperature changes are possible across the temperature discontinuities formed by the resulting threads or seams. These temperature discontinuities can produce large errors of measured surface heat flux. Unlike a conventional gauge, the new gauge is not screwed or welded into place, but instead a thermoplug and annulus are electrical-discharge-machined (EDM) into the specimen material. The EDM process leaves no interface between the material and the thermoplug, thus inherently increasing gauge accuracy by eliminating the interface and the associated temperature discontinuity. The EDM process is also conducive to accurate fabrication of minute gauges.

Gauges can be fabricated in a variety of sizes. Thermoplug diameters are currently 0.040 in. (1.02 mm), and lengths are about 0.060 in. (1.52 mm). Wall thicknesses nominally vary from about 0.010 in. (0.25 mm) to 0.020 in. (0.51 mm) (see figure). Annulus depths range from 0.060 in. (1.52 mm) to 0.100 in. (2.54 mm). Annulus widths are typically 0.020 in. (0.51 mm).

Temperatures are measured with commercial coaxial (single-wire) thermocouple assemblies, which are modified by swaging them to a diameter of 0.010 in. (0.254 mm) and then by stripping them to expose a 0.0015 in. (0.038 mm) diameter Chromel* or Alumel* (or equivalent) thermoelement (wire). Pairs of Chromel and Alumel wires are joined and spotwelded to the sides of the thermoplug to form hot junctions. The junctions are located circumferentially 120° from each other along the length of the thermoplug. The wires are extended from the junctions in a direction perpendicular to the cylindrical plug surface and are then routed through the annulus to the back of the gauge. The wires are carefully positioned so that they do not touch metal surfaces. The coaxial thermocouple assemblies are then extended from the rear of the material gauge (see figure) and laid side by side within grooves electrical-discharge-machined into the material. The grooves and assemblies are covered with metallic, material welded to the specimen. The thermocouple assemblies are extended to remote data systems for temperature-data storage. A cover is welded over the plug to seal thermally insulating air within the annulus. The air minimizes heat loss from the thermoplug. To measure temperature near the active surface, individual Chromel and Alumel thermoelements in the coaxial thermocouple assemblies are joined and spotwelded to the bottom of a hole electrical-discharge-machined from the annulus side into the wall (see figure). The hole is nominally located 0.010 in. (0.254 mm) below the active surface.

The gauges measure both transient and steady-state surface heat flux. Temperature as a function of time is recorded at each thermocouple location. The surface heat flux and rate of change of surface heat flux are calculated from temperature-vs.-time data, known properties of the gauge material, thermocouple positions measured from the active surface of the

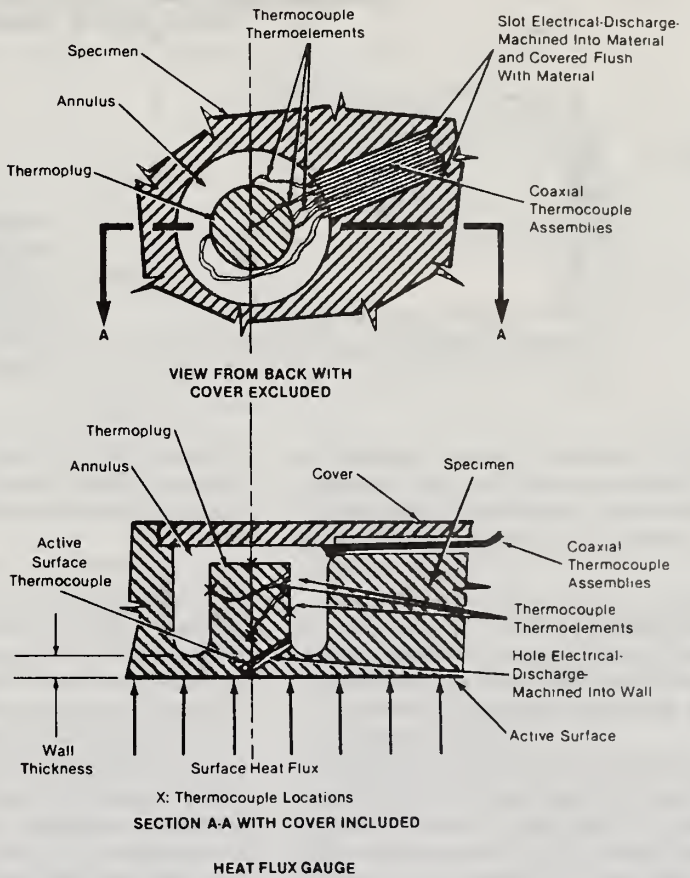

The **Integral Thermoplug Gauge** measures the flux of heat across a specimen of material. In comparison with conventional gauges that are screwed or welded in place, the integral thermoplug gauge is more accurate.

gauge, and thermoplug length. A gauge of this type functions at temperatures ranging from cryogenic to the melting temperatures of metals and alloys.

This work was done by Curt H. Liebert and John Koch, Jr., of **Lewis Research Center.**

This invention is owned by NASA, and a patent application has been filed. Inquiries concerning nonexclusive or exclusive license for its commercial development should be addressed to the Patent Counsel, Lewis Research Center. Refer to LEW-14967/TN.

Lewis Research Center
Technology Utilization Officer: Daniel G. Soltis
Mail Stop 7-3
21000 Brookpark Road
Cleveland, OH 44135
(216) 433-5567
Patent Counsel:
Gene E. Shook
Mail Code 301-6
21000 Brookpark Road
Cleveland, OH 44135
(216) 433-5753

FOR ADDITIONAL INFORMATION: *Contact: Director, Technology Transfer Division, P.O. Box 8757, BWI Airport, MD 21240; (301) 621-0100 Ext. 241*
REFER TO THE NUMBER LISTED AT THE END OF THIS ARTICLE

NASA Tech Brief
National Aeronautics and Space Administration
Langley Research Center, Hampton, Virginia

Licensing Opportunity

Mixed-Mode-Bending Delamination Apparatus

Double-cantilever-beam and end-notch-flexure loads are applied simultaneously.

Failures in structural composites often develop as delamination between laminated plies. Typically these delaminations are initiated and grow as a result of combined peeling (opening) stresses and sliding (shear) stresses. Therefore, studies of resistance to delamination should account for the effects of combined opening and shear stresses, referred to as mode I and mode II stresses, respectively.

Although most delamination tests are currently conducted by use of single-mode specimens, various mixed-mode test procedures have been introduced. Unfortunately, each of these mixed-mode test procedures has one or more limitations. For example, with some tests, only a narrow range of mode I/mode II ratios can be tested, and others require difficult time-consuming numerical analyses of the test results. Therefore, the mixed-mode-bending delamination apparatus was developed to apply mode I and mode II loads simultaneously to a simple test coupon to measure delamination resistance.

The figure illustrates a test conducted with the apparatus. The specimen is loaded in a manner that represents a combination of two well-known procedures used in pure mode I and mode II testing. The upward load on the right end is like that used in a double-cantilever-beam (DCB) test for mode I delamination. The downward load is like that used in an end-notch-flexure (ENF) test for mode II delamination. These loads can be applied simultaneously to produce combined mode I and mode II delamination in the specimen.

The combined load is produced by applying a single load to a beam attached to the specimen. Bonded hinges on the end of the specimen are attached to the loading beam and to the base of the apparatus by use of grips. The left end of the specimen rests on a supporting roller. A center roller loads the specimen downward, and, simultaneously, the right end of the specimen is loaded upward. These two loads are in proportion to the applied load, and their relative magnitudes depend on the loading distance, c. By varying c, a wide range of mode I/mode II ratios for mixed-mode delamination testing can be produced.

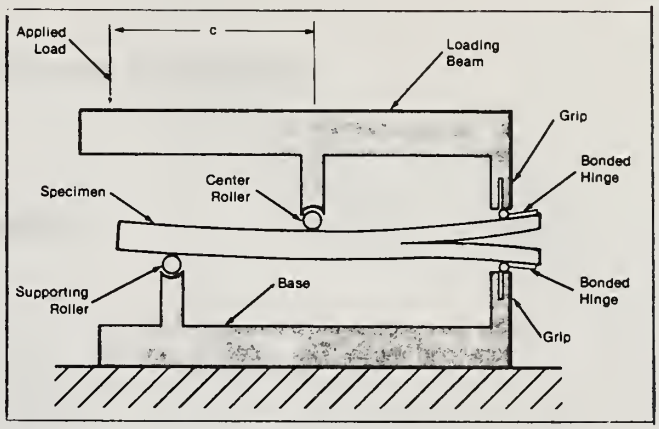

The **Mixed-Mode-Bending Delamination Apparatus** generates two types of delamination stress simultaneously in the specimen from a single externally applied point load.

The mode I and mode II loading on the specimen can be expressed in terms of the applied load, which can be measured by use of a conventional test machine. Then simple equations related to DCB and ENF testing can be used to resolve the measured mixed-mode response into its mode I and mode II components. For example, mixed-mode delamination toughness can be determined by measuring the applied load during an increment of delamination growth and can then be resolved into mode I and mode II components. Also, these simple equations for pure mode I and mode II testing provide for selection of c to obtain desired mode I/mode II test ratios.

In this technique, the individual mode I and mode II contributions to delamination in the specimen can be analyzed by use of simple beam-theory equations, thereby eliminating the need for time-consuming, difficult numerical analysis. Also, this technique allows a wider range of mode I/mode II ratios than are possible with many other methods. Mixed-mode delamination testing is of interest in all fields that utilize composite materials. Composite materials are used mostly in the aerospace field, but are also used in automobiles, lightweight armored military vehicles, boats, and sporting equipment. This technique could also be useful in the general lumber, plywood, and adhesive industries.

This work was done by John H. Crews Jr., and James R. Reeder of **Langley Research Center**. *Further information may be found in NASA TM-100662 [N89-10945], "A Mixed-Mode Bending Apparatus for Delamination Testing."*

Copies may be purchased [prepayment required] from the National Technical Information Service, Springfield, Virginia 22161, Telephone No. (703) 487-4650. Rush orders may be placed for an extra fee by calling (800) 336-4700.

This invention is owned by NASA, and a patent application has been filed. Inquiries concerning nonexclusive or exclusive license for its commercial development should be addressed to the Patent Counsel, Langley Research Center. Refer to LAR-13985

Langley Research Ctr.
Technology Utilization
Officer John Samos
Mail Stop 139A
Hampton, VA 23665
Patent Counsel
George F. Helfrich
Mail Code 279
Hampton, VA 23665
(804) 864-3523

Environmental Science & Technology

0036 Indoor Air Quality Simulator for Personal Computers

Testing & Instrumentation

0037 An Assessment of Soil-Gas Measurement Technologies

Other Items of Interest

0056 Air/Sea Temperature Probe Developed

United States
Environmental Protection
Agency

Air and Energy Engineering
Research Laboratory
Research Triangle Park NC 27711

Research and Development

EPA **Project Summary**

Indoor Air Quality Simulator for Personal Computers

The results of this project are the IAQPC (indoor air quality simulator for personal computers), a User's Guide, and a Technical Manual. The IAQPC was developed to address the problem of indoor air contamination. The program requires a large amount of data, but all values have defaults, many of which will be applicable to many situations. The program uses menus for the data input and to specify output.

This Project Summary was developed by EPA's Air and Energy Engineering Research Laboratory, Research Triangle Park, NC, to announce key findings of the research project that is fully documented in two separate reports and one computer diskette (see Project Report ordering information at back).

Computer Requirements

The minimum required computer setup which will run the IAQPC includes an IBM-PC or compatible with two floppy disk drives, DOS Version 2.0 or later, and 350 K of memory. The recommended hardware configuration includes a PC (or a PC-compatible) with a hard disk, a math coprocessor, and a color monitor (e.g., an Enhanced Graphics Adapter [EGA]). Other computers or less memory may work but have not been tested.

Input/Output Options

The IAQPC gives concentration profiles to cover up to 62 days based on information entered on a building layout, the HVAC (heating, ventilation, and air-conditioning) system parameters, and source (machines, cigarettes) and sink (walls, floors) data.

The general building layout is chosen from one of six standard configurations. The building must be single-story and may have up to 20 rooms. The room volumes and the cross-sectional areas of the interconnections between the rooms (doors, vents, cracks) may be entered. The HVAC parameters include the amount of outdoor air entering the building and the schedule of the HVAC system. Airflows for the building are calculated by the program.

The IAQPC can model up to six pollutants. These are selected in one menu. Note that at this point no pollutant interactions are modeled, so any of the pollutant slots may be used for any pollutant; however, it is much simpler to keep track of the output if the pollutants are referred to by name. Source production rates are entered, then the locations for the sources are chosen. Sinks are modeled through the same process.

The IAQPC provides graphical representations of the layout, source/sink locations, calculated airflows, and source cycles. The concentrations calculated by the program may be displayed both as linear and semilog plots.

Table 1. Program Flowchart Showing Menus and Functions[a]

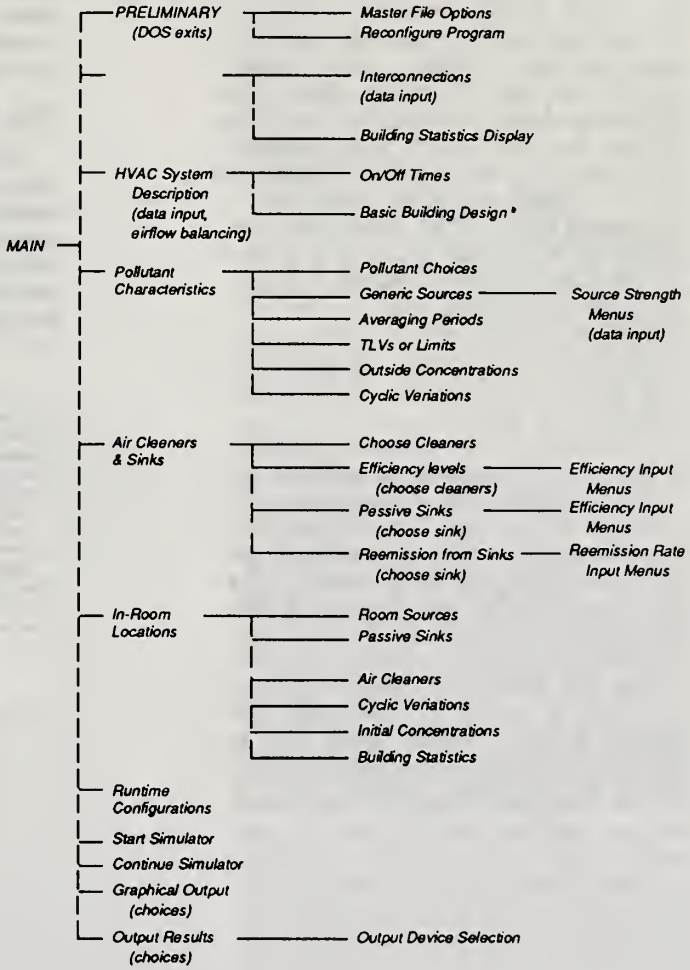

[a]Menus are in bold print.
[b]This menu can be reached in two ways.

Program Design/Menu Setup

The IAQPC uses a series of menus (as shown in Table 1) to enter data, run the

program, and select output(s). The menu approach was chosen so that the data can be entered in an easy, simple to understand way. The menus were prepared so that related information can be entered in the same location. A great deal of data is needed to describe an indoor environment. This means that data input could be messy and difficult. However, the approach used in IAQPC makes this input as easy as possible.

The IAQPC's menu system begins with the Main Menu or the Preliminary Menu, as chosen in the Reconfigure Program option. The Main Menu gives access to all the data input, modeling, output option menus, and the Preliminary Menu. The Preliminary Menu contains the master file options, the exit options, and a program configuration menu. Data entry begins with the Main Menu where the user chooses the type of data to enter. The arrow keys, pressing the first letter of the choice, or a mouse may be used to select a choice. From this step the data entry may be in the next menu or may be three more menus deep. The on-screen instructions and the user's manual will help the user find a way through the program.

Another part of this approach to make data entry as simple as possible is the data file structure. This program saves the data in a series of files. One of these files, the Master File, saves the names of the other data files that were used for the particular run. In this way, a system of data files may be built up to operate as a library. For example, a source strength file with values that apply to several buildings or cases could be set up, then used with several different building design files to determine the effect of the building layout on the concentrations. At least one set of files is included with the program. As the experimental data base grows and the number of analyzed test cases increases, more sample cases will be provided. With these, a case similar to the user's own building may be chosen as a base to simplify data entry.

The User's Guide

The guide introduces the IAQPC and contains menu instructions, a step-by-step tutorial, and brief descriptions of the meanings and reasonable inputs for the variables. It should be extremely helpful for fist-time users, but will also act as a quick reference for experienced users.

The Technical Manual

The technical manual provides the theoretical background of the program, offers details on the algorithms, and includes the program listings. This manual should be useful to the experienced user and to those who are interested in the fundamentals of the program.

P. Lawless and M. Owen are with Research Triangle Institute, Research Triangle Park, NC 27709.
Leslie E. Sparks is the EPA Project Officer, (see below).
The complete report consists of two volumes entitled "IAQPC Indoor Air Quality Simulator for Personal Computers:," and one diskette:
"Volume 1" (Order No. PB91-205153/AS; Cost: $31.00, subject to change) is the Technical Manual.
"Volume 2" (Order No. PB91-205161/AS; Cost: $17.00, subject to change) is the User's Guide.
The disk (Order No. PB91-507871/AS; Cost: $130.00, subject to change) contains the executable files for IAQPC.
Volumes and disk of this report will be available only from:
National Technical Information Service
5285 Port Royal Road
Springfield, VA 22161
Telephone: 703-487-4650
The EPA Project Officer can be contacted at:
Air and Energy Engineering Research Laboratory
U.S. Environmental Protection Agency
Research Triangle Park, NC 27711

United States
Environmental Protection
Agency

Air and Energy Engineering
Research Laboratory
Research Triangle Park NC 27711

Research and Development

EPA Project Summary

An Assessment of Soil-Gas Measurement Technologies

Introduction

A fairly wide range of methods for characterizing the radon potential of land areas has evolved over the last decade through research programs in this country and abroad. This reviews published technologies that could support soil-based estimators of radon potential. Basic technologies concentrate on measuring (1) radon in soil gas, (2) radon flux from the surface, or (3) radium content. Approaches may also include attendant measures of soil characteristics and other factors to support predefined indexes of radon potential.

Fundamental Considerations

Soil and rock are the main source of radon in buildings. Although broad spatial trends of indoor radon are in rough proportion to soil radium concentrations, the emanation and subsequent migration in the soil and ultimately into buildings is determined by processes and characteristics at work in the soil, in the building, and in the surrounding environment.

Quantitative estimates of radon potential for soils are predicated on a volume of soil in flow communication to a building, a supply of radon to the pore spaces of the soil, and transport mechanisms to convey radon into the building. The situation is complicated by a number of factors. The soil volume of interest is not defined by physical boundaries; rather, the strength of the transport mechanisms coupling the building to the soil defines the basic limits of migration. Radon emanation rates to the soil pores are controlled by the radium content of the soil grains, and are further tempered by soil moisture.

In most soils, the pore space contains both air and water, providing the opportunity for radon to partition between the air and water phases. If the volume portion of the pore space occupied by water is small, radon emanation is directed primarily to the gas phase. As the volume fraction of water grows, however, it does so at the expense of the gas phase. The gas phase vanishes at complete saturation.

Radon delivered to the soil pores can migrate through the ground by: (1) diffusion, in which the radon moves with respect to the pore fluid in order to equalize concentration gradients; and (2) forced convection, in which the pore fluid moves under the influence of external forces, carrying the radon along with it. Diffusion can occur with or without forced convection.

Measurement Technologies

While the basis for judging radon potential is still evolving, measurement strategies have converged along basic themes addressing (1) radium content, (2) soil gas, and (3) radon flux. Other types of measurements have been developed to quantify moisture, bulk density, permeability, porosity, and other soil properties that relate to the production and migration of radon in the soil. Concerns have been raised about representative sampling. While measurements of radon potential based on invariant soil properties could alleviate some of these concerns, representative soil conditions would still need to be defined for this approach and model relationships would still be required to adjust measured values.

Measurement strategies for estimating radon potential hinge on detecting the radioactivity in a known sample volume (or mass) whose history has been controlled to represent one or more processes germane to the production and migration of radon in the soil. Radium content is measured by isolating a defined volume of soil to retain the emanating fraction. At radioactive equilibrium, the activity concentration of radon and radon progeny is equated with the radium concentration. Soil-gas measurements, on the other hand, seek to isolate radon in the pore spaces without affecting emanation or transport. Flux-based measurements rely on natural or induced transport through the soil column to deliver the radon to a sampling volume defined over a specified area of the soil.

Basic approaches for measuring the radium content of soils involve sealing a soil sample in a leak-proof container, storing the sealed sample for a long enough period of time to establish radioactive equilibrium, and analyzing for radionuclides of interest using gamma spectroscopy. Protocols frequently accommodate concurrent analysis of moisture content, laboratory estimates of radon emanation, and other analyses by subdividing field samples. Variations in procedure include repeated analyses to evaluate the secular equilibrium between radium and radon.

Basic technologies for measuring radon concentrations in soil gas have evolved along three complementary pathways: (1) gas extraction from depth using hollow tubes,

(2) analysis of bulk soil samples, and (3) in situ detection. The reconnaissance probe for soil-gas extraction is a relatively simple system consisting of a small-diameter (6- to 9-mm) thick-walled carbon steel tube that is driven to sampling depth (75 cm, nominal) using a slide hammer. While the reconnaissance probe is intended for collecting grab samples of soil gas, it has been suggested that the system can be used for determining soil permeability. The permeameter probe is further equipped for controlled flow extraction to allow for estimates of soil permeability from pressure/flow relationships as well as radon concentration. The packer probe is a more complex apparatus that features inflatable packers to intercept surface air.

Basic approaches for determining soil-gas concentrations from bulk samples of soil generally involve sealing the sample under known conditions and measuring the evolution of radon in the sample with time.

Technical Considerations

Currently, there are no hard and fast criteria to provide an unambiguous reference for judging the performance of measurement technologies for radon potential. While there is little doubt that site-specific measurements can be used to determine the radon potential of land areas, interpretations are driven by empirical correlations and theoretical considerations. A broad consensus, however, highlights the importance of examining the abundance of radon in the soil and its propensity to migrate into buildings. Ideally, then, methods would provide information on the undepleted soil concentration, diffusion coefficient, and permeability through various combinations of direct measurements and model assumptions.

Each measurement approach reviewed in this report can provide useful information to evaluate radon potential. Technologies geared to measuring (1) radium concentrations in bulk soil samples or (2) soil gas concentrations are readily applied to the problem of estimating the undepleted radon concentration in soil gas. Measurements of unattenuated flux provide estimates of diffusive transport which, in turn, could be used to estimate soil-gas concentrations at depth. The induced flux method, although untested, may provide the means to directly simulate radon entry for slab-on-grade and crawl space construction. Laboratory measurements of exhalation, on the other hand, while not readily extrapolated to the soil environment, may provide clues to the relative strength of radon sources through comparative tests.

Radium-based measurements have the distinct advantage of being suited to testing water-saturated soils. Soil-gas-based measurements (extraction probes, in situ detection, flux), on the other hand, generally fail to obtain samples from saturated soils because the gas volume is nearly zero. Recognition factors to avoid generally saturated conditions can be built into protocols, as can rules to invalidate samples from saturated layers encountered at depth.

Practical Considerations

Practical decisions are likely to be guided by two absolutes: (1) avoidance of clearly inappropriate technologies, and (2) meeting the schedule demands of the situation. For the radium-based measurements, the all-weather capability must be judged against the lengthy time period necessary to achieve radioactive equilibrium. Delays could be shortened by taking more counts during the ingrowth period to extrapolate data to equilibrium levels. For soils with a low emanation fraction, a number of days may need to elapse to resolve the trend, but turnaround time could, in concept, be reduced to a matter of days. Further, initial count data offer information to provide a rough estimate without extended waits.

Conclusions and Recommendations

Each available technique for measuring radon in the soil provides some useful and informative data, but the means to apply these data are still evolving. How this evolution will affect future strategies and protocols for soil measurements remains to be seen. In the end, the utility of soil-based measurements is probably more sensitive to the interpretive framework than to the technologies employed to collect the data.

A firm and quantitative basis needs to be established for formally comparing different soil-measurement technologies. Achieving this basis would most likely require replicated testing of the various technologies across a range of soil types and sampling conditions. Allied to this, existing multicomponent data bases should be analyzed to place different measurement parameters on a common basis. The virtues of measurements directed toward invariant soil properties warrant further investigation from technical and practical standpoints, and the current range of accepted practice for soil-gas measurements needs to be assembled and compiled in a manner suited to consensus review.

Harry E. Rector is with GEOMET Technologies, Inc., Germantown, MD 20874.
David C. Sanchez is the EPA Project Officer (see below).
The complete report, entitled "An Assessment of Soil-Gas Measurement Technologies," (Order No. PB91- 219 568; Cost: $17.00, subject to change) will be available only from:
National Technical Information Service
5285 Port Royal Road
Springfield, VA 22161
Telephone: 703-487-4650
The EPA Project Officer can be contacted at:
Air and Energy Engineering Research Laboratory
U.S. Environmental Protection Agency
Research Triangle Park, NC 27711

Manufacturing, Machinery & Tools

0038 AGARD Handbook on Advanced Casting

0039 Composite Recycling

0040 Paint Spray Guide Developed

0041 Bearing-Cartridge Damping Seal—Ball bearings would carry reduced loads and be cooled more effectively. (Licensing Opportunity)

0042 Computer-Aided Design of Sheet-Material Parts—The old manual graphical 'development' technique is computerized. (Licensing Opportunity)

Testing & Instrumentation

0043 Computerized Profilometer for Inspection of Welds—Subjective inputs in inspection are reduced with consequent enhancement of precision. (Licensing Opportunity)

Department of Defense Fact Sheet

AGARD Handbook on Advanced Casting

The Advisory Group for Aerospace Research & Development (AGARD) is an activity of the North Atlantic Treaty Organization (NATO) formed to provide scientific and technical support for aerospace research within the member countries. As such, AGARD is a major publisher of scientific and technical materials in that field. The rationale for this handbook publication is explained in the introduction:

"The need to cut costs has in recent years led not only to the development of new materials but also to the further development of economic manufacturing processes like 'advanced casting technology.' Advances in casting technology could lead to increased use of castings for the manufacture of vital aircraft components, which in turn leads to reduced cost.

"Castings are favorable in terms of cost and weight and offer the possibility of combining into one casting a whole number of material-intensive machining and sheet-metal parts which were previously joined by riveting at high cost. Moreover, the process affords the design engineer greater freedom of design. It should be noted that the design should be made suitable for casting, i.e. the design engineer and foundry should get in touch as early as possible during component development. Only thus will it be possible to make maximum use of all the advantages of the process.

"So far, the lack of confidence of design and stress engineers in casting has stood in the way of a more widespread use of castings for primary structures. However, today there are precise and reliable data concerning castings available. They are collected in this handbook on 'Advanced Casting' to aid engineers in the application of cost-saving castings.

"Preference is given to the casting alloys A357, A201 and TiAl6V4, for structures in aircraft, on account of the high strength values of these alloys.

"The handbook should provide the user with practical information i.e. design data, mechanical values and quality assurance methods, but not with the manufacturing data because they are the 'know-how' of the foundry. This handbook was created to help the user with basic information for properly designing a casting. It provides specific information on design data and includes practical tips on how to prepare a drawing for a casting."

The handbook is organized into the following chapters:

1. Introduction - Includes principles of investment, sand, and titanium casting along with candidate materials and application.

COMPLEX CONFIGURATION

MANUFACTURING COST COMPARISON

F-20 VERTICAL STABILIZER

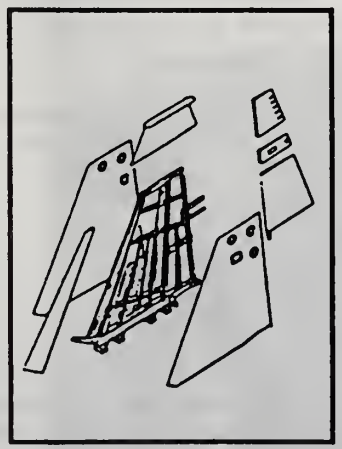

BUILDUP DESIGN AND ATTACHING STRUCTURES

NON-RECURRING	RECURRING
100	100

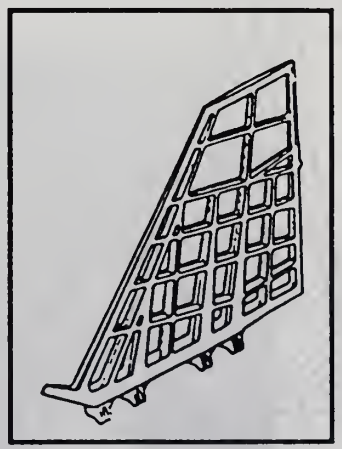

CASTING DESIGN A357-T6 ALUM ALLOY

NON-RECURRING	RECURRING
42	28

2. Casting Design - Includes method selection, design to cost, design details (cavities, loft lines, welded joints, etc.), tolerances, surface roughness, materials, surface protection, and repair..

3. Mechanical Data - Mechanical properties, strength behavior, fatigue behavior crack propagation, eye bolt joints, riveted joints, and weld repair.

4. Applications - A357, D357, A201, Ti6Al-4V

5. Quality Assurance Methods/Corrosion Behavior - Specifications, QA at the foundry and buyers, corrosion in A357, A201, TiAl6V4.

6. Damage Tolerant Design with Castings - Durability design, initial flaw size, crack growth rate, critical flaw size, metallographic controls, design allowables, casting factors.

This handbook is abundantly supplied with tables, figures, sketches, and photos, examples of which are reproduced here.

This is a valuable reference work for those interested in design and manufacture of aerospace castings. Preparation of this handbook was an international effort. Dietmar Mietreh edited the handbook and coordinated the working group that contributed. The appendix contains a full list of the contributors for further contact. Some of the U.S. contributors include:

Wright-Patterson AFB - C.L. Harmsworth
ALCOA - M.R. Dunke
Boeing Company - D.L. McLellan
Consolidated Aluminum Corp. - N.J. Davidson
General Dynamics Corporation - B.L. Ribeiro
Hitchcock Industries - F.H. Muehlegger
Howmet Turbine Components - G. Askey
Avery Kearney and Co.
Northrop Corp - K.J. Oswald
Precision Cast Parts - J. Thorne
Progress Casting Group - D.E. Leitlen
TiTech, International - E.A. Williams

This handbook is available from the National Technical Information Service, 528 Port Royal Road, Springfield, VA 22161. 703-487-4650.

The figure below gives a graphical description of the recommended diameter-to-length ratio.

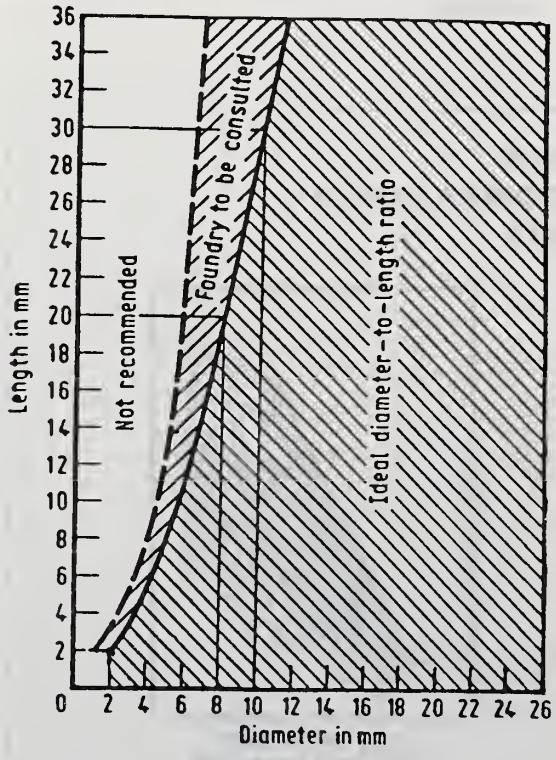
Length in mm
Diameter in mm
Not recommended
Foundry to be consulted
Ideal diameter-to-length ratio
0 2 4 6 8 10 12 14 16 18 20 22 24 26
2 4 6 8 10 12 14 16 18 20 22 24 26 28 30 32 34 36

Fan Frame

This complex gas turbine engine component is the largest one-piece titanium production class casting of its kind.

There are three major concentric elements combined in this state-of-the-art casting: heavy-walled flanges which support twelve hollow, thin wall airfoil struts, along with heavy engine mount bosses and an internal housing which supports the main turbine axle. Several through-core and blind-end cores are contained throughout this intricate casting.

The development of this casting design resulted in the elimination of 90-plus separate piece fabrication, a significant weight reduction, and a superior airflow path, all of which increase total engine performance.

Technical data: Ti-6Al-4V Alloy
HIP and heat treated
51in. (1295 mm) diameter)
300 lb (133 kg) net casting weight
Specification: General Electric

Courtesy: Precision Castparts Corp.

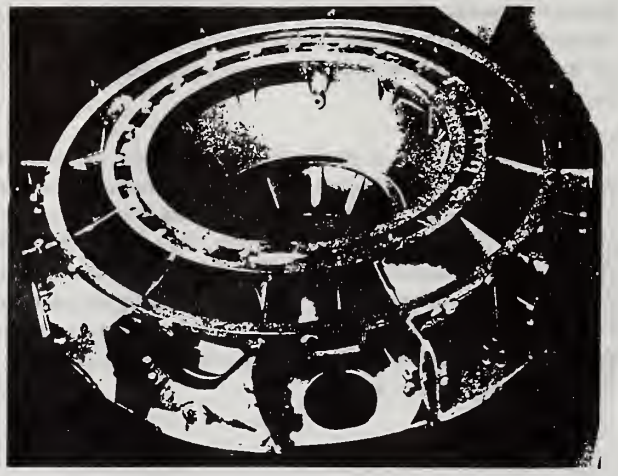

NAVY Manufacturing Technology Program

Composite Recycling

In composite manufacturing, offal from the process can be as much as 30-40% of the preimpregnated (prepreg) material used. This scrap is typically collected and disposed of in a landfill. Some of the material that is involved in the manufacturing process can also be considered as hazardous waste. As composite materials increase in use, the quantity and the problems of disposal will increase as well.

The hazardous material has to be separated and disposed of in a dedicated manner. The non-hazardous material also presents a complex separation and disposal problem. It is usually contaminated with packing material and separations used to cover the prepreg plies. Thus the question of reuse of such material has several considerations.

The elements of the GLCC program will:

- Identify and characterize the types and quantities of offal generated.
- Identify possible uses of the various materials.
- Evaluate manufacturing specimens and verify alternate end use.
- Determine the cost of the proposed process versus the potential environmental benefit in reuse of the materials.

Full scale systems will be designed and developed for recycling. As each system is proven, a prototype production facility will be developed leading to industrialization of the process and products.

The start-up phase for this program is underway. It involves efforts of three GLCC members: McDonnell Douglas Corporation, Production Products Inc., and Amalga Composites, Inc. After initial decisions regarding the best approaches, other member firms will be added.

There are a number of benefits seen as a result of this program.

First, quantities of hazardous waste will be minimized in manufacturing. Reuse of the offal material will cut drastically the disposal costs and these cost savings will reduce the ultimate cost of parts made by these composites. The parts made through reuse material will themselves be products that will provide commercial and economic development opportunities.

For more information, contact:
John Holland, P.E.
Vice President, Technology
Telephone: (414) 947-8900

Gerber Cutter with Prepreg Scrap

Paint Spray Guide Developed

The Naval Civil Engineering Laboratory (NCEL), Port Hueneme, California, has developed a users guide that provides instructions and cost evaluation information for converting water curtain particulate emission control systems to dry filter operations. Engineering and logistical issues are addressed, and example design plans are provided. Construction and operating permit requirements mandated by regulatory agencies are discussed. Cost estimates that may be used to perform comprehensive cost evaluation analyses are provided. In addition, sample calculations that illustrate how to use cost data are included.

For Additional Information:

Backup material on this effort is available from:

Navy Domestic Technology Fact Sheet Reader Reply Service
Code E211
Naval Surface Weapons Center
Dahlgren, VA 22448-5000
(703) 663-8921

Refer to 160904/TN

NASA Tech Brief
National Aeronautics and Space Administration
Marshall Space Flight Center, Alabama

Licensing Opportunity

Bearing-Cartridge Damping Seal

Ball bearings would carry reduced loads and be cooled more effectively.

In a proposed design for an improved ball-bearing cartridge, a damping seal in the form of a thin-layer fluid journal bearing would be incorporated into the cartridge. The damping seal would act as an auxiliary bearing, relieving the bearing balls of significant portions of both the static and the dynamic bearing loads. The damping from the seal would reduce the dynamic loads even further by reducing the amplitude of vibrations in the second vibrational mode of the rotor, which mode occurs when the rotor is turning at nearly the full operating speed. The damping-seal-cartridge design is intended for use in the high-pressure-oxygen turbopump of the Space Shuttle main engine, but the design concept should also be applicable to other turbomachinery bearings.

The bearing cartridge would be mounted with 0.001-in. (0.025-mm) radial clearance in the backup support attached to the stator. The outer races of the bearing would be mounted with 0.0005-in. (0.013-mm) radial clearance in the bearing cartridge (see figure). Because the static lateral loads would remain greater than the dynamic lateral loads throughout each turn of the rotor, the bearings and cartridge would be held to one side within their radial clearances.

The damping seal would be formed by the fluid in the gap between the knurled inner surface of the cartridge and the smooth outer surface of a spacer on the rotor. The damping seal would be 1 in. (2.54 cm) long and located between the two ball bearings. A small volume of the pumped fluid (in this case, liquid oxygen) would flow along the axis of the rotor, then along six radial roles to holes in the spacer that are aligned 50° from radial backward from the rotation. This arrangement would partly deswirl the flow as it entered the damping-seal gap. Deswirling would reduce the undesired cross-coupling stiffness while maintaining the desired direct stiffness and damping for optimum rotordynamic performance. As it emerged from the damping-seal gap, this flow would discharge directly into the heat-generating zone of the ball bearings, thereby helping to remove heat from the bearings and consequently prolonging their operating life.

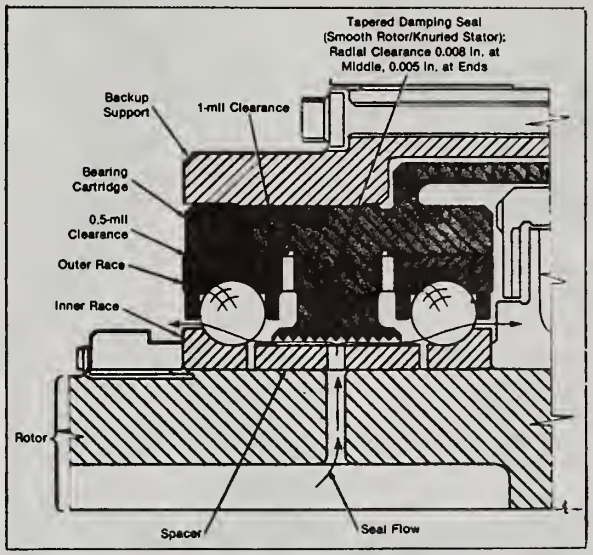

The **Damping Seal** would be incorporated into the bearing cartridge to divert loads from the ball bearings and damp vibrations of the rotor.

The design of the seal is limited by the available supply pressure and rate of flow. The seal is designed to impose the controlling resistance in its flow circuit and to provide maximum stiffness versus leakage, thus providing maximum support for the rotor in the face of the limited supply flow. The design that results from this combination of requirements calls for the knurled cartridge surface and a gap that tapers from 0.008 in. (0.20 mm) radial clearance at the middle to 0.005 in. (0.13 mm) at the ends. (The gap and the knurl are exaggerated for clarity in the figure.)

This work was done by David G. Goggins, Joseph K. Scharrer, and Wei C. Chen of Rockwell International Corp. for **Marshall Space Flight Center.**

Inquiries concerning rights for the commercial use of this invention should be addressed to the Patent Counsel, Marshall Space Flight Center. Refer to MFS-29657/TN.

George C. Marshall Space Flight Center
Technology Utilization Officer Ismail Akbay
Code AT01
Marshall Space Flight Center,
AL 35812
(205) 544-2223
Patent Counsel
Leon D. Wofford, Jr.
Mail Code CC01
Marshall Space Flight Center,
AL 35812
(205) 544-0024

FOR ADDITIONAL INFORMATION: *Contact: Director, Technology Transfer Division, P.O. Box 8757, BWI Airport, MD 21240; (301) 621-0100 Ext. 241*
REFER TO THE NUMBER LISTED AT THE END OF THIS ARTICLE

NASA Tech Brief
National Aeronautics and Space Administration
Marshall Space Flight Center, Alabama

Licensing Opportunity

Computer-Aided Design of Sheet-Material Parts

The old manual graphical "development" technique is computerized.

A computer-aided-design system partly automates the tedious process of designing and guiding the assembly of small pieces of flat sheet material into large surfaces that approximate smoothly curved surfaces that have complicated three-dimensional shapes. The system was conceived for use in making rocket-engine nozzles — specifically, for designing the small pieces of brazing foil, called "preforms," that are assembled edge to edge to cover the surface of each nozzle prior to brazing in a furnace. Previously, the foil covers were patchworks of manually trimmed, small pieces that had random, nonoptimum shapes and did not fit the surfaces of the nozzle in some spots. Clearly, computer-aided design can be used to advantage not only in the rocket-engine application but in other applications that require the design of sheet-material parts.

In effect, this computer-aided design system provides an improved, accelerated version of the old technique of manual graphical "development" of flat sections of sheet metal that are to be joined at their edges and/or folded to make three-dimensional vessels, ducts, and the like. In contrast with the manual graphical technique, the computer-aided technique rapidly yields accurate dimensions for the small pieces. This capability provides for flexibility in that it enables the designer to assess quickly and easily the effects of changes in design in making engineering compromises among various sizes and shapes.

At the beginning of the design process, the data that specify the three-dimensional surface to be covered or constructed are fed into the computer from an engineering drawing of the surface or from an equivalent computer data file. From this base of information and with the help of the computer, the designer can develop the geometric data on the pieces. Different shapes can be created, then translated and/or rotated onto the surface as required. This process enables the designer to obtain an optimized design fairly quickly.

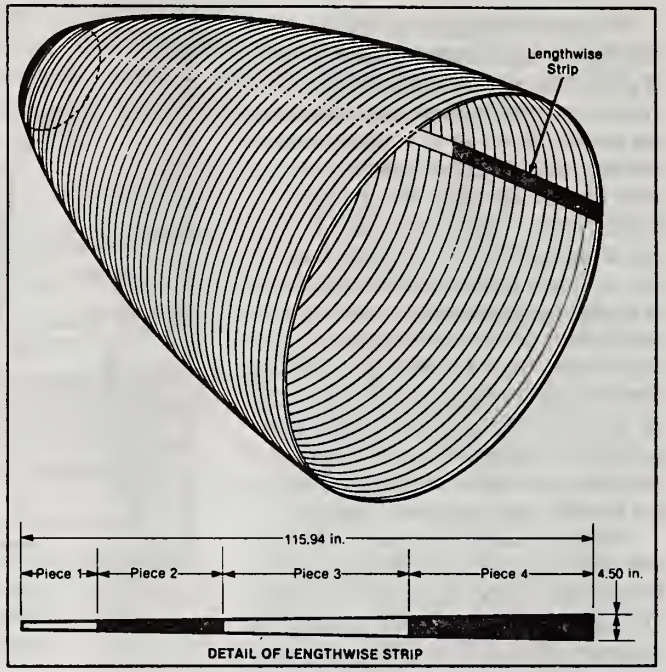

A **Curved Surface of Revolution** is approximated by flat lengthwise strips that can be cut with the help of templates and assembled edge to edge. In this case, each strip is divided into four pieces.

The system can plot the outline of a tentatively designed piece in full size; the shape can be cut out of the plotting paper and placed on a model of the surface to determine whether the tentative design provides a good fit. The system can create drawings of templates that are used to cut out the pieces (see figure). It can also create indexing-aid drawings, which assist in assembly by showing how to mark each piece to show where to place it on the surface to be covered or constructed.

The system can save time and money in both design and fabrication. For example, it can be used to maximize the sizes and/or optimize the shapes of parts in such a way as to reduce the amount of scrap left after cutting the parts out of sheet stock. Alternatively, it could help the designer achieve an acceptable fit with fewer parts, thereby reducing the fabrication time.

This work was done by Jeffrey L. Gilbert, Vincent Y. Paternoster, Maureen L. Levitt, and Mark R. Osterloh of Rockwell International Corp. for **Marshall Space Flight Center.**

Inquiries concerning rights for the commercial use of this invention should be addressed to the Patent Counsel, Marshall Space Flight Center. Refer to MFS-29759/TN.

George C. Marshall Space Flight Center
Technology Utilization Officer Ismail Akbay
Code AT01
Marshall Space Flight Center,
AL 35812
(205) 544-2223
Patent Counsel
Leon D. Wofford, Jr.
Mail Code CC01
Marshall Space Flight Center,
AL 35812
(205) 544-0024

FOR ADDITIONAL INFORMATION: *Contact: Director, Technology Transfer Division, P.O. Box 8757, BWI Airport, MD 21240; (301) 621-0100 Ext. 241*
REFER TO THE NUMBER LISTED AT THE END OF THIS ARTICLE

NASA Tech Brief
National Aeronautics and Space Administration
Marshall Space Flight Center, Alabama

Licensing Opportunity

Computerized Profilometer for Inspection of Welds

Subjective inputs in inspection are reduced with consequent enhancement of precision.

A third-generation profilometer for the inspection of butt welds includes a hand-held probe unit that operates in conjunction with a computer. In comparison with first- and second-generation profilometers, this one increases precision by reducing subjective inputs and the concomitant variations in outputs among different operators. In addition, the training of operators is simplified.

A contour gauge in the hand-held probe unit acquires a surface profile or cross section (see figure) and reproduces the profile mechanically in the input-image aperture of an array of optoelectronic sensors. A microprocessor in the hand-held probe unit collects the raw image data (64 pairs of *x*, *y* coordinates) and sends them to the computer via a standard serial data link. The computer processes these data into a dimensionally correct cross section of the weld, locates the centerline, and computes the peak angle and mismatch of the weld. The results of these computations are sent over a parallel data port to a printer/plotter, which prints the peak angle and mismatch and plots the cross section.

The computerization of the third-generation profilometer retains the capabilities of the first- and second-generation profilometers to measure the peak angles and mismatches of butt welds and extends measurement capabilities into the field of image analysis. This makes the profilometer an expandable system in the sense that the computer program can be made to extract and quantify subtle features in a weld profile. For example, it could be made to detect a weld bead, measure its width and height, and assess its symmetry. With modifications of the hand-held probe and further modifications of the software, the profile-analysis capability could be extended to include such other inspection functions as rapid, objective measurements of diameters, concentricities, angles, and general profiles, as well as tooling-setup functions for which rapid, objective measurements are required.

Yet another advantage of computerization is that output data are more readily processable into forms that can be used by the same or another computer. This feature is desirable for the development of data bases and for the development of systems that perform other analyses; e.g., to determine statistics on the qualities of manufactured products for use in controlling manufacturing processes.

The **Hand-Held Probe Unit** is positioned across a weld, in contact with the workpiece, to obtain a profile.

This work was done by M.A. Badinger, F.N. Stone, and G.J. Drouant of Martin Marietta Corp. for **Marshall Space Flight Center.**

Inquiries concerning rights for the commercial use of this invention should be addressed to the Patent Counsel, Marshall Space Flight Center. Refer to MFS-28548/TN.

George C. Marshall Space Flight Center
Technology Utilization Officer Ismail Akbay
Code AT01
Marshall Space Flight Center,
AL 35812
(205) 544-2223
Patent Counsel Leon D. Wofford, Jr.
Mail Code CC01
Marshall Space Flight Center,
AL 35812
(205) 544-0024

Materials

0044 Carbon Foam Features Exceptional Properties

0045 High-Temperature Polymers Reported

0046 Controlled Temperature Gradient Improves Freezing Alloy—Better microstructure increases fatigue life. (Licensing Opportunity)

0047 Correlating DSC and X-Ray Measurements of Crystallinity—The degree of crystallinity is roughly proportional to the heat of fusion.

0048 LaRC-RP41: a Tough, High-Performance Composite Matrix—A new polymer exhibits increased toughness and resistance to microcracking. (Licensing Opportunity)

0049 New Polyimide has Many Uses—Low-toxicity and low-mutagenicity monomer is the key to a new high-performance polyimide. (Licensing Opportunity)

0050 Superfiber for Strong, Light Fabrics—Polyolefin fiber resists chemicals and abrasion.

Other Items of Interest

0038 AGARD Handbook on Advanced Casting

0039 Composite Recycling

Department of Defense Fact Sheet

Strategic Defense Initiative Organization

Carbon Foam Features Exceptional Properties

Numerous potential applications have emerged for an extremely versatile, low-density carbonized foam, which was developed at Sandia National Laboratories (Albuquerque, N.M.) under SDI an DOE funding. The process used to make the foam permits a wide range of properties to be discretely controlled. As a result of this control, electrical conductivity can be finely tailored to suit a particular application.

Among those properties which can be specified in the manufacturing process are pore size, density, and internal structure or morphology. Foam densities are low, and can range from 0.03 g/cc to 0.60 g/cc. Pore size can range from several tenths of a micron to tens of microns.

While the outward appearance of the foam remains constant, internal cellular structure can be varied. Internal structure can be isotropic - that is, voids or pores can be uniformly distributed throughout the form, much like pores in a sponge. In the isotropic version, the pores are not oriented in a specific direction, so a fluid flowing through the foam must follow a more tortuous path. Hence, isotropic foam would make a good filter. Isotropic carbonized foam provides a uniform structure, allowing it to conduct heat or electricity uniformly in all directions.

Internal structure also can be anisotropic - that is, pores can be arranged so that void areas are contiguous. Anisotropic foam is oriented differently in different directions; the void areas form tube-like structures, or channels, which allow flow along a single axis. Hence, anisotropic foam is better suited for high velocity flow, because it allows a clear path for material to flow through.

This flexibility of structure allows foams to be custom-made to suit particular applications. Both types of foams can be used for a catalyst support. A metal coats all the surfaces of the foam and acts as the catalyst. The foam provides more surface area - leading to a greater reaction rate. Carbon is desirable because it doesn't react with most chemicals, and it is a good thermal conductor, so it can get rid of heat that builds up during the reaction.

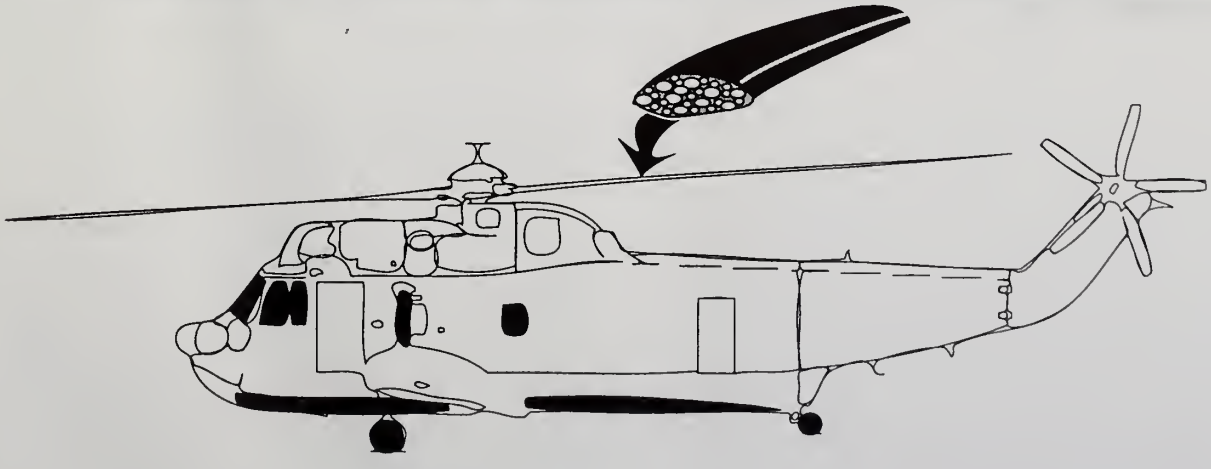

Dr. Sylwester, inventor of the foam, reports that Sandia has developed its own spinoffs - an electrically conducting composite material - made by filling the foam voids with an insulating polymer. The resulting material can be used in micro-electrode sensor arrays for electrochemistry. In the foam, each individual carbon cell wall acts like an electrode, while the polymer filler acts like an insulator surrounding a conducing wire. Thus, the foam can conduct electricity, and the polymer filler provides insulation and structural integrity.

Metal-coated carbon foam could also lead to improved battery electrodes. Also, because carbon is biocompatible, the foam could be used in implants and artificial bones.

Meanwhile, Applied Sciences (Yellow Springs, Ohio) is developing a technique that uses off-the-shelf carbon foam to create a carbon composite 3-D preform, which is like a skeleton that supports a final composite structure. The technique is less complex, and may significantly lower costs and improve properties over conventional preforms, which use multidirectional weaving, spinning, or knitting to provide the lightweight porous support structure. Starting with the carbon foam substrate, a layer of carbon is vapor-deposited, creating an isotropic, 3-D graphite honeycomb structure.

This graphitic foam can then be reinforced by growing catalytic-carbon fibers within the preform. Resulting preforms can be subsequently densified using conventional matrix materials, such as epoxy and pitch. The composite preforms show high stiffness-to-weight, and good strength-to-weight. They also readily conduct heat and electricity. The preforms can serve in aerospace structural components, brakes, centrifuge rotors, flywheels, helicopter blades, and nose cones.

Another company, Ultramet (Pacoima, Cal.), is coating reticulated carbon foam with rhenium to make tiny hot rocket nozzles. The foam can withstand 1,000 degrees Fahrenheit higher temperature than the NASA shuttle tiles. Coating carbon foam with a metal or metal oxide, such as platinum, rhenium, or thorium , protects against oxidation. Thoria (a thorium oxide), for instance, can endure up to 3,400 degrees Fahrenheit, without cracking or chipping.

The coatings extend the material's life, and permit significantly higher combustion temperatures, resulting in higher specific impulse, The lightweight foam requires less fuel, allowing greater payloads or longer missions. Coated carbon foam can be applied in kinetic energy weapons, rockets, heat transfer pipes, and as protective coatings for aircraft and gas turbine engine blades.

Ultramet is also infiltrating carbon foam with refractory metals or ceramics to create sandwich panels, structural members, and furnace components.

FOR ADDITIONAL INFORMATION: Contact: Technology Applications Office, Strategic Defense Initiatives Organization, OSD/SDIO/TNI, The Pentagon, Washington, DC 20301-7100; (703)693-1563.

High-Temperature Polymers Reported

A researcher from the Naval Research Laboratory (NRL), Washington, D.C., reports the development of a new class of phthalonitrile-based polymers that offers a promise of bridging the gap between currently used high-temperature polymers and ceramics/metals.

The polymers are easily processed by melt condensation of the phthalonitrile units into a void-free thermosetting material. The resins are readily polymerized in one step with an appropriate amine curing agent by heating the mixture above the melting point until gelation and vitrification occur (C-stage). This is followed by postcuring at elevated temperatures to improve the physical properties. An alternative process involves heating the polymerization mixture to distinct stages or to a specific viscosity (B-stage). Upon cooling, the B-staged prepolymer is a frangible, glassy solid that can be stored indefinitely at ambient temperature without further reaction.

Preliminary laboratory-scale investigations of these phthalonitrile-based polymers indicate that they can withstand temperatures up to 370°C (700°F). The glass transition temperature or softening temperature can be varied as a function of the curing and postcuring conditions. The mechanical properties are similar to current state-of-the-art high-temperature thermosetting polymers such as PMR-15.

The nonreactivity of the prepolymers at ambient conditions is particularly appealing for the preparation of laminates and as low-flow materials for fiber-reinforced composites.

For Additional Information:

Backup material on this effort is available from:

Navy Domestic Technology Fact Sheet Reader Reply Service
Code E211
Naval Surface Weapons Center
Dahlgren, VA 22448-5000
(703) 663-8921

Refer to 160302/TN

NASA Tech Brief
National Aeronautics and Space Administration
Marshall Space Flight Center, Alabama

Licensing Opportunity

Controlled Temperature Gradient Improves Freezing Alloy

Better microstructure increases fatigue life.

A controlled gradient of temperature in the advancing zone of solidification increases the fatigue life of a directionally solidified nickel-base superalloy. The improved solidification process eliminates, reduces, or controls the microstructure of deleterious brittle phases, including carbides and γ/γ' eutectic. The improved process also reduces microsegregation and makes discrete carbides (if present) become fine and blocky.

Unlike a pure metal, an alloy melts and freezes over a range of temperatures rather than at a single temperature: it is completely molten above the liquidus temperature, completely frozen below the solidus temperature, and consists of liquid (of one composition) between dendritic solid regions (of another composition) at intermediate temperatures. The gradient of temperature through the advancing liquid/solid zone in a directionally solidifying specimen of alloy affects the final, solidified microstructure by influencing the width of the solid/liquid zone and the time spent solidifying.

In the improved process, the spatial and temporal distribution of temperature between the advancing liquidus and solidus surfaces is tailored as follows: Below the liquidus temperature, the gradient of temperature is kept small and caused to make a transition to a temperature plateau in the liquid/solid zone. After the plateau, the gradient of temperature is large and remains so during the remainder of solidification (see figure).

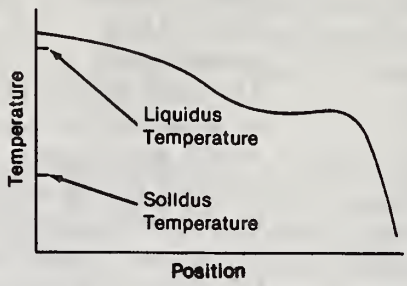

When the **Temperature as a Function of Position** along a directionally solidifying specimen of alloy looks something like this, the resulting solidified microstructure favors increased fatigue life. The combination of different thermal gradients that yields the best mechanical properties must be determined by experimental studies.

The fatigue life of MAR-M246(Hf) alloy solidified in the improved process is increased by a factor of 10 to 100 over that of the same alloy produced by more-conventional high-temperature-gradient directional solidification. The use of controlled temperature gradients is also expected to improve the properties of other alloys, of both directionally-solidified polycrystalline and single-crystal forms.

This work was done by Deborah Schmidt, Wendy S. Alter, and William D. Hamilton of **Marshall Space Flight Center.**

Inquiries concerning rights for the commercial use of this invention should be addressed to the Patent Counsel, Marshall Space Flight Center. Refer to MFS-28314/TN.

George C. Marshall Space Flight Center
Technology Utilization Officer Ismail Akbay
Code AT01
Marshall Space Flight Center,
AL 35812
(205) 544-2223
Patent Counsel
Leon D. Wofford, Jr.
Mail Code CC01
Marshall Space Flight Center,
AL 35812
(205) 544-0024

FOR ADDITIONAL INFORMATION: *Contact: Director, Technology Transfer Division, P.O. Box 8757, BWI Airport, MD 21240; (301) 621-0100 Ext. 241*
REFER TO THE NUMBER LISTED AT THE END OF THIS ARTICLE

NASA Tech Brief
National Aeronautics and Space Administration
NASA's Jet Propulsion Laboratory, Pasadena, California

Correlating DSC and X-Ray Measurements of Crystallinity

The degree of crystallinity is roughly proportional to the heat of fusion.

An experiment has demonstrated that there is an approximate linear correlation between the degree of crystallinity of a multiphase polymer (as calculated from x-ray diffraction measurements) and the heat of fusion of the polymer [as calculated from differential scanning calorimetry (DSC) measurements]. This correlation is the basis of a simple new technique for estimating the degree of crystallinity of specimens of the polymer from DSC measurements alone.

The experiment was performed with specimens of polyvinylidene fluoride (PVDF), the microstructure of which consists of interspersed regions of an amorphous phase and two crystalline phases (α and β). PVDF was selected for study because its piezoelectric and pyroelectric properties make it an important material for use in sensors, because its dielectric properties make it an important material for use in capacitors, and because these properties depend on microstructural characteristics and crystallinity.

Each specimen of PVDF was placed in an x-ray diffractometer and rotated (to average out orientational effects) while it was exposed to Cu Kα x-rays. The raw scattering pattern (intensity vs. angle) of each semicrystalline specimen, was recorded, then normalized with respect to the thickness of the specimen and corrected for air scatter, Lorentz polarization, background counts, and incoherent scatter. Next, each specimen was heated on the diffractometer to 168 °C (almost the melting temperature for most specimens) to eliminate the crystalline phases and obtain a scattering pattern for the amorphous phase. After normalization and correction, this pattern was subtracted from the pattern from the semicrystalline condition to obtain the crystalline component of the scattering pattern.

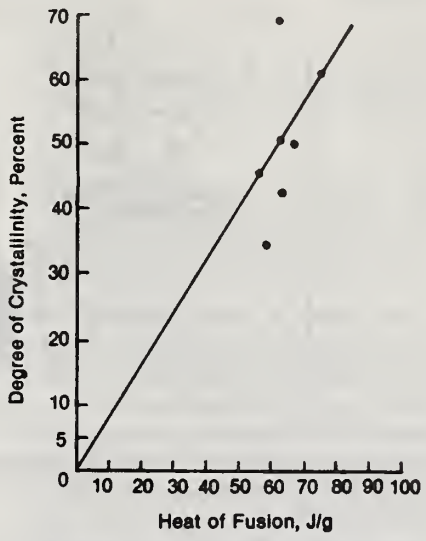

The Degrees of Crystallinity of specimens of PVDF (as determined via x-ray diffraction) are correlated with their heats of fusion (as determined via differential scanning calorimetry).

From previous studies, it is known that the integral, over all angles, of the normalized and corrected intensity of scattering from one of the phases is proportional to the amount of that phase in the specimen. In this case, the constants of proportionality were obtained by calculating a linear regression between the integrated α-phase and integrated amorphous-phase intensities of different specimens and a similar regression for the β and amorphous phases. The resulting constants of proportionality were applied to the integrated scattering intensities of the specimens to obtain the fractions of α, β, and amorphous phases. The degree of crystallinity of each specimen was then calculated as the sum of fractions of the α and β phases.

The heat of fusion of each specimen was calculated by integrating to obtain the area under the endothermic portion of its DSC curve. The figure illustrates the correlation between the calculated degree of crystallinity and the calculated heat of fusion. In applying the new technique to other specimens of PVDF or another polymer, one would first calibrate by taking x-ray diffraction and DSC data to obtain a correlation like this one. Thereafter, one would estimate the degree of crystallinity of new specimens from DSC measurements alone by use of the proportionality indicated by this correlation.

This work was done by Shiao-Pink S. Yen, Lynn E. Lowry, and Clyde P. Bankston of Caltech for **NASA's Jet Propulsion Laboratory.** *NPO-17958/TN*

FOR ADDITIONAL INFORMATION: *Contact: Director, Technology Transfer Division, P.O. Box 8757, BWI Airport, MD 21240; (301) 621-0100 Ext. 241*
REFER TO THE NUMBER LISTED AT THE END OF THIS ARTICLE

NASA Tech Brief
National Aeronautics and Space Administration
Langley Research Center, Hampton, Virginia

Licensing Opportunity

LaRC-RP41: a Tough, High-Performance Composite Matrix

A new polymer exhibits increased toughness and resistance to microcracking.

Recently, work has been done on the interpenetrating-polyimide-network (IPN) approach to developing tough, microcracking-resistant, high-temperature matrix resins for use in aircraft and aerospace structural components. One such polymer was designated LaRC-RP40. This simultaneous semi-IPN was prepared from easy-to-process, but brittle, cross-linking PMR-15® and tough, but difficult-to-process, linear NR-150B2®. Both of these raw materials are commercially available. The combination exhibited significant improvements in toughness, resistance to microcracking, and glass-transition temperature over those of PMR-15. These results encouraged further exploration of this approach for the development of a wider range of polymers of basic technological and economic interest.

In an experiment, cross-linking PMR-15 and linear LaRC-TPI were combined to provide a new, sequential semi-2-IPN designated as LaRC-RP41. LaRC-RP41 was synthesized from PMR-15 imide prepolymer undergoing cross-linking in the immediate presence of LaRC-TPI polyamic acid, which was also undergoing simultaneous imidization and linear chain extension. This synthesis is shown in the figure. LaRC-RP41 was prepared and tested both in neat form and as the matrix of a composite reinforced with graphite fibers. Neat and composite specimens of PMR-15 and LaRC-TPI were similarly prepared and tested.

In comparison with PMR-15, LaRC-RP41 showed significantly improved toughness and resistance to microcracking. However, the glass-transition temperature and mechanical performance at elevated temperature were substantially lower than those of PMR-15. The LaRC-TPI phase acts as an effective plasticizer, rather than as a reinforcement, and it controls the toughness, microcracking behavior, and elevated-temperature mechanical performance of LaRC-RP41.

LaRC-RP41 exhibited apparent two-phase microstructure. The stability of the phases was affected by time and temperature in service as well as by the presence of graphite fibers. Thus, any efforts based on the exploitation of relationships between properties and microstructure to develop high-performance semi-IPN's must take into account the stability of the phases of a semi-IPN.

Synthesis of Semi-Interpenetrating Polyimide is demonstrated in the preparation of LaRC-RP41.

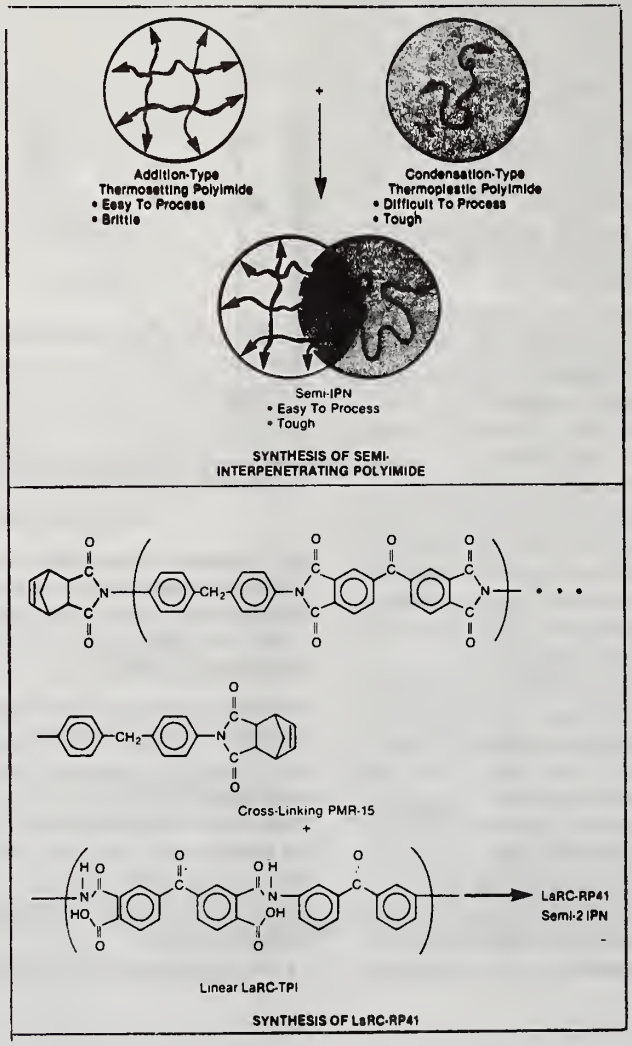

LaRC-RP41 has potential as a high-temperature matrix resin, adhesive, and molding resin. Applications could include automobiles, electronics, aircraft, and aerospace structures.

This work was done Ruth H. Pater, Norman J. Johnston, Ricky E. Smith, and John J. Snoha of **Langley Research Center,** *Carol R. Gautreaux of Analytical Services and Materials, Inc., and Rakasi M. Reddy of Old Dominion University.*

This invention is owned by NASA, and a patent application has been filed. Inquiries concerning nonexclusive or exclusive license for its commercial development should be addressed to the Patent Counsel, Langley Research Center. Refer to LAR-14338/TN.

Langley Research Ctr.
Technology Utilization
Officer John Samos
Mail Stop 139A
Hampton, VA 23665
Patent Counsel
George F. Helfrich
Mail Code 279
Hampton, VA 23665
(804) 864-3523

NASA Tech Brief
National Aeronautics and Space Administration
Langley Research Center, Hampton, Virginia

Licensing Opportunity

New Polyimide Has Many Uses

Low-toxicity and low-mutagenicity monomer is the key to a new high-performance polyimide.

High-performance polyimide adhesives are used in the aerospace industry; for example, in joining metals to metals or metals to composite structures. In addition, they are rapidly being put to new uses as matrix resins for composites, molding powders, and films. These materials display a number of high-performance characteristics; for example, resistance to high temperatures and to solvents, improved flow for better wetting and bonding, high modulus of elasticity, and resistance to chemicals and hot water. One area of application is the manufacture of lighter and stronger aircraft and spacecraft structures.

LaRC-TPI is a thermoplastic polyimide well known as a high-performance material. Its structure is derived from 3,3′-, 4,4′-benzophenonetetracarboxylic dianhydride (BTDA) and 3,3′-diaminobenzophenone (3,3′-DABP), and it is prepared in 2-methoxyethyl ether (diglyme). Invented at NASA Langley Research Center, it is now a commercially available product. However, the commercialization of the 3,3′-DABP component of LaRC-TPI has not occurred in the United States because it has been shown to be a mutagen. Therefore, only experimental samples of this chemical can be purchased in this country for research purposes.

A new polyimide, identified as LaRC-IA, exhibits flow and adhesive properties similar to those of LaRC-TPI. This novel polymer is prepared from the low-toxicity, commercial diamine 3,4′-oxydianiline (3,4′-ODA) and the commercially available dianhydride 4,4′-oxydiphthalic anhydride (ODPA) in 2-methoxyethyl ether (diglyme). This polymer (see figure) has been prepared in both ultra-high-molecular-weight (exact stoichiometry of diamine and dianhydride) form and in a controlled-molecular-weight form, which has a 2.5-percent offset in stoichiometry (excess diamine) with a 5.0-percent level of phthalic anhydride as an end cap.

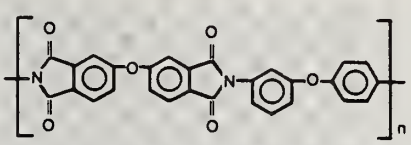

LaRC-IA is a thermoplastic polyimide made from 3-4′-oxydianiline and 4,4′-oxydiphthalic anhydride. It has good processing characteristics, low toxicity, and no mutagenicity.

The controlled-molecular-weight form allows for greatly improved processing of the polymer for moldings, adhesive bonding, and the fabrication of composites. The version that has the higher molecular weight affords tougher films and coatings. The glass-transition temperature of the polymer, as determined by differential scanning calorimetry, is between 230 and 240 °C. The overall polymer structure with oxygen flexibilizing linkages in both the dianhydride and the diamine, as well as a meta linkage in the diamine, affords adequate flow properties for making this polymer useful as a molding powder, adhesive, and matrix resin for composite materials.

Adhesives, composite matrix resins, neat resin moldings, and coating films made of the new polymer have been found to exhibit properties identical or superior to those of commercially available polyimides. The end-capped version of ODPA/3,4′-ODA has been used to prepare graphite-reinforced composites because this version exhibits melt flow superior to that of the non-end-capped version. This higher level of melt flow is important in making large, composite objects that have complicated shapes. Potential applications for this polyimide are wide ranging. With and without end capping, it can be employed to prepare unfilled moldings, coatings and free films, adhesive tape, adhesively bonded substrates, prepregs, and composites.

This work was done by Terry L. St. Clair, Donald J. Progar, Janice Y. Smith, and Ricky E. Smith of **Langley Research Center.**

This invention is owned by NASA, and a patent application has been filed. Inquiries concerning nonexclusive or exclusive license for its commercial development should be addressed to the Patent Counsel, Langley Research Center. Refer to LAR-14163/TN.

Jet Propulsion Lab.
NASA Resident Office
Technology Utilization Officer Gordon S. Chapman
Mail Stop 180-801
4800 Oak Grove Drive
Pasadena, CA 91109
(818) 354-4849
Patent Counsel Paul F. McCaul
Mail Code 180-801
4800 Oak Grove Drive
Pasadena, CA 91109
(818) 354-2734
Technology Utilization Mgr. for JPL Norman L. Chalfin
Mail Stop 156-211
4800 Oak Grove Drive
Pasadena, CA 91109
(818) 354-2240

FOR ADDITIONAL INFORMATION: *Contact: Director, Technology Transfer Division, P.O. Box 8757, BWI Airport, MD 21240; (301) 621-0100 Ext. 241*
REFER TO THE NUMBER LISTED AT THE END OF THIS ARTICLE

NASA Tech Brief
National Aeronautics and
Space Administration
Lyndon B. Johnson Space Center, Houston, Texas

Superfiber for Strong, Light Fabrics

Polyolefin fiber resists chemicals and abrasion.

A new ultrahigh-molecular-weight fiber offers major advantages as a fabric for space suits, diving suits, sporting goods, sails, and ultralight aircraft. The polyolefin fiber has an extremely high modulus of elasticity, low elongation, high specific strength, low specific gravity, resistance to chemicals, low moisture absorption, and high resistance to damage by flexure and abrasion.

The fiber is available in a variety of weave patterns, including plain, herringbone and other twill, and basket-weave patterns (see figure). Besides plain fabric, the fiber is available as plain braided cord, braided cord woven into link nets, flat woven tape, and webbing. Its high strength per unit weight — higher than that of any other polymeric fiber — allows space suits, diving suits, or balloons to be pressurized to 8.3 lb/in.^{2} (57 kPa). Its light weight gives wearers greater mobility.

The new fiber consists of elongated, highly aligned, highly crystalline polyethylene molecules. This structure not only results in a high strength-to-weight ratio but also gives high resistance to tearing and ripping.

In comparison with Kevlar (or equivalent) aromatic polyamid fiber — until now, a material of choice in high-strength applications — the new material can be made into 40 percent more fiber per pound and has 7 to 20 times the resistance to abrasion. Moreover, because its coefficient of friction is low, little heat is generated during abrasion.

Chemically, the new material is nearly inert. It is hardly affected by either alkaline or acidic compounds. When exposed to a broad range of chemicals for a period of 6 months, the fibers retained all their original strength in almost every instance. In addition, because water molecules cannot attach themselves to the polymer chains, the material absorbs little moisture and remains lightweight under wet or humid conditions.

This work was done by Frederic S. Dawn and Joseph J. Kosmo of **Johnson Space Center.** *MSC-21659/TN*

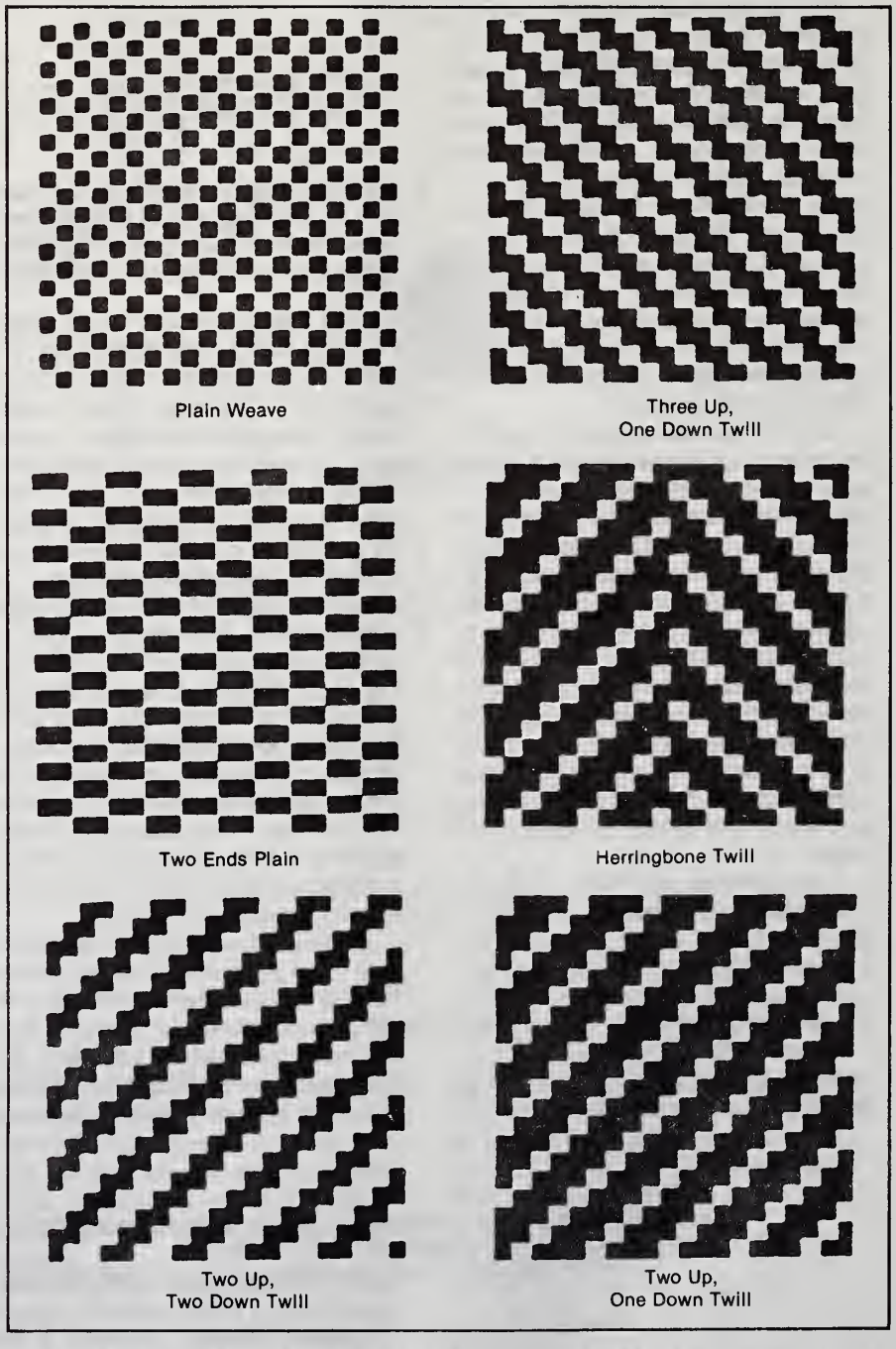

Fibers Can Be Woven in many patterns, a few of which appear here. The fabrics offer a combination of desirable properties not found in nylon, polyester, or aramid fabrics.

FOR ADDITIONAL INFORMATION: *Contact: Director, Technology Transfer Division, P.O. Box 8757, BWI Airport, MD 21240; (301) 621-0100 Ext. 241*
REFER TO THE NUMBER LISTED AT THE END OF THIS ARTICLE

Medicine & Biology

0051 Chronic Adult Periodontitis Studied

0052 Confirmation for the Good Cholesterol

Testing & Instrumentation

0053 Biological Sensors

Other Items of Interest

0002 Milk Doesn't Block Cereal's Iron

Chronic Adult Periodontitis Studied

The Naval Dental Research Institute (NDRI), Great Lakes, Illinois, evaluated serum and gingival tissue antibody levels to oral microbial antigens in human chronic adult periodontitis. Antibody levels against antigens from eight oral micro-organisms were measured in sera and gingival tissue extracts from adult periodontitis patients and healthy subjects by an enzyme linked immunosorbent assay. The antibody levels of diseased serum samples were significantly higher than those of healthy serum samples. Analysis of diseased sera indicated that antibody levels against *Bacteriodes gingivalis* antigens were significantly higher than antibody levels against all the other antigens tested except for those from B. *intermedius* and B. *asaccharolyticus*. Extracts from diseased gingival tissues had significantly higher levels of antibody against B. *gingivalis* antigens than against antigens from all of the other micro-organisms tested, including B. *intermedius* and B. *asaccharolyticus*. These results suggest selective, specific, and localized antibody production during or following the establishment of chronic adult periodontitis.

FOR ADDITIONAL INFORMATION: Backup material on this effort is available from: Navy Domestic Technology Fact Sheet Reader Reply Service, Code E211, Naval Surface Weapons Center, Dahlgren, VA 22448-5000; (703)663-8921. Refer to 160804/TN.

Lawrence Berkeley Laboratory

Confirmation for the Good Cholesterol

The first direct experimental evidence that high density lipoprotein (HDL) - the "good cholesterol" - can protect against heart disease has been obtained by scientists from the Lawrence Berkeley Laboratory.

After several months on high fat diets, transgenic mice genetically engineered to have high levels of humans HDL and apolipoprotein AI (ApoA-I), the main protein component of HDL, showed almost no signs of atherosclerosis. Non-transgenic mice fed the same diets developed numerous fatty deposits in their arteries - a precursor to atheroscleratic plaques.

"Our results are consistent with numerous epidemiological surveys in humans which demonstrated that individuals with high HDL levels were protected from developing heart disease," says the leader of this research, Edward Rubin, with LBL's Research Medicine and Radiation Biophysics, and Cell and Molecular Biology divisions.

"This direct study on the transgenic mice is consistent with indirect human epidemiological studies suggesting that therapeutic interventions which raise the level of ApoA-I and HDL in plasma may decrease the risk of atherosclerosis in susceptible individuals," Rubin says.

Rubin and his colleagues introduced human DNA containing the ApoA-I gene into a strain of mice which is extremely susceptible to diet-induced atherosclerosis. Transgenic and non-transgenic littermates were then housed in the same cages and fed one of two high fat diets for up to 18 weeks.

Following these atherogenic diets, arterial vessels from each animal were examined for fatty deposits. On one diet, the transgenics were completely free of such deposits. Small deposits did appear in the transgenics on the second atherogenic diet but the quantity was sevenfold less than that observed in the non-transgenics.

Blood was also collected from each mouse for lipoprotein measurements. Analyses showed that HDL levels in the the transgenic mice were nearly double that of the non-transgenics, while the levels of LDL and other non-HDL cholesterols were approximately the same for all the animals.

In addition to HDL quantity differences, there were also differences in HDL composition and size distribution between the transgenic and non-transgenic mice.

Says Rubin, "It is possible that alternations in the concentrations as well as the physical and chemical properties of HDL may be contributing to the resistance of the transgenic mice to the development of fatty deposits."

Rubin cautions it is important to note that the relationship between the fatty deposits measured in this study and the mature atherosclerotic plaques which can form in mice following longer dietary exposure has not been examined.

"We've shown that a high plasma concentration of human ApoA-I and HDL in transgenic mice has a direct inhibitory effect on the early stages of atherogenesis," he says. "Long-term studies will be necessary to assess the impact of ApoA-I and HDL on the formation of mature atherosclerotic plaques."

FOR ADDITIONAL INFORMATION: Public Information Department, ATTN: Lynn Yarris, Lawrence Berkeley Laboratory, Berkeley, CA 94720; Telephone (415)486-5375.

Lawrence Berkeley Laboratory

Biological Sensors

In a fusion of the fields of materials science, chemistry, and biotechnology, Lawrence Berkeley Laboratory (LBL) scientists are creating sensors able to lock onto and detect targeted biological molecules and organisms.

The sensors have a broad range of potential applications. Doctors could identify within moments which bacterial or viral strain has infected a patient. Researchers could screen for new enzymes, and technicians could sample air and water for particular contaminants.

The new diagnostic devices rely upon bioelectric thin films developed by a team led by Mark Bednarski of LBL's Center for Advanced Materials (CAM).

While the team continues to conduct fundamental research to further develop the technology, they have filed a patent application and begun commercial development with the assist of a grant from the California Competitive Technology Program.

These biologically sensitive films are possible due to recent advances in materials science, particularly in the synthesis of chemicals and enzymes. Researchers create the films with a micro-fabrication process called molecular self-assembly.

Researchers have discovered that certain organic molecules, when placed in contact with a surface, form highly ordered arrays. The degree of molecular organization can extend beyond that achieved by etching with the photolithographic technologies used to create silicon semiconductors.

Self-assembled films are generated by manipulating the fundamental forces - such as hydrogen bonding - that control the interactions between molecules. Bednarski and his colleagues have pushed molecular self-assembly well beyond its previous limits, becoming the first to fabricate complex molecules at the surface of films. In an important advance, the team has fabricated an array of molecules structured to bind to different biological sites.

Their invention relies on a film containing "ligands" on its surface. Ligands are molecular structures that comprise one-half of a biological lock and key mechanism. They are shaped so that only agents with a matching structure can bind to them. Through molecular self-assembly, films can be fabricated so that a virus, bacteria, antibody, or enzyme, each of which has a uniquely shaped binding site, will attach to a matching ligand structure.

After a sample containing specific biological molecules is applied to the sensor, ligand sites designed to bind these molecules are occupied almost immediately.

When a targeted virus, bacteria, enzyme, or contaminant binds to a specific surface site, the respective molecular chain to which it is attached becomes deformed. This produces a stressed surface that can be detected optically and electronically.

The best medical sensors currently available rely on cumbersome, time-consuming assay techniques to detect specific pathogens. When dealing with low concentrations of pathogens, they are often inaccurate. The new sensors, on the other hand, can detect low concentrations and provide immediate results. They will enable a doctor to make an on-the-spot diagnosis and a patient to receive the added benefit of more immediate medical care.

Most current diagnostic devices depend upon monoclonal antibodies, bioengineered agents which lock onto pathogens. This is a drawback in that pathogenic organisms mutate and no longer are responsive to the same antibodies.

The new sensors, however, cannot be thwarted by mutations because viral or bacterial protein receptors are among the least likely parts of the micro-organism's genome to mutate.

Ligands, integral in the detection of pathogens, ultimately may be used - apart from the sensors - in drugs to prevent infections. The drugs, would act by unleashing a flood of ligands that have a strong affinity for particular pathogens. Viruses and bacteria that bind to these ligands would be tied up and unable to cause infections. Though this pharmaceutical strategy is unproved, researchers elsewhere are exploring its deployment against a number of diseases, including AIDS.

FOR ADDITIONAL INFORMATION: Contact Dr. Pepi Ross, (415)486-6467.

Natural Resources Technology & Engineering

0054 Azimuthal Anisotrophy in Radar Backscatter From the Ocean—Minima are offset from the nominal crosswind directions.

Other Items of Interest

0037 An Assessment of Soil-Gas Measurement Technologies

NASA Tech Brief
National Aeronautics and Space Administration

Azimuthal Anisotropy in Radar Backscatter From the Ocean

Minima are offset from the nominal crosswind directions.

A report describes an experimental and theoretical study of the azimuthal anisotropy in radar backscatter from the surface of the ocean. An important objective of this and related studies is to enhance the ability to sense the speed and direction of the surface wind remotely by use of airborne or spaceborne radar.

The essence of this kind of remote sensing is to synthesize knowledge of the relationship between wind and waves with knowledge of the radar backscattering properties of waves and thereby obtain a technique to infer wind data from radar backscattering data. Often, researchers in this field mathematically model the backscattering cross section by a simple Fourier series; e.g., $\theta_0 = A_0 + A_1 \cos(\theta) + A_2 \cos(2\theta)$, where θ is the azimuthal angle (that is, the ground-track angle) between the radar beam and the wind, and A_0, A_1, and A_2 are coefficients that depend on the speed of the wind, the angle of incidence of the radar beam, and the polarization of the radar beam.

In at least partial agreement with experimental data, this and similar models show a maximum cross section in the upwind direction ($\theta = 0°$), another maximum in the downwind direction ($\theta = 180°$), and minimums near the crosswind directions ($\theta \approx 90°$ or 270°). A_1 and A_2 characterize the up/down-wind anisotropy and the depth of the crosswind anisotropy, respectively. The offset between the directions of each minimum and the nearby crosswind direction increases as A_1/A_2 increases.

In the experimental part of this study, the surface of the ocean was scanned azimuthally by an airborne radar at a frequency of 14.6 GHz. Backscattering cross sections in horizontal and vertical polarizations were measured as functions of θ at various angles of incidence. The backscattering data were initially fitted with a simple Fourier series to obtain rough estimates of the azimuthal locations of the extrema of σ_0. Data within 45° of these estimated locations were then fitted with second-order polynomials, and from these polynomial fits new locations of the extrema were determined. This process was repeated five times to refine the estimate for each extremum.

To provide a physical basis for analysis of the locations of the extrema, the radar-backscattering properties of ocean waves were computed via a two-scale mathematical model, in which the height of the surface of the ocean is divided into a large-scale and a small-scale component, the scattering from the large-scale component is quasi-specular, and the scattering from the small-scale component is more like Bragg scattering. In this case, the small-scale component dominated.

For horizontal polarization, the minimums in the experimental cross sections were found to be significantly offset from the crosswind directions towards the downwind direction. These offsets were substantially smaller for vertical polarization. The offsets predicted by the two-scale model for horizontal and vertical polarizations were found to agree, at least qualitatively, with the experimental offsets.

This work was done by F.K. Li, G. Neumann, S.J. Shaffer, and S.L. Durden of Caltech for **NASA's Jet Propulsion Laboratory**. *To obtain a copy of the report, "Studies of the Location of Azimuth Modulation Minima for Ku-Band Ocean Radar Backscatter."*
NPO-17422/TN

FOR ADDITIONAL INFORMATION: *Contact: Director, Technology Transfer Division, P.O. Box 8757, BWI Airport, MD 21240; (301) 621-0100 Ext. 241*
REFER TO THE NUMBER LISTED AT THE END OF THIS ARTICLE

Physical Sciences

0055 Molecular Engineering Theory Guides New Polymer Blends

Testing & Instrumentation

0056 Air/Sea Temperature Probe Developed

0057 Telescope Would Image X and (r) Rays—The advantages of focusing optics would be made available at high photon energies. (Licensing Opportunity)

0058 Ultra-High-Spectral-Resolution X-Ray/EUV Monochromator—Multilayer Bragg-reflection coats would be combined with diffraction gratings. (Licensing Opportunity)

Sandia National Laboratory

Molecular Engineering Theory Guides New Polymer Blends

Scientists at Sandia National Laboratories have developed a new technical approach that could guide chemists in the development of novel polymer blends and copolymers.

Using computer codes based on a theory developed at Sandia, a polymer chemist can infer the approximate solubility and phase behavior of hypothetical polymer mixtures before going into the laboratory.

The Sandia research has captured the interest of BIOSYM Technologies Inc., a company that develops and markets software for scientific and industrial applications. BIOSYM, based in San Diego, Calif., is collaborating with Sandia to develop a commercial software package based on the new polymer theory.

Although alloying of metals has been practiced for centuries, the blending of polymers to produce new engineering materials is relatively new. Because of their chainlike nature, polymers mix in a more complex manner than metals, and researchers are now engaged in understanding the relationship between the polymer blend miscibility and molecular structure.

Sandia researchers developed a tractable theory that allows quantitative calculation of the average intermolecular packing and thermodynamic properties of polymer melts and blends. The Sandia approach applies to long chain polymers ideas originally developed by Professor David Chandler and co-workers. Chandler - now at the University of California at Berkeley - and his co-workers successfully used this earlier theory, called the RISM theory, to describe small molecule liquids.

The Sandia theory differs from previous polymer theories in several respects. It is a continuous space description that does not assume the polymer molecules are confined to regularly spaced lattice positions. It also includes the effects of nonrandom packing, chain connectivity, and compressibility. These effects are known to play an important role in accurately predicting the thermodynamics of mixing of polymers.

Previously, chemists have relied on the well-known Flory-Huggins theory, developed in the 1950s, to guide them in designing new polymer alloys. John G. Curro, supervisor of Sandia's Physical Properties of Polymers Division, says Sandia researchers now believe that this theory leads to overly pessimistic predictions regarding the ability of two polymers to successfully mix. Non-random mixing, not included in the Flory-Huggins theory, has the effect of stabilizing the miscible mixture and forestalling the tendency of polymers to separate into two different phases. "Much of the polymer blend development work in the past has followed trial-and-error procedures. The new theory has the potential to change this," Curro says.

Curro states that chemists could use the new theory to identify promising new alloy systems based on hypothesized polymer structures. This would reduce the time-consuming and costly synthesis and characterization work of current materials development strategies.

BIOSYM Technologies Inc. has formed a consortium of more than 40 polymer manufacturing companies for the purpose of modeling synthetic polymers. In response to the expressed need of polymer manufacturers to integrate molecular modeling techniques into their polymer development activities, BIOSYM approached Sandia about developing commercial software based on their polymer blend theory. Dana Honeycutt of BIOSYM has been working with Sandia on this project.

University of Illinois materials science and engineering professor Kenneth Schweizer, a former Sandia researcher and co-developer of the Integral Equation approach with Curro, also is continuing to work with Sandia and BIOSYM. Schweizer was awarded the 1991 John H. Dillon Medal by the High Polymer Physics Division of the American Physical Society in part for his work on polymer alloys.

"Until now, we had performed our calculation using idealized models of polymer chain structure in order to examine qualitative trends and universal aspects of polymer mixture behavior. Before commercial exploitation of the new theory is possible, additional development needs to be done to incorporate local chemical structure details into the model so that quantitative predictions can be made on real polymer blends and copolymer systems," Curro explains.

That work can be accomplished through collaboration with industrial partners. The joint research and development project, aimed at furthering the development of the Sandia theory, is expected to run for several years. An initial version of the software will be available to the consortium this fall.

FOR ADDITIONAL INFORMATION: Technical Contact: John G. Curro (505)844-3963, Department of Energy, Sandia National Laboratories, Albuquerque, NM 87185-5800.

Air/Sea Temperature Probe Developed

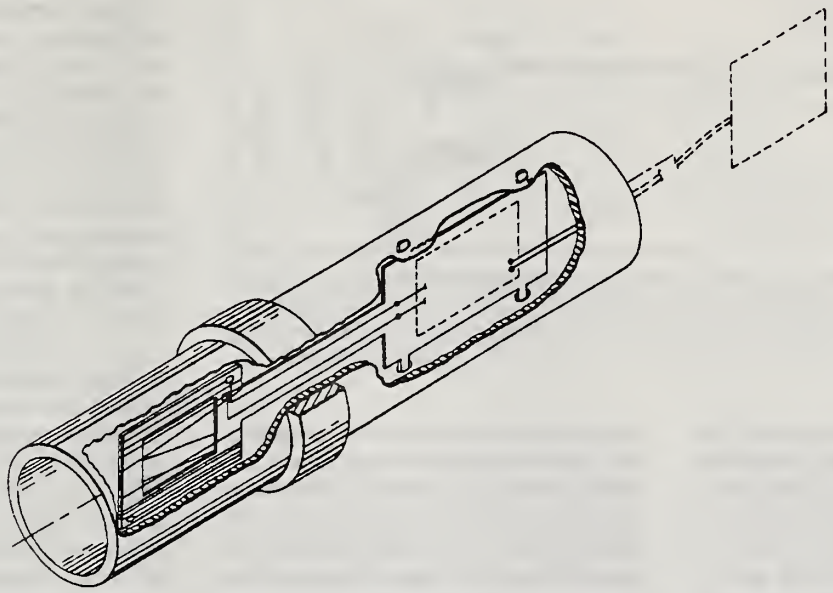

Figure 2. Air/sea temperature probe

The Naval Ocean Systems Center (NOSC), San Diego, California, has developed an inexpensive air/sea temperature probe (Figure 2) that can detect air and ocean surface temperatures beyond the thermal influence of a ship under way at sea. This is achieved because the probe has an extremely quick air temperature time constant of less than 100 milliseconds.

The probe comprises of a temperature transducer formed as bifilar wire looped several times around an electrically non-conductive open frame. The resistance of the wire corresponds to ambient temperature. A signal processing network detects the resistance of the wire and provides an electrical pulse modulated output functionally related to the resistance. The pulse modulated signal is provided to an opto-isolator, which in turn propagates a second pulsed electrical signal that is propagated via electrical wires to a receiver located on the ship. The temperature transducer and electrical circuitry are mounted within a tubular-shaped thermal radiation shield having low reflectivity and thermal conductance.

The probe is very simple to operate. It may be hand thrown or launched into a trajectory, which carries it beyond the thermal influence of the ship. The time constant of the transducer is low enough so that by the time it

reaches the apogee of its trajectory, it senses ambient air temperature. As the probe descends to the ocean surface, it constantly provides air temperature telemetry to the shipboard receiver. When the probe impacts the ocean surface, it then detects ocean near surface temperature.

For Additional Information:

Backup material on this effort is available from:

Navy Domestic Technology Fact Sheet Reader Reply Service
Code E211
Naval Surface Weapons Center
Dahlgren, VA 22448-5000
(703) 663-8921

Refer to 160602/TN

NASA Tech Brief
National Aeronautics and Space Administration
Marshall Space Flight Center, Alabama

Licensing Opportunity

Telescope Would Image X and γ Rays

The advantages of focusing optics would be made available at high photon energies.

A proposed telescope would form images of sources of γ rays (photon energies from 30 to 100 keV), hard x rays (photon energies from 3 to 30 keV), and soft x rays (photon energies from 0.2 to 3 keV). The telescope would offer the advantages of grazing-incidence focusing optics, which were previously available only at photon energies of less than 10 keV. The telescope was conceived for use in astrophysical studies in outer space. With modifications, it could be used in terrestrial laboratory vacuum systems to image x or γ rays from pulsed plasmas, for example.

The version of the telescope illustrated in the figure would include two coaxial, spherical, grazing-incidence reflectors. The reflector substrates would be made of sapphire, ground to within 1/20 visible-light wavelength of the desired surface figures, and polished to roughnesses of less than 3 Å root-mean-square. The polished surfaces of both reflectors would be coated with Bragg-reflecting alternating layers of high- and low-atomic-number materials (e.g., tungsten and carbon). The spacing of the layers would be chosen so that, at the wavelength or photon energy at which the image is to be formed, the peak Bragg reflection would occur at the design grazing angle of incidence. The surface figures would be chosen according to the field of view and other optical requirements: typically, the primary reflector would be a paraboloid, while the secondary would a hyperboloid.

At photon energies less than a value (typically, 0.5 keV) that depends on the density of electrons in the high-atomic-number surface layers, the reflectors would operate by conventional grazing-incidence reflection. This means that the telescope would also focus visible light, which is undesired in the intended application. Therefore, to prevent visible light from reaching the imaging detector at the focus, the telescope would include a filter, which would typically be made of aluminum foil 2,500 Å thick on a nickel mesh. Such a filter would be opaque to visible light but highly transmissive for extreme-ultraviolet and higher-energy photons. This filter could be mounted in a wheel along with other foil filters designed to isolate different portions of the soft x-ray spectrum. Thus, by rotation of the wheel to bring one of the filters into the focused beam, one could select an image in x rays or hard γ rays (formed by Bragg reflection) or by soft x rays (formed by conventional grazing-incidence reflection).

The imaging detector could be photographic film or any of a variety of arrays of electronic γ-ray or x-ray detectors. If high sensitivity and/or real-time imaging capability were not required, photographic film would ordinarily be preferred because of its high spatial resolution. The specific photographic film could be chosen from among the many commercially available x- and γ-ray films.

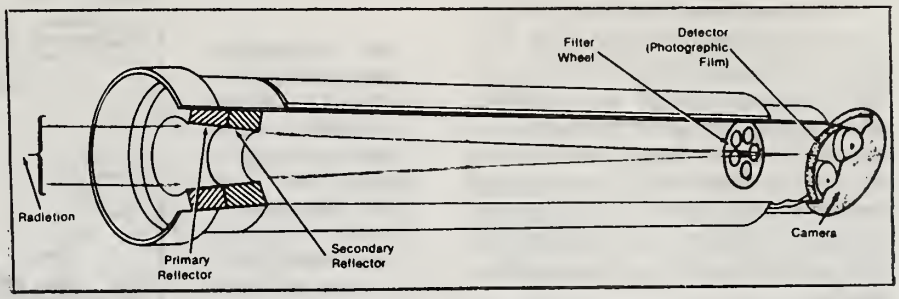

The **γ-Ray and/or X-Ray Telescope** would contain-reflecting, grazing-incidence reflectors. One pair of reflectors is shown here, but multiple coaxial nested pairs could be used to form images simultaneously at multiple γ-ray or hard-x-ray photon energies or to enhance the collection area at a single photon energy.

This work was done by Richard B. Hoover of **Marshall Space Flight Center.**

Inquiries concerning rights for the commercial use of this invention should be addressed to the Patent Counsel, Marshall Space Flight Center. Refer to MFS-28484/TN.

George C. Marshall Space Flight Center
Technology Utilization Officer Ismail Akbay
Code AT01
Marshall Space Flight Center,
AL 35812
(205) 544-2223
Patent Counsel
Leon D. Wofford, Jr.
Mail Code CC01
Marshall Space Flight Center,
AL 35812
(205) 544-0024

FOR ADDITIONAL INFORMATION: *Contact: Director, Technology Transfer Division, P.O. Box 8757, BWI Airport, MD 21240; (301) 621-0100 Ext. 241*
REFER TO THE NUMBER LISTED AT THE END OF THIS ARTICLE

NASA Tech Brief
National Aeronautics and Space Administration
Marshall Space Flight Center, Alabama

Licensing Opportunity

Ultra-High-Spectral-Resolution X-Ray/EUV Monochromator

Multilayer Bragg-reflection coats would be combined with diffraction gratings.

A proposed monochromator for soft x rays and extreme ultraviolet (EUV) radiation would include diffraction gratings and mirror surfaces coated with alternating layers of high- and low-atomic-number materials to produce Bragg reflection (see figure). The instrument would have moderate throughput and a very high spectral resolution. It would have a relatively low cost and could be constructed and aligned easily.

The multilayer coat on the grating would reflect electromagnetic radiation in a narrow band of wavelengths, with peak reflection at a middle wavelength that would meet the Bragg condition, $n\lambda = 2D \sin\theta$, where D is the center-to-center spacing of successive layers of the same material in the multilayer, θ is the angle between the incident beam and the surface of the grating or mirror, n is an integer that specifies the order of the diffraction, and λ is the wavelength. The grating structure would disperse the selected wavelength band into a series of diffraction orders on either side of the specularly reflected zeroth diffraction order. Where radiation in one of these dispersed orders struck the mirror, the mirror would reflect only the portion of the beam, the wavelength and angle of incidence of which satisfied the Bragg condition. The desired wavelength could be selected by adjusting the angle of the grating and mirror. Typically, the grating and mirror would be maintained parallel to each other, and the angle θ between them and the input beam would be adjusted by a parallelogram linkage.

In some applications, additional slits or other apertures might be required to reject undesired wavelength components. Foil filters could be used at the input to limit the wavelength range accepted.

In preparation for coating, the mirror and grating substrates would have to be made optically flat to within 1/20 wavelength of visible light, with a root-mean-square roughness of less than 3 Å. Surface roughnesses in the range 0.5 to 3 Å could be produced by advanced flow polishing, float polishing, or ion polishing. Suitable substrate materials include silicon carbide, fused silica, and sapphire.

To make a typical grating surface, 500 to 1,500 lines per mm would be cut into the substrate by mechanical or holographic ruling or by anisotropic etching. Suitable pairs of materials for multilayer coating include rhenium/carbon, tungsten/carbon, and molybdenum/silicon. A typical coat could consist of as few as 20 or as many as 1,000 layers.

By changing the grating and mirror components, one could configure the monochromator to operate at any wavelength from 10 to somewhat more than 400 Å. Alternatively or in addition, the instrument could be constructed with multiple sets of gratings and mirrors arranged like slats in a venetian blind. One grating-and-mirror pair would cover a portion of that range with a wavelength ratio of about $\sqrt{3}$ as the angle of incidence of the input beam varied from 30° to 60°.

The instrument is intended for use with high-intensity x-ray/EUV beams now available from synchrotrons, laser plasma sources, free-electron lasers, wigglers, and the like. Its monochromatic output beam of accurately known wavelength would be very useful in the testing and calibration of x-ray telescopes, x-ray microscopes, photographic films, and photodetectors; in research in biological and biomedical disciplines, x-ray crystallography, the properties and processing of materials, and x-ray lasers; and in x-ray lithography.

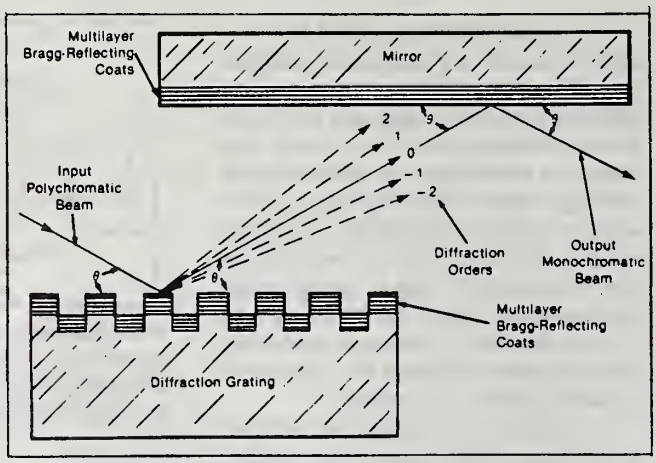

The **Ultra-High-Spectral-Resolution X-Ray/EUV Monochromator** would depend on Bragg reflection from multilayer coats and diffraction by a multilayer-coated grating to select a narrow wavelength band from an input beam.

This work was done by Richard B. Hoover of **Marshall Space Flight Center.**

Inquiries concerning rights for the commercial use of this invention should be addressed to the Patent Counsel, Marshall Space Flight Center. Refer to MFS-28482/TN.

George C. Marshall Space Flight Center
Technology Utilization Officer Ismail Akbay
Code AT01
Marshall Space Flight Center,
AL 35812
(205) 544-2223
Patent Counsel Leon D. Wofford, Jr.
Mail Code CC01
Marshall Space Flight Center,
AL 35812
(205) 544-0024

FOR ADDITIONAL INFORMATION: *Contact: Director, Technology Transfer Division, P.O. Box 8757, BWI Airport, MD 21240; (301) 621-0100 Ext. 241*
REFER TO THE NUMBER LISTED AT THE END OF THIS ARTICLE

Transportation & Components

0059 Research in Helicopter Noise—Progress in aeroacoustical theory and experiments is reviewed.

NASA Tech Brief
National Aeronautics and
Space Administration

Research in Helicopter Noise

Progress in aeroacoustical theory and experiments is reviewed.

A report summarizes continuing U.S. Army programs of research into the causes of noise generated by helicopters. There are many such causes, most of which are related to aerodynamic phenomena around rotor blades and fuselages. Among the most notable advancements of recent decades have been computer codes for the prediction of high-speed impulsive noise, a technique for the measurement of noise in flight, and a joint Army/helicopter-industry test program in an anechoic wind tunnel.

One of the three main topics discussed in the report is high-speed impulsive noise. Experimental data have been taken by a quiet airplane instrumented with microphones, flying in formation with a helicopter. High-speed impulsive noise manifests itself in such measurements as strong negative pressure peaks observed during level flight at high speeds. This type of noise has been shown to be caused by effects of the thicknesses of rotor blades and transonic flow around the blades. High-speed impulsive noise has also been studied with models in wind tunnels. From flight and wind-tunnel tests, it has become clear that high-speed impulsive noise can be scaled and that the primary scaling parameter is the mach number of the advancing tip of the rotor blade.

The theoretical analysis of high-speed impulsive noise is based on an equation for the far-field acoustic pressure in terms of monopole and dipole integrals over the surfaces of rotor blades and the surrounding volume. Comparisons between theoretical predictions and experimental data are presented.

The second main topic is noise caused by interactions between rotor blades and vortices. This phenomenon is not as well understood as is high-speed impulsive noise. It is known, however, that this type of noise can be scaled for low advance ratios and that the scaling parameters are the mach number of the advancing tip of the rotor blade, the advance ratio, the coefficient of thrust of rotor colitity, and the angle of the plane defined by the path of the tips of the rotor blades. Techniques of computational fluid dynamics are now emerging for the understanding of the interactions between blades and vortexes and the noise caused by them.

The third topic is the joint Army/helicopter-industry test program. Acoustic and aerodynamic measurements are taken in a wind tunnel with advanced, dynamically scaled, pressure-instrumented model rotor systems to relate the important aerodynamic phenomena to near- and far-field acoustic radiation. Topics of study include high-speed impulsive noise, blade/vortex-interaction noise, and low-frequency harmonic noise.

This work was done by Yung H. Yu, Frederic H. Schmitz, and Andrew H. Morse of **Ames Research Center.** *"Aeroacoustic Research Programs at the Army Aviation Research and Technology Activity."* *ARC-12171/TN*

FOR ADDITIONAL INFORMATION: *Contact: Director, Technology Transfer Division, P.O. Box 8757, BWI Airport, MD 21240; (301) 621-0100 Ext. 241*
REFER TO THE NUMBER LISTED AT THE END OF THIS ARTICLE

*U.S. Government Printing Office: 1991 — 311-885/60002

U.S. DEPARTMENT OF COMMERCE
National Technical Information Service
Springfield, VA 22161

NTIS ORDER FORM

Use this form ONLY to order reports designated as available from NTIS.

TELEPHONE ORDERS (703) 487-4650 FAX (703) 321-8547 TELEX 89-9405

Rush Service
1-800-553-NTIS

For Subscription Questions
(703) 487-4630

For Tracing an Order
(703) 487-4660

For Editorial Questions
(703) 487-4805

If your address label on this Tech Notes is NOT correct, call the NTIS Subscriptions Department on (703) 487-4630.

1 ADDRESS INFORMATION

Last Name .....

Title .....

Company/Organization .....

Address .....

.....

City/State/ZIP .....

Telephone Number .....

2 METHOD OF PAYMENT

☐ Charge my NTIS Deposit Account .... – .....

☐ Check/Money order enclosed payable to NTIS for $ .....

☐ Purchase order **ADD $7.50 per order** (U.S., Canada, and Mexico only)

Purchase order number .....

Charge my ☐ American Express ☐ VISA ☐ MasterCard

Account Number. ..... Exp. .....

Signature .....
(Required to validate order)

3 ORDER SELECTION (Use only for reports stated as available from NTIS)

NTIS Order Number	*Price**	*Quantity*	*Total Price*
..... /NAC	.....	.....	.....
..... /NAC	.....	.....	.....
..... /NAC	.....	.....	.....
..... /NAC	.....	.....	.....
..... /NAC	.....	.....	.....
		Handling fee	$3.00
		Total	.....

10/91

NTIS PRICE SCHEDULE *

This schedule converts into actual prices the price codes cited in those Tech Notes having a report available from NTIS.

Price Code	*Price*
A01	$9.00
A02	12.50
A03	17.00
A04 through A05	19.00
A06 through A09	26.00
A10 through A13	35.00
A14 through A17	43.00
A18 through A21	50.00
A22 through A25	59.00
A99	Contact NTIS for price

These prices are for customers in U.S., Canada, and Mexico. Other addresses should write for the price listing, number PR-360-4.

Prices effective October 1, 1991

- Agriculture & Food
- Computers
- Electrotechnology
- Energy
- Engineering
- Environmental Science & Technology
- Manufacturing, Machinery, & Tools
- Materials
- Medicine & Biology
- Natural Resources Technology & Engineering
- Physical Sciences
- Transportation & Components

Route To:

PENN STATE UNIVERSITY LIBRARIES
A0000720104O2

EPARTMENT OF COMMERCE
al Technical Information Service
eld, Va. 22161

AL BUSINESS
for Private Use, $300

AN EQUAL OPPORTUNITY EMPLOYER

BULK RATE
POSTAGE & FEES PAID
NTIS
Permit No. G-292